3 A Primer in Three-Dimensional Radiative Transfer

Anthony B. Davis and Yuri Knyazikhin

3.1 Introduction

3.1.1 Three-Dimensional?

Technically speaking, only the 2-stream model in homogeneous (or layered) plane-parallel, cylindrical, or spherical geometries can be truly one-dimensional (1D) because there is no angular dependence to worry about, only the axial flow of radiant energy in a highly symmetric medium with equally symmetric source distributions. By strict mathematical standards, azimuthally-averaged or -symmetric radiative transfer in a plane-parallel medium is already 2D (one spatial and one angular coordinate). By the same token, it is patently 3D if there is also azimuthal variation (one extra angular coordinate) as, e.g., when solar illumination is off-zenith. However, it is generally understood that, independently of the how angles are treated, all plane-parallel radiative transfer (RT) theory is called "1D:" at most stratification in the vertical z direction is allowed. So only spatial variability counts here. Then what about patently 2D cases, so often used in sensitivity studies, where optical properties and/or sources vary at most in the horizontal y and vertical z directions? Well, this is still considered "3D" RT for the legendary simplicity. So when we say we are treating 3D radiative transfer it only means that we are making no assumptions about the translational or rotational symmetry of the optical medium's macro-structure nor about the sources of radiation. To make things worse, we will see that the most general 3D problem in RT is trivially solvable as long as there is no scattering: only emission and absorption are present and no coupling exists between the radiation beams. Mathematically speaking, this solution is a simple 1D integration beam-by-beam, where opposite directions count separately (since they are not coupled). And then there is the possibility of time-dependence.

Having somewhat clarified and somewhat obfuscated what is meant by "dimension" in the RT literature, we can ask about the history of RT theory that acknowledges that we live in a 3D world. This question of chronology breaks into two more specific ones covered asymmetrically in the next few paragraphs. First, how did we get to modern radiometry and formulate the radiative transfer equation (RTE)? Then, skipping much on the solution of the RTE in slab geometry with angular details (for planetary or stellar atmospheres) or spherical geometry in a 2-stream mode (for stellar interiors), how did 3D radiative transfer per se develop from the dawn of scientific computing to circa 1980 in application to the *natural* sciences

(atmospheric and, to some extent, astrophysical questions)? We cover the first topic simply by tracing a thread through the contributions of many celebrated scientists, primarily to build historical context. The second topic is covered with detailed references to the seminal papers by the pioneers of 3D radiative transfer because we have occasionally found it refreshing to go back to the early publications in our field.

We have decided, somewhat arbitrarily, that post-1980 literature is best covered in the specialized chapters of this volume. We have also decided that applications to *engineered* systems is another story altogether, an interesting one in its own right that we could not do justice to. We will simply acknowledge that the engineering community has had to struggle with 3D radiation transport, primarily from thermal sources, in increasingly intricate geometries. One is bound to find significant overlap between our concerns and theirs. Indeed, both atmospheric scientists and engineers will start with simple geometries either because they are tractable or because they are viable designs. However, in the end, both will have to consider the complexity of how turbulent reacting flows interact with radiation. It might be rewarding for both communities to draw more on each other's experience with 3D RT.

3.1.2 From Radiometry to Radiative Transfer

As far as we know, the earliest physically correct analysis of radiometric data (i.e., based on the intuitive notion of radiant energy conservation) were by Galileo Galilei (1564 -1642) and Johannes Kepler (1571-1630), discussing their respective observations of the Moon and of Mars. This is of course only about the propagation of radiant energy (whatever they understood that to be) across empty space; so the problem at hand is fully 3D but in the simple case where there is no scattering, nor absorption for that matter. Let us acknowledge the forefathers of general-purpose (hence 3D) radiometry: Lambert, Bouguer, de Beer, Helmholtz, and others. We must mention in passing the founders of particle transport theory (on which modern RT is based), Maxwell and Boltzmann, who worked in the earliest years of the atomic theory of matter when it was still highly controversial. Then come the pioneers of RT per se (i.e., with the complication of scattering): Schuster, Eddington, Peierls, and Schwarzschild. They were soon followed by the giants of 1D RT theory: Milne, Sobolev, Ambartsumian, and Chandrasekhar. The onset of the nuclear age brought us phenomenal advances in computational transport theory driven by the 3D geometry of weapons and reactors. We should commemorate from this period the brilliant contributions by von Neumann, Ulam, Metropolis, Teller, Marshak, Davison, Vladimirov, Germogenova, and others.

On a parallel track, we can trace the progress of "elementary" radiation-matter interaction science, defined operationally as what provides RT with its emission, absorption, and scattering coefficients and terms. This is the bridge between RT and mainstream optics, drawing on both sides of its celebrated duality between waves and particles. Here the modern era opens arguably with Leonardo da Vinci's (1452-1519) notes on smoke plumes and unfolds with Newton and Huygens. The fundamental link between spectroscopy and thermal physics was established by Fraunhofer, Kirchhoff, Planck, and Einstein. There are too many important contributions

of early quantum theorists and experimenters to attempt even a partial list that is meaningful. Because scattering is what makes RT so interesting and challenging, especially in a 3D setting, we will recall the classic work, still in use, by Rayleigh, Lorenz, Mie, and Raman.

Computing absorption and/or scattering coefficients and emission terms is one thing, and deriving the full RTE from first principles in optics is another. The difficulty hinges on the connecting the radiance field that plays a central photon transport theory and the fundamental quantities of scalar or, better still, electro-magnetic (EM) wave theory. The crux of the matter is the loss of wave theoretical (i.e., amplitude and phase) information in the spatial coarse-graining to scales of a few wavelengths where a statistical description of the wave field applies. For remarkable efforts to bridge this gap between radiometry and optics, see Ishimaru (1975) who works from scalar waves and Wolf (1976) who works from vector waves in the frame of classic or quantum EM theory. In the meantime, the theory of radiative transfer we are concerned with in this chapter and volume remains a phenomenology not rigorously connected to optics per se.

3.1.3 The Genesis of 3D Radiative Transfer ($\lesssim$1980)

We have thus fast-forwarded to the last half of the XXth century and set the stage for 3D RT as we presently understand it, that is, in application to astrophysical or geophysical rather than man-made systems; we are also interested in theoretical studies of abstract media that are based on at least some analytical work on the 3D RT equation or an approximation thereof. With these selection rules, we have traced the beginning of 3D RT to Richards' investigation (Richards, 1956) of a point-source in a homogeneous scattering slab medium that is finitely thick, not in boundary-free 3D space, while Giovanelli and Jefferies (1956) looked at variable sources in more generality. Around the same time, Chandrasekhar (1958) considered a collimated "pencil-beam" source impinging on a uniform semi-infinite medium. But Giovanelli's paper (Giovanelli, 1959) stands out as the earliest study of 3D variability effects as we still think of them most often: the slab medium is internally variable and results are compared to the prediction of a standard 1D (internally uniform) model. During the 60s, the first 3D RT papers appeared in the atmospheric literature per se: Romanova (1968b,a) on the pencil-beam problem in a uniform medium, Weinman and Swartztrauber (1968) on uniformly illuminated media with a horizontal sine-wave structure. In the 70s, we continue to see the same two classes of problem addressed with increasing sophistication. On the one hand, we have pencil-beams (now readily materialized with laser technology) illuminating a uniform scattering plane-parallel medium (Romanova, 1971a,b), or the closely related (essentially adjoint) problem of surface albedo blurring by the intervening atmosphere (Odell and Weinman, 1975; Otterman and Fraser, 1979; Kaufman, 1979). On the other hand, we have uniformly illuminated but internally variable slabs (van Blerkom, 1971; Avaste and Vainikko, 1973; McKee and Cox, 1974; Romanova, 1975; McKee, 1976; Aida, 1977a,b; Wendling, 1977), or simply non-plane-parallel media such as upright cylinders with circular sections (Barkstrom and Ar-

duini, 1977) or perpendicular parallelepipeds (Davies and Weinman, 1977; Davies, 1978). The methodologies were almost invariably Monte Carlo simulation for numerical results (if any) and either the diffusion or small-angle approximations for the analytical work (if any). The noteworthy exceptions were (1) Chandrasekhar's pencil-beam study in purely scattering media which used neither approximations nor numerics but established the formal connection between horizontal transport away from the beam and the problem of an absorbing/scattering medium under uniform illumination problem, and (2) Avaste and Vaynikko's "mean-field" theory for a stochastic binary (cloudy/clear) medium with a random (Poissonian) distribution of transitions. Two other notable publications were Cannon's article (Cannon, 1970), a penetrating analysis of numerical results on line transfer in a 2D medium using a finite-difference technique to solve the RT equation (not an approximation), and the compilation by Mullamaa et al. (1972), a poorly distributed report (even in translation), where the linear mixture of 1D results that became known as the "independent pixel/column approximation" (IPA or ICA) was first introduced, at least in the former Soviet Union. This brings us up to Marchuk et al.'s landmark volume on the Monte Carlo technique (Marchuk et al., 1980). Developments beyond 1980 are better covered in the specialized chapters that follow. We will only mention Ronnholm et al. (1980) who reinvented the important IPA/ICA technique in the Western literature. The IPA/ICA is used extensively in Chaps. ???, ???, ???, and ???.

3.1.4 Overview

This introductory chapter is organized as follows. In the next section, we review the basic concepts of radiometry and radiative transfer (RT) that are prerequisite for the following sections and chapters. Before formulating the radiative transfer equation (RTE) in Sect. 3.7, we follow a logical but physically backwards flow from detectors (Sect. 3.2) and sinks (Sect. 3.3) to sources (Sect. 3.6), via scattering (Sect. 3.4) and propagation (Sect. 3.5). Once we have the RTE in hand (Sect. 3.7), we examine boundary conditions and integral formulations (Sect. 3.8). At that point, numerical solutions of couple of 3D RT problems are presented, primarily to illustrate less familiar boundary shapes (non-flat lower boundary and compact cloud shapes). Green functions, adjoint RT theory and reciprocity are covered in Sect. 3.10. We summarize in Sect. 3.11 and offer our perspective on the future of research into the fundamental aspects of RT theory. A compendium of Suggested Reading complements the usual list of References. At the end of the volume, an Appendix lists in tabular form the most common notations as well as some useful constants and definitions.

3.2 Radiometric Quantities

We recall and apply the definitions of all the important quantities used in radiometry and RT theory. Ultimately, radiometry is just a theory of light detection in the sense of photon gathering, just before conversion into electrical current or charge, heat, or whatever else that can become an instrument reading.

3.2.1 Flux/Irradiance in a Collimated Beam

The most basic quantity in radiometry is flux, a.k.a. irradiance. It is at once an observable that can be sampled at any point with the proper equipment and a field that exists everywhere, like gravity. Figure 3.1 shows a simple experiment where a collimated beam impinges on a detection area δA for a certain time interval δt. Our goal is to count the number of light quanta that are detected by crossing the surface, each carrying energy in the amount of $h_{\mathrm{P}}\nu$ (h_{P} is the Planck constant and ν the frequency). If δA and δt are small enough, this number δN is certainly proportional to the kinetic volume in the figure; specifically,

$$\delta N = \frac{\delta E}{h_{\mathrm{P}}\nu} \propto \delta V = \cos\theta_0 \delta A \times c\delta t \tag{3.1}$$

where c is the speed of light and θ_0 is the incidence angle of the beam away from the normal to the small/flat detection surface. The dependencies on δA and δt are fully expected while the "$\cos\theta_0$" factor takes a little more thought (δA has to be projected perpendicularly to the beam to get δN right). This is known as Lambert's cosine law of radiometry and it is in fact a requirement for radiometers to follow this law which, in practice, is not easy to achieve at large incidence angles.

Some radiometric devices count photons, others respond to radiant energy, so we allow for both possibilities in (3.1). The proportionality factor in (3.1) is

$$f_{\mathrm{col}} = \lim_{\delta A, \delta t \to 0} \frac{\delta N \text{ (or } \delta E)}{\cos\theta_0 \delta A \times c\delta t}, \text{ in m}^{-3} \text{ (or J/m}^3\text{)} \tag{3.2}$$

is thus the density of photons (or radiant energy) in space at the point where δN was obtained. It is a characteristic property of the beam — its strength — as is its direction of propagation, $\boldsymbol{\Omega}_0$ in Fig. 3.1. The other quantities relate the specifics of its measurement, either the outcome δN (or δE) or the controlled parameters δA (aperture) and δt (exposure).

A more conventional characterization of beam strength is by its flux (or irradiance) content,

$$F_0 = cf_{\mathrm{col}}, \text{ in m}^{-2}\text{s}^{-1} \text{ (or W/m}^2\text{)}. \tag{3.3}$$

The result of the above measurement is thus

$$\frac{\delta E}{\delta t} = F_{\boldsymbol{n}}^{(\pm)}(\boldsymbol{\Omega}_0)\delta A = \cos\theta_0 F_0 \delta A = |\boldsymbol{n} \bullet \boldsymbol{\Omega}_0| \, F_0 \delta A \tag{3.4}$$

where the subscript $\boldsymbol{n}$ identifies the orientation of the detector and the superscript $(\pm)$ the direction from which the beam is coming, specifically $\pm = \mathrm{sign}(\boldsymbol{n} \bullet \boldsymbol{\Omega})$. In the case of Fig. 3.1, the outcome is $(-)$.

For illustration, we imagine an isotropic point-source of power P (in W) and a detector at some distance d subtending a solid angle $\delta\boldsymbol{\Omega} = \cos\theta\delta A/d^2$; see Fig. 3.2. The reading of the device is

$$\frac{\delta E}{\delta t} = P\frac{\delta\boldsymbol{\Omega}}{4\pi} = \frac{P}{4\pi d^2}\cos\theta\delta A. \tag{3.5}$$

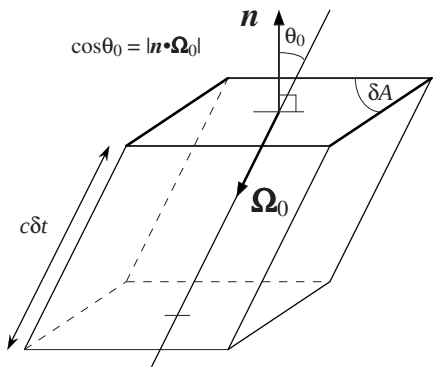

Fig. 3.1. Flux transfer by an oblique collimated beam.

By comparison with (3.4), we have

$$F_0 = \frac{P}{4\pi d^2}. \tag{3.6}$$

So flux diminishes with distance, as required by the overall conservation of energy flowing through spheres of any radius d. Strictly speaking, this well-known "$1/d^2$" decay applies only in absence of absorbing/scattering material; otherwise, it is only one of several terms as we will see in Sects. 3.3 and 3.8.

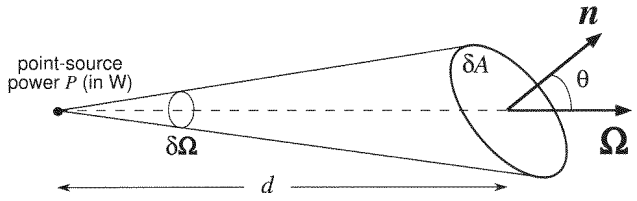

Fig. 3.2. Flux from a distant point-source transferred through an optical vacuum.

3.2.2 Intensity/Radiance in a Diffuse Light Field

The experiment in Fig. 3.3 is a generalization of that in Fig. 3.1 where exposure time is now represented by a stop-watch icon rather than by a kinetic volume. Light is now admitted into $\delta V = \delta A \cos\theta \times c\delta t$, but only from a finite solid angle $\delta\boldsymbol{\Omega}$ around $\boldsymbol{\Omega}$. The outcome is now

$$\delta N(\boldsymbol{\Omega}) = \frac{\delta E}{h_{\mathrm{P}}\nu} \propto \delta V \times \delta\boldsymbol{\Omega} = (\delta A \cos\theta \times c\delta t) \times \delta\boldsymbol{\Omega}, \tag{3.7}$$

and the relevant *diffuse* beam property is

$$f_{\rm dif} = \lim_{\delta V, \delta \mathbf{\Omega} \to 0} \frac{\delta N \text{ (or } \delta E)}{\delta V \times \delta \mathbf{\Omega}}, \text{ in m}^{-3}\text{sr}^{-1} \text{ (or J/m}^3\text{/sr)} \tag{3.8}$$

in comparison with the *collimated* beam property in (3.2).

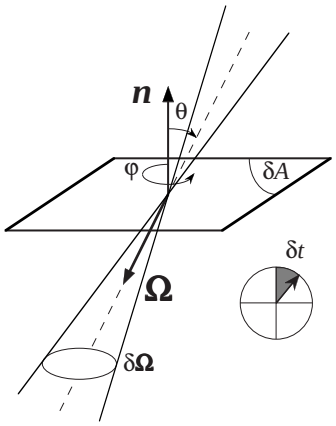

Fig. 3.3. Radiance in a diffuse light field.

Here again, a more conventional characterization of beam strength uses radiance or (specific) intensity

$$I(\mathbf{\Omega}) = c f_{\rm dif}, \text{ in m}^{-2}\text{s}^{-1}\text{sr}^{-1} \text{ (or W/m}^2\text{/sr)} \tag{3.9}$$

and the associated measurement outcome is

$$\delta E = |\boldsymbol{n} \bullet \mathbf{\Omega}| \, I(\mathbf{\Omega}) \delta \mathbf{\Omega} \delta A \delta t. \tag{3.10}$$

From this point on, it is important to bear in mind that polarization and wavenumber filters may be used in conjunction with radiometers. So the most general description of the light field anywhere in space-time calls for an intensity I dependent on all of the quantum mechanical parameters of the photon population:

- wavenumber ν (or energy $E = h_{\rm P}\nu$);
- direction of travel $\mathbf{\Omega}$ (or momentum $\boldsymbol{p} = (E/c)\mathbf{\Omega}$);
- statistical state of polarization (or spin).

In this volume we will be concerned exclusively with the first two and, in this chapter, mostly with the second. The most popular representation of polarization uses Stokes' radiance "vector" where $I(\boldsymbol{x}, \mathbf{\Omega})$ is complemented by three other quantities. For more details, we refer the interested reader to Chandrasekhar (1960).

Imagine a diffuse source at a certain distance d from a detector, as illustrated in Fig. 3.4. The throughput in radiant energy can be evaluated in two different ways:

$$\delta E = I_{\rm det}(\mathbf{\Omega})\delta A_{\rm det}\cos\theta_{\rm det}\delta\mathbf{\Omega}_{\rm det}\delta t,$$
$$\delta E = I_{\rm src}(\mathbf{\Omega})\delta A_{\rm src}\cos\theta_{\rm src}\delta\mathbf{\Omega}_{\rm src}\delta t,$$

respectively from the detector's and source's viewpoints, where

$$\delta\mathbf{\Omega}_{\rm det} = \delta A_{\rm src}\cos\theta_{\rm src}/d^2,$$
$$\delta\mathbf{\Omega}_{\rm src} = \delta A_{\rm det}\cos\theta_{\rm det}/d^2.$$

This shows that, by definition, radiance is conserved across optical vacuum,

$$I_{\rm det}(\mathbf{\Omega}) = I_{\rm src}(\mathbf{\Omega}). \tag{3.11}$$

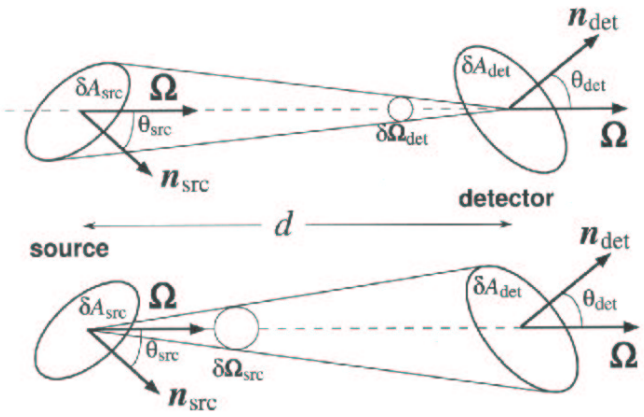

Fig. 3.4. Conservation of radiance in a beam across an optical vacuum.

We can now revisit the concept of flux from the previous subsection without the assumption of a collimated beam. Indeed, by comparing (3.10) and (3.4) we can define the *element* of flux

$$\delta F_{\boldsymbol{n}}^{(-)}(\mathbf{\Omega}) = |\boldsymbol{n}\bullet\mathbf{\Omega}|\, I(\mathbf{\Omega})\delta\mathbf{\Omega}. \tag{3.12}$$

At this point, we need an analytical representation of the beam direction $\mathbf{\Omega}$ on the unit sphere Ξ. We will use both Cartesian and spherical (pole at $\hat{\mathbf{z}}$) coordinates:

$$\mathbf{\Omega}(\theta,\varphi) = \begin{pmatrix}\Omega_x\\ \Omega_y\\ \Omega_z\end{pmatrix} = \begin{pmatrix}\sin\theta\cos\varphi\\ \sin\theta\sin\varphi\\ \cos\theta\end{pmatrix} = \begin{pmatrix}\sqrt{1-\mu^2}\cos\varphi\\ \sqrt{1-\mu^2}\sin\varphi\\ \mu\end{pmatrix}, \tag{3.13}$$

for $-1 \leq \mu = \cos\theta \leq 1,\ 0 \leq \varphi < 2\pi$. From there, the element of solid angle is given by

$$\mathrm{d}\boldsymbol{\Omega} = \mathrm{d}\mu\mathrm{d}\varphi = \sin\theta\mathrm{d}\theta\mathrm{d}\varphi. \tag{3.14}$$

This enables us to define the two *hemispherical* fluxes with respect to an arbitrary plane at any point in space:

$$F_{\boldsymbol{n}}^{(\pm)} = \int\limits_{\pm\boldsymbol{n}\bullet\boldsymbol{\Omega}>0} |\boldsymbol{n}\bullet\boldsymbol{\Omega}|\, I(\boldsymbol{\Omega})\mathrm{d}\boldsymbol{\Omega}. \tag{3.15}$$

These in turn can be combined algebraically to define the *net* flux in any direction:

$$F_{\boldsymbol{n}} = F_{\boldsymbol{n}}^{(+)} - F_{\boldsymbol{n}}^{(-)} = \oint\limits_{\Xi} (\boldsymbol{n}\bullet\boldsymbol{\Omega})\, I(\boldsymbol{\Omega})\mathrm{d}\boldsymbol{\Omega}. \tag{3.16}$$

In classic plane-parallel — often called one-dimensional (1D) — RT, there is only an interest in vertical fluxes (assuming the slab is horizontal), obtained for $\boldsymbol{n} = \hat{\boldsymbol{z}}$. In 3D RT, there is also an interest in horizontal fluxes, $\boldsymbol{n} = \hat{\boldsymbol{x}}, \hat{\boldsymbol{y}}$.

Consider two extreme situations that we will encounter frequently in the following chapters and where we need to know how to relate radiance/intensity and irradiance/flux:

- Collimated beam: $f_{\mathrm{dif}} = f_{\mathrm{col}}\delta(\boldsymbol{\Omega}-\boldsymbol{\Omega}_0)$ in (3.8) where f_{col} was defined in (3.2). We have
$$I(\boldsymbol{\Omega}) = F_0\delta(\boldsymbol{\Omega}-\boldsymbol{\Omega}_0). \tag{3.17}$$
- Isotropic (Lambertian) emittance into a hemisphere by a surface element: $I(\boldsymbol{\Omega}) \equiv I_{\mathrm{L}},\ \forall\mu > 0,\ \forall\varphi \in [0, 2\pi)$. The associated hemispherical flux is therefore
$$F_{\mathrm{L}} = \pi I_{\mathrm{L}}. \tag{3.18}$$

There is a popular non-dimensional representation of radiance in solar problems, especially for satellite imaging analysis, that makes use of both these examples. If the mono-directional radiance field in (3.17) is incident on a scattering medium, then a field of diffusely reflected radiance is generated that we will denote $I_{\mathrm{TOA}}(\mu,\varphi)$, with $\mu > 0$. In atmospheric applications, the uppermost level is colloquially called the Top-of-Atmosphere (or "TOA"). As we will see further on in our discussion of "secondary" sources, the albedo of a surface (or of a plane-parallel medium) is defined as the ratio of outgoing-to-incoming fluxes, measured perpendicular to the surface (or upper boundary). We now assume that the surface (boundary) is horizontal. Then the incoming flux is $\mu_0 F_0$, a quantity we will frequently encounter. We do not necessarily know the out-going flux, a hemispherical integral. In fact, often we have only one directional sample of the out-going radiance distribution, say, the nadir radiance (propagating vertically upward) in every pixel of a satellite image $I_{\mathrm{TOA}}(\boldsymbol{\Omega} = \hat{\boldsymbol{z}})$. However, with a Lambertian hypothesis, we can use (3.18)

to predict the flux and, from there, we can define the *apparent* albedo of the (generally composite surface/atmosphere) medium. This is known as the "Bi-directional Reflectance Factor" or

$$\text{BRF} = \frac{\pi I_{\text{TOA}}(\hat{\mathbf{z}})}{\mu_0 F_0}. \tag{3.19}$$

Note that the BRF, unlike the original out/in flux-ratio concept, is not bounded between 0 and 1; notwithstanding, this is often called "TOA reflectance" in satellite remote sensing. Sections 3.6.2 and 3.9 cover reflection properties of surfaces and atmosphere-surface systems in more detail, including angular integrals that are flux ratios and are between 0 and 1.

3.2.3 Scalar/Actinic and Vector Fluxes

So far, we have illustrated the operational principles of radiometric measurement using radiance $I(\boldsymbol{x}, \boldsymbol{\Omega})$ which will generally depend on both position $\boldsymbol{x}$ and direction $\boldsymbol{\Omega}$. Other quantities can be defined by integration over direction-space. There are both theoretical and practical reasons for doing this.

We start with the *actinic* (a.k.a. scalar) flux

$$J(\boldsymbol{x}) = \oint\limits_{4\pi} I(\boldsymbol{x}, \boldsymbol{\Omega}) \mathrm{d}\boldsymbol{\Omega} \tag{3.20}$$

which can be related to photon (or radiant energy) density. We already encountered a photon density in (3.2) but here it is understood, as usual, irrespective of direction of travel:

$$U(\boldsymbol{x}) = J(\boldsymbol{x})/c, \text{ in } \mathrm{m}^{-3} \text{ (or J/m}^3\text{)}. \tag{3.21}$$

Next in the hierarchy, we have the *vector* flux

$$\boldsymbol{F}(\boldsymbol{x}) = \oint\limits_{4\pi} \boldsymbol{\Omega} I(\boldsymbol{x}, \boldsymbol{\Omega}) \mathrm{d}\boldsymbol{\Omega} = \begin{pmatrix} F_x \\ F_y \\ F_z \end{pmatrix} \tag{3.22}$$

where $F_x = F_{\hat{\mathbf{x}}}$, etc. This vector field tells us about the mean flow of radiation in space. It can be used to compute the outcome of the radiometric measurements described in (3.16). Specifically, we have

$$F_{\boldsymbol{n}}(\boldsymbol{x}) = \boldsymbol{n} \bullet \boldsymbol{F}(\boldsymbol{x}). \tag{3.23}$$

In essence, $J(\boldsymbol{x})$ and $\boldsymbol{F}(\boldsymbol{x})$ represent respectively the monopolar/isotropic (0th-order) and dipolar (1st-order) components of the radiance field $I(\boldsymbol{x}, \boldsymbol{\Omega})$ in spherical-harmonic expansion. So there are higher-order terms that add more and more angular details; they will be used extensively in the following chapter. Only the 2nd-order term has a special name through its connection with the radiation pressure tensor, cf. Mihalas (1979).

3.3 Sinks

We consider all the important mechanisms for removal of photons from a population of interest. In an inward zoom, we go from boundaries to bulk, to a point. We then consider detailed processes unfolding along a beam. At that point, we have a closer look at what is going on inside the elementary kinetic volume.

3.3.1 Boundary Losses

Consider some large region M (cf. Fig. 3.5). We can compute the energy budget in steady state from the radiance field at its boundary denoted (as in mathematical topology) by ∂M. To that effect, we use integrals over the resulting elements of flux:

$$\left.\frac{\delta E}{\delta t}\right|_{\mathrm{out}(+)/\mathrm{in}(-)} = \oint_{\boldsymbol{x}\in\partial\mathrm{M}} \mathrm{d}S(\boldsymbol{x}) \int_{\pm\boldsymbol{n}(\boldsymbol{x})\bullet\boldsymbol{\Omega}>0} |\boldsymbol{n}(\boldsymbol{x})\bullet\boldsymbol{\Omega}|\, I(\boldsymbol{x},\boldsymbol{\Omega})\mathrm{d}\boldsymbol{\Omega} \geq 0 \qquad (3.24)$$

where $\mathrm{d}S(\boldsymbol{x})$ is an element of the boundary of the region.

From (3.24) and various definitions, the net radiative budget for region M is

$$\begin{aligned}\left.\frac{\delta E}{\delta t}\right|_{\mathrm{in}} - \left.\frac{\delta E}{\delta t}\right|_{\mathrm{out}} &= -\oint_{\boldsymbol{x}\in\partial\mathrm{M}} \mathrm{d}S(\boldsymbol{x}) \oint_{4\pi} \boldsymbol{n}(\boldsymbol{x})\bullet\boldsymbol{\Omega} I(\boldsymbol{x},\boldsymbol{\Omega})\mathrm{d}\boldsymbol{\Omega} \\ &= -\oint_{\boldsymbol{x}\in\partial\mathrm{M}} \boldsymbol{F}(\boldsymbol{x})\bullet\boldsymbol{n}(\boldsymbol{x})\mathrm{d}S(\boldsymbol{x}) = \int_{\mathrm{M}} (-\nabla\bullet\boldsymbol{F})\mathrm{d}\boldsymbol{x} \qquad (3.25)\end{aligned}$$

where the last step used the divergence theorem for the vector field $\boldsymbol{F}(\boldsymbol{x})$. If there is neither sources nor sinks *inside* M, the result of (3.25) will clearly be null. Since M is an arbitrary volume, this establishes that radiation flows are irrotational (divergence-free) in conservative optical media. In other words, flux lines start and end at the boundaries where the sources as well as the sinks are to be found.

We now assume are in the case with internal sources only, i.e., $\delta E_{\mathrm{in}}/\delta t = 0$ and $\delta E_{\mathrm{out}}/\delta t > 0$. For instance, think of the Sun or a planet in the thermal part of the electro-magnetic (EM) spectrum. Then, for all practical purposes, the boundary ∂M is absorbing the energy produced in the bulk of M, none is entering from the boundaries, hence the notion of "absorbing" boundary conditions introduced in Sect. 3.8 below.

3.3.2 Bulk Losses

We return again to Fig. 3.5, this time in the absence of sources in the bulk of M (so they must all be accounted for with $\delta E_{\mathrm{in}}/\delta t$). We can estimate the total absorptance in the region, namely,

$$A = 1 - \frac{\delta E_{\mathrm{out}}/\delta t}{\delta E_{\mathrm{in}}/\delta t} = \frac{-\int_{\mathrm{M}} \nabla\bullet\boldsymbol{F}\mathrm{d}\boldsymbol{x}}{\delta E_{\mathrm{in}}/\delta t} \geq 0. \qquad (3.26)$$

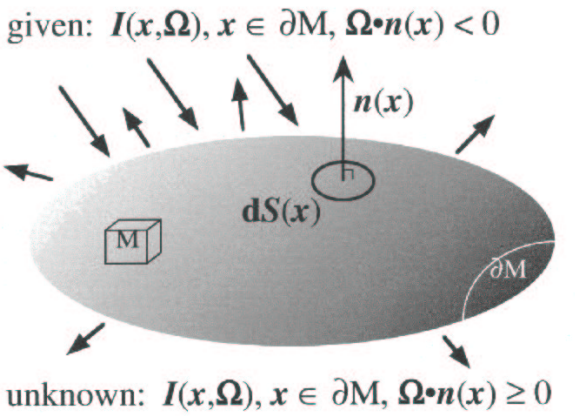

Fig. 3.5. Steady-state radiative energy budget of a macroscopic region.

The inequality is certainly true in the shortwave (solar) spectrum where the source is at the upper boundary of the medium. So the net effect of the Sun is always a *heating* of the atmosphere/surface system. How much and where this heating occurs is discussed in more detail in Chap. ??? but it is fair to say that the effect of clouds is far from well-understood, and this is at least partially due to 3D RT effects in the observations as well as in the radiation physics.

By contrast, in the long-wave (thermal infrared) spectrum, the sources are internal so the sign of (3.26) can go either way depending on the wavelength, the region of interest, and overall (vertical and horizontal) atmospheric structure. Chapter ??? will provide some insight into this important 3D RT problem. The net effect, which has to balance solar heating in the climate system, is of course a *cooling*.

3.3.3 Local Loss

The simplest description of matter-radiation interaction is photon depletion when a narrow beam crosses an optical medium, cf. Fig. 3.6 with the "$-$" sign representing a net loss (we assume $\delta I \geq 0$). Noting that the surface used in Sect. 3.3.1 is in fact quite general, we have basically expressed here the flux-divergence theorem in (3.25) for an "elementary" volume inside the medium. Along the horizontal cylinder the net transport is 0; to the left, there is an in-flux; to the right, an out-flux. So the divergence integral is simply the difference from left to right.

Operationally, we have

$$\delta I \propto I \times \delta s \tag{3.27}$$

and the proportionality constant, defined as

$$\sigma = \lim_{\delta s \to 0} \frac{\delta I / I}{\delta s}, \text{ in m}^{-1}, \tag{3.28}$$

is the *extinction coefficient* or simply "extinction." This inherent optical property of matter is non-negative (except in laser cavities, and other situations where stimulated emission dominates the underlying quantum physics).

Much of 3D RT is predicated on σ's propensity to vary with position $\boldsymbol{x}$ in the atmosphere. Vertical variability of σ is a given because of its strongly stratified structure and of course solar and thermal sources as well as sinks are unevenly distributed vertically. So *atmospheric* RT is generally considered to become 3D when σ varies in one (or both) horizontal direction(s). In this case, σ is often left uniform in the vertical, but sources and/or boundaries will still drive vertical gradients in radiance. There are notable exceptions to this rule since horizontal variability in radiance can be excited in a uniform atmosphere by non-uniform illumination (cf. "off-beam" lidar techniques in active cloud remote sensing) or non-uniform surface albedo (cf. pixel "adjacency" effects mediated by aerosol particulates in passive solar remote sensing). Non-flat terrain, even without an overlaying atmosphere, is also 3D RT problem attracting considerable attention.

Time-dependence of σ is never a concern here because the time for photons to propagate through the system (tens of μs at most) is short by comparison to the turnover time in any atmospheric dynamics. More importantly, σ can depend on photon state variables: frequency ν, direction $\boldsymbol{\Omega}$, and polarization. In this volume, we will account fully for the former, touch on the second (in Chap. ???), and neglect the latter completely.

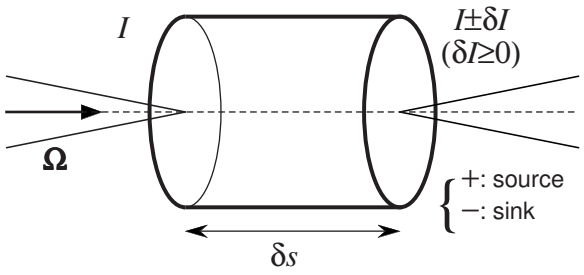

Fig. 3.6. Accounting for sources and sinks of radiance in a beam interacting with matter over a short distance.

3.3.4 Loss Along a Beam

The calculus problem in (3.28), namely,

$$\mathrm{d}I/I = \mathrm{d}\ln I = -\sigma(\boldsymbol{x})\mathrm{d}s, \tag{3.29}$$

is easily solved.

First define *optical* distance as the running integral of σ along the given beam direction $\boldsymbol{\Omega}_0$ from some given starting point $\boldsymbol{x}_0$:

$$\tau(d;\boldsymbol{x}_0,\boldsymbol{\Omega}_0) = \int_0^d \sigma(\boldsymbol{x}_0 + \boldsymbol{\Omega}_0 s)\mathrm{d}s. \tag{3.30}$$

To address the problem of *cumulative* extinction, we will consider $\{\boldsymbol{x}_0,\boldsymbol{\Omega}_0\}$ to be fixed parameters. When it is not convenient to put them in sub-indices, we will separate parameters from the independent variables, in this case d, by a semi-colon. An alternative notation for optical distance emphasizes only the starting and ending points:

$$\tau(\boldsymbol{x}_0,\boldsymbol{x}) = \int_0^1 \sigma(\xi\boldsymbol{x}_0 + (1-\xi)\boldsymbol{x})\mathrm{d}\xi. \tag{3.31}$$

One can easily go from one notation to the other using $\tau(\boldsymbol{x}_0,\boldsymbol{x}) = \tau(d;\boldsymbol{x}_0,\boldsymbol{\Omega}_0)$ where $d = ||\boldsymbol{x}-\boldsymbol{x}_0||$ and $\boldsymbol{\Omega}_0 = (\boldsymbol{x}-\boldsymbol{x}_0)/d$.

The solution of the ordinary differential equation (ODE) in (3.29) is therefore

$$I(d;\boldsymbol{x}_0,\boldsymbol{\Omega}_0) = I(0;\boldsymbol{x}_0,\boldsymbol{\Omega}_0)\exp[-\tau(d;\boldsymbol{x}_0,\boldsymbol{\Omega}_0)]. \tag{3.32}$$

This is the exponential law of direct transmission with respect to *optical* distance. Consider a uniform medium where optical distance is simply

$$\tau(d;\boldsymbol{x}_0,\boldsymbol{\Omega}_0) = \sigma d,\ \forall \boldsymbol{x}_0,\boldsymbol{\Omega}_0; \tag{3.33}$$

thus

$$I(d) = I_0\exp[-\sigma d]. \tag{3.34}$$

This is Beer's law of exponential transmission with respect to *physical* distance, sometimes called the Lambert-Bouguer-Beer law to be more accurate historically. It is obviously of more limited applicability than (3.32).

For future reference, we will define a general notation for *direct* transmission between two arbitrary points $\boldsymbol{x}_0$ and $\boldsymbol{x}$:

$$T_{\mathrm{dir}}(\boldsymbol{x}_0 \to \boldsymbol{x}) = \exp[-\tau(\boldsymbol{x}_0,\boldsymbol{x})]. \tag{3.35}$$

The arrow is used in the notation for the argument of T_{dir} to emphasize causality: the photons were at $\boldsymbol{x}_0$ before going to $\boldsymbol{x}$. This is not to be interpreted as a dependence on the direction of propagation which would violate reciprocity in a fundamental way. Even in vegetation canopies (cf. Chap. ???) where extinction depends on direction, we have $\sigma(\boldsymbol{x},\boldsymbol{\Omega}) = \sigma(\boldsymbol{x},-\boldsymbol{\Omega})$. So it is understood that $T_{\mathrm{dir}}(\boldsymbol{x}_0 \to \boldsymbol{x}) = T_{\mathrm{dir}}(\boldsymbol{x} \to \boldsymbol{x}_0)$ since $\tau(\boldsymbol{x}_0,\boldsymbol{x}) = \tau(\boldsymbol{x},\boldsymbol{x}_0)$.

Optical distance *across* a medium is called optical "thickness" and sometimes (less correctly) optical "depth" (which should vary with z, normally away for a source and/or boundary). Opaque objects such as clouds and fog layers have, by

definition, considerable optical thickness. Equivalently, the amount of directly transmitted or "uncollided" light predicted in (3.35) with positions on either side of the medium will be somewhere between small and negligible. For an empirical investigation of how optically thick this means, from a human observer's perspective, we refer to Bohren et al. (1995).

3.3.5 A Look Inside the Elementary Kinetic Volume

Extinction Mechanism. We now study the detailed mechanism of extinction illustrated schematically in Fig. 3.7. This is about a population of streaming photons colliding with a static population of massive particles. Here, "static" is with respect to the speed of light of course, while "massive" is in comparison with photon mass-equivalent energy $h_{\mathrm{P}}\nu/c^2$ where $h_{\mathrm{P}}\nu$ is at the most an eV or so in energy units for solar problems. This is important because, otherwise, efficient momentum transfer between radiation and matter would make the collision cross-sections dependent on the light field and the whole RT problem becomes patently nonlinear. [1] In all atmospheric applications, the smallest particles are diatomic molecules with already many MeV of mass in energy-equivalent units. So all we have to do is estimate the number of particles in the sample volume $\delta A \times \delta r$ in Fig. 3.7: $\delta N = n\delta A\delta r$ where n is the ambient particle density. Multiplying this by the (mean) cross-section $\mathtt{s}$ and dividing by δA yields the element of probability for an interaction which, by definition (3.28), is $\sigma\delta r$, and should be small. We thus find

$$\sigma = \mathtt{s} \times n. \tag{3.36}$$

In this sense, extinction is the interaction cross-section per unit of volume, equivalently, the probability of collision per unit of length.

For cloud droplets, density n as well as the mean cross-section $\mathtt{s}$ are highly variable in space — 3D RT oblige! — and in time. This variability notwithstanding, it is good to have some typical numbers in mind. The density of (activated) cloud condensation nuclei or "CCN" is often quoted as hundreds to thousands per cm^3 in marine and continental air-masses respectively, so we can use that as an estimate of droplet concentration. At VIS/NIR wavelengths, we have

$$\mathtt{s} \approx 2\pi\langle r^2\rangle \tag{3.37}$$

where r is the droplet radius and $\langle\cdot\rangle$ denotes an average carried over the distribution of droplet radii. The factor of 2 is the asymptotic value of the "efficiency factor" in Lorenz-Mie theory for scattering dielectric spheres that are much larger than the wavelength (cf. Sect. 3.4.4).

[1] The RT equation can become nonlinear in other ways than by momentum transfer. The quantized energy levels of absorbing atoms or molecules can depend on the photon population in non-LTE situations. This happens frequently in tenuous astrophysical media and in photochemically active regions of the atmosphere.

If we are to make an equivalent monodisperse assumption for the droplets, the best is to use the "effective" droplet radius

$$r_{\rm e} = \frac{\langle r^3 \rangle}{\langle r^2 \rangle}. \tag{3.38}$$

In terrestrial liquid water clouds, r_e is $\approx 10\,\mu$m, give or take a factor of 2 or so. This puts the extinction coefficient σ in (3.36) for clouds in a range from almost nil (aerosol levels) to 1/10 or even 1 m^{-1}.

An independent way of estimating this range is to use the observed optical depths of cloud layers to obtain a vertically-averaged σ. Optical depth is simply optical distance τ measured vertically from cloud bottom to cloud top and it ranges from somewhat less than 10 to several 100 in the bulk of the cloud. This is for physical thickness h, equated with d in (3.33). Again excluding cloud edges, we can take h in the range from a few hundred meters to a couple of km. The lower end for h gives us back our upper limit for σ and we anticipate of course less for an average, say $\tau/h = 25/0.5 = 50$ km$^{-1} = 0.05$ m^{-1}.

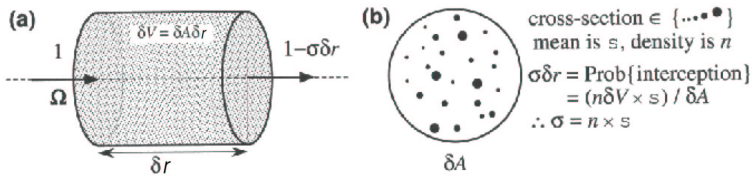

Fig. 3.7. Mechanism of optical extinction by a dilute medium of scattering/absorbing particles. **(a)** Geometrical parameters of the kinetic volume. **(b)** What the volume looks like to the incoming photon beam.

Absorption vs. Scattering. Upon collision with an atmospheric particle, a photon can be either absorbed or scattered. In both cases, it is a loss for the beam; in the latter case, it becomes a source for another beam (cf. Sect. 3.4). So the extinction cross-section (per particle) has to be broken down into its scattering and absorption components, $\mathtt{s} = \mathtt{s}_{\rm s} + \mathtt{s}_{\rm a}$, and similarly for the extinction coefficient in (3.36):

$$\sigma = \sigma_{\rm s} + \sigma_{\rm a}. \tag{3.39}$$

The conventional representation of this breakdown uses the *single-scattering* albedo:

$$\varpi_0 = \sigma_{\rm s}/\sigma \le 1, \tag{3.40}$$

and single-scattering *co*-albedo,

$$1 - \varpi_0 = \sigma_{\rm a}/\sigma. \tag{3.41}$$

It is noteworthy that in nuclear reactor theory, the counterpart of ϖ_0 describes the mean number of neutrons produced after collision with a nucleus and is typically larger than unity, and that is precisely what makes sustained chain reactions possible. So in this context σ_a can be formally negative (anti-absorption).

In atmospheric RT, scattering and absorption can be traced to both gaseous constituents (i.e., molecules) and particulates (i.e., aerosol and cloud droplets). All coefficients depend on wavelength λ. The spectral features of gases tend to vary faster with λ, especially for absorption. This is discussed, as needed, in various parts of this volume.

3.4 Scattering

Scattering is the process that makes 3D RT such a challenge because photon transport through a scattering medium is fundamentally nonlocal, as will be shown in Sect. 3.8. We describe here the basic concepts and popular models for photon scattering. When we get to our brief survey of physical theories of light-particle interaction, it will become clear that we can not treat absorption and scattering separately. So, although the new quantity introduced here is the phase function, we will revisit the partition of extinction σ into σ_s and σ_a.

3.4.1 The (Poorly-Named) Scattering Phase Function

Figure 3.8 illustrates the redistribution of radiant energy between different beams through scattering. Our goal is to estimate the element of scattered flux δF_s. It is surely proportional to the small solid angle into which the scattering occurs $\delta\boldsymbol{\Omega}$ and to the small loss of flux δF_0 incurred when the incoming photons cross the sample volume (conditional to scattering rather than absorption); the latter term is equal to the scattering coefficient times the small length δs. In summary, we have

$$\delta F_\mathrm{s} \propto \delta F_0 \times \delta\boldsymbol{\Omega} = F_0 \sigma_\mathrm{s} \delta s \times \delta\boldsymbol{\Omega}. \tag{3.42}$$

We define the scattering *phase function* as

$$p(\boldsymbol{x}, \boldsymbol{\Omega}_0 \to \boldsymbol{\Omega}) = \lim_{\delta F_0, \delta\boldsymbol{\Omega} \to 0} \frac{\delta F_\mathrm{s}}{\delta F_0 \times \delta\boldsymbol{\Omega}}, \text{ in sr}^{-1}. \tag{3.43}$$

The explicit notation tells us that this property will generally depend on position $\boldsymbol{x}$. Using the above definitions, the integral of $p(\boldsymbol{x}, \boldsymbol{\Omega}_0 \to \boldsymbol{\Omega})$ over all final directions $\boldsymbol{\Omega}$ will be unity (since the sum of all the δF_s in Fig. 3.8 has to equal δF_0). [2] As a first example, we take everywhere isotropic scattering:

$$p(\boldsymbol{x}, \boldsymbol{\Omega}_0 \to \boldsymbol{\Omega}) \equiv 1/4\pi. \tag{3.44}$$

[2] It is important to note that there is another popular normalization convention for the phase function, often denoted $P(\cdot)$ for that matter; even in this volume both conventions and notations are used. The phase function's integral is then equated to 4π; in this case, it is a non-dimensional quantity and $\mathrm{d}\boldsymbol{\Omega}$ is always divided by 4π wherever $P(\cdot)$ is used.

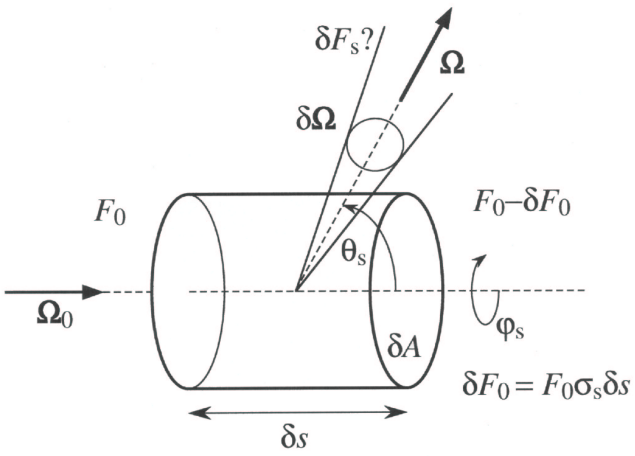

Fig. 3.8. Schematic of scattered flux and radiance.

More general formulations include changes in polarization and wavenumber mediated by scattering. In the former case, one needs a phase matrix; in the latter case, one talks about inelastic scattering since photon energy is changed (and consequently the energy of the scattering entity too, by an equal amount in the opposite direction).

We note in passing that these so-called "phase functions" and "phase matrices" have very little to do with "phases" in the wave (or *coherent*) optics sense of the word since here energies are added and subtracted, not the complex amplitudes used in EM as well as scalar-wave theory. In this respect, we recall that all of RT theory is entirely about *incoherent* optics while (coherent) wave theory contributes at most scattering and absorption cross-sections, one particle at a time. The origin of the "phase function" terminology in fact goes back to early lunar and planetary astronomy were the "phase angle" is defined, following the deflection of the light rays, as the angle between the axis going from the Sun to the celestial body of interest and the line between the celestial body and Earth. It is therefore the equivalent of the scattering angle $\theta_s = \cos^{-1}(\mathbf{\Omega}_0 \bullet \mathbf{\Omega})$. In the course of the Moon's monthly "phases," it varies from 0 at new Moon (in a solar eclipse configuration if *exactly* 0) to π at full Moon (in a lunar eclipse configuration if *exactly* π). The astronomical phase function's purpose is simply to capture the dependence of total planetary brightness (hence photometry) not explained by celestial mechanics, i.e., relative distances. For a given body (hence radius), phase angle is the dominant term but albedo, and the regional variability thereof, also matter.

As for extinction, we can have a closer look at the mechanics of scattering at the individual collision level. To isolate the inherent property of the scattering medium,

we compute

$$\lim_{\delta s,\delta\mathbf{\Omega}\to 0}\frac{\delta F_{\mathrm{s}}/F_0}{\delta s\times\delta\mathbf{\Omega}}=\sigma_{\mathrm{s}}(\boldsymbol{x})p(\boldsymbol{x},\mathbf{\Omega}_0\to\mathbf{\Omega})=n(\boldsymbol{x})\times\frac{\mathrm{d}\mathtt{s}_{\mathrm{s}}}{\mathrm{d}\mathbf{\Omega}}(\boldsymbol{x},\mathbf{\Omega}_0\to\mathbf{\Omega}) \tag{3.45}$$

where the last expression is obtained by straightforward generalization of (3.36) to *differential* cross-sections, again averaged over the population of particles in the sample volume sorted by size and/or type.

By energy (flux) conservation, we have

$$\oint_{4\pi}p(\boldsymbol{x},\mathbf{\Omega}_0\to\mathbf{\Omega})\mathrm{d}\mathbf{\Omega}\equiv 1,\ \forall\mathbf{\Omega}, \tag{3.46}$$

and for any $\boldsymbol{x}$ where scattering occurs. By reciprocity (cf. Sect. 3.10.3), we have $p(\boldsymbol{x},-\mathbf{\Omega}\to-\mathbf{\Omega}_0)=p(\boldsymbol{x},\mathbf{\Omega}_0\to\mathbf{\Omega})$, hence

$$\oint_{4\pi}p(\boldsymbol{x},\mathbf{\Omega}_0\to\mathbf{\Omega})\mathrm{d}\mathbf{\Omega}_0\equiv 1,\ \forall\mathbf{\Omega}_0, \tag{3.47}$$

and for any $\boldsymbol{x}$. In the remainder of this section, we will assume the spatial variability the phase function is implicit, and drop $\boldsymbol{x}$ from its arguments.

3.4.2 Phase Functions with Axial Symmetry

In most atmospheric applications (ice clouds being a notable exception), it is reasonable to assume that scattering is axi-symmetric around the incoming beam. Mathematically,

$$p(\mathbf{\Omega}_0\to\mathbf{\Omega})\equiv p(\mathbf{\Omega}_0\bullet\mathbf{\Omega})=p(\mu_{\mathrm{s}}). \tag{3.48}$$

where the scattering angle θ_{s} is given by $\mu_{\mathrm{s}}=\cos\theta_{\mathrm{s}}=\mathbf{\Omega}_0\bullet\mathbf{\Omega}$.

This enables an expansion of the phase function in spherical harmonics without the complication of azimuthal terms:

$$p(\mu_{\mathrm{s}})=\left(\frac{1}{4\pi}\right)\sum_{l\geq 0}\omega_l P_l(\mu_{\mathrm{s}}), \tag{3.49}$$

where the coefficient is often factored as $\omega_l=(2l+1)\eta_l$. These coefficients can be computed from

$$\eta_l=\frac{\omega_l}{2l+1}=2\pi\int_{-1}^{+1}P_l(\mu_{\mathrm{s}})p(\mu_{\mathrm{s}})\mathrm{d}\mu_{\mathrm{s}}. \tag{3.50}$$

The orthogonality relation of the Legendre polynomials is used here, that is,

$$\int_{-1}^{+1}P_n(x)P_{n'}(x)\mathrm{d}x=\frac{\delta_{nn'}}{n+1/2} \tag{3.51}$$

where $\delta_{nn'}$ is the Kronecker symbol ($= 1$ if $n = n'$, $= 0$ otherwise). Specific values of the polynomials can be obtained efficiently by recursion, but their analytical expressions are best derived from the generating function

$$\Phi(x,z) = \sum_{n\geq 0} P_n(x) z^n = (1 - 2xz + z^2)^{-1/2} \tag{3.52}$$

for any z inside the unit circle of the complex plane. Using

$$P_n(x) = \frac{1}{n!} \left(\frac{\partial}{\partial z}\right)^n \Phi(x,z)\bigg|_{z=0}, \tag{3.53}$$

we find

$$\begin{aligned} P_0(x) &= 1, \\ P_1(x) &= x, \\ P_2(x) &= (3x^2 - 1)/2, \end{aligned} \tag{3.54}$$

and so on.

We have $\eta_0 = \omega_0 = 1$ by conservation for any phase function, and the only non-vanishing coefficient for isotropic scattering in (3.44) and (3.49). Also of considerable interest is

$$g = \eta_1 = \frac{\omega_1}{3} = 2\pi \int_{-1}^{+1} \mu_s p(\mu_s) \mathrm{d}\mu_s, \tag{3.55}$$

the *asymmetry factor*, or mean cosine of the scattering angle. This correctly presents the phase function as a probability density function (PDF) in angle space. Any deviation of the phase function from isotropy corresponds to a directional correlation between incident and scattered photons.

We will be introducing several kinds of averages in upcoming sections and chapters. So those that concern photon scattering and propagation events deserve a special notation, which we borrow from the probability literature: $\mathcal{E}(\cdot)$ which stands for (mathematical) *expectation* of the random variable in the argument. Thus, we can recast the asymmetry factor in (3.55) as

$$g = \mathcal{E}(\mathbf{\Omega}_0 \bullet \mathbf{\Omega}) = \oint_{4\pi} \mathbf{\Omega}_0 \bullet \mathbf{\Omega} \mathrm{d}P(\mathbf{\Omega}|\mathbf{\Omega}_0) \tag{3.56}$$

where $\mathrm{d}\Pr(\mathbf{\Omega}|\mathbf{\Omega}_0) = p(\mathbf{\Omega}_0 \bullet \mathbf{\Omega})\mathrm{d}\mathbf{\Omega}$. The "|" in a PDF separates the random variable from the given (fixed) quantities.

3.4.3 Henyey–Greenstein Models

The most popular 1-parameter model for single-scattering in atmospheric radiation and elsewhere is by far the Henyey–Greenstein (HG) phase function

$$p_{\mathrm{HG}}(g;\mu_s) = \left(\frac{1}{4\pi}\right) \frac{1 - g^2}{(1 + g^2 - 2g\mu_s)^{3/2}} \tag{3.57}$$

which, like the expression "phase function" itself, comes to us from astronomy. It was indeed proposed first by Henyey and Greenstein (1941) to model scattering by interstellar dust, i.e., the stellar astronomer's counterpart of aerosol as a nuisance in surface remote sensing in the solar spectrum. Interstellar dust grains also have in common with aerosol huge spatial variability in quantity and in quality. As for the aerosol, they cause trouble for one kind of observation but have inherent interest in other studies: aerosol matters in climate, cloud physics and pollution; interstellar dust matters in life-cycles of stars and planets.

In spherical harmonics, (3.57) yields

$$\eta_l = g^l. \tag{3.58}$$

Indeed, $4\pi p_{\mathrm{HG}}(z;x)$ is identical to $\sum_{n\geq 0}(2n+1)P_n(x)z^n = 2\partial\Phi(x,z)/\partial z + \Phi(x,z)$ from (3.52); the above coefficients then follow by comparison with (3.49).

A related 3-parameter model is the *double* Henyey–Greenstein (DHG) phase function

$$p_{\mathrm{DHG}}(g_{\mathrm{f}}, g_{\mathrm{b}}, f; \mu_{\mathrm{s}}) = f \times p_{\mathrm{HG}}(g_{\mathrm{f}}; \mu_{\mathrm{s}}) + (1-f) \times p_{\mathrm{HG}}(-g_{\mathrm{b}}; \mu_{\mathrm{s}}). \tag{3.59}$$

We have $g = fg_{\mathrm{f}} - (1-f)g_{\mathrm{b}}$, and so on (for higher-order spherical harmonics). Two other constraints beyond this expression for g can be invoked to uniquely determine all three parameters.

3.4.4 Physical Theories for Scattering and Absorption

The above HG phase functions are convenient models but they have no physical basis. More accurate computations of scattering properties from first (EM or other) principles yield Rayleigh and, for spherical particles, Lorenz-Mie phase functions. However, not all optically important particles in the atmosphere are tiny nor spherical, far from it. Scattering and absorption of course come together in a physically correct theory at the single particle level, basically they come as direct consequences of the existence of interfaces with a discontinuity in the complex index of refraction m, which generally has real ($\neq 1$) and imaginary (≥ 0) parts.

Rayleigh Scattering by Molecules. Rayleigh scattering can be computed using the classic theory of equilibrium thermodynamical fluctuations in molecular density around the mean n, semi-classical or pure quantum mechanics. It leads to the cross-section (per molecule)

$$\mathtt{s}_{\mathrm{Ray}}(\lambda) = \frac{24\pi^3}{n^2\lambda^4}\left(\frac{m^2-1}{m^2+2}\right)^2\left(\frac{6+3\delta}{6-7\delta}\right) \tag{3.60}$$

where λ is the wavelength, m is the index of refraction of dry air at STP, and δ is its depolarization ratio, a weakly λ-dependent term accounting for the anisotropy of (tri-atomic) air molecules. At solar wavelengths, δ can be set to ≈ 0.031. We also have $m - 1 \approx 2.781\,10^{-4} + 5.67\,10^{-3}/\lambda^2$, where λ is expressed in μm.

To a first approximation, scattering by clear air is isotropic. However, an accurate calculation of Rayleigh differential cross-section leads to

$$p_{\mathrm{Ray}}(\mu_{\mathrm{s}}) = \frac{3}{16\pi}(1+\mu_{\mathrm{s}}^2). \tag{3.61}$$

Equivalently, we have $\eta_0 = 1$ and $\eta_2 = 1/10$ with all other Legendre coefficients in (3.49) vanishing.

Lorenz-Mie Scattering by Cloud Droplets. Being too small (by definition) for their shapes to be affected by gravity and/or hydrodynamic flow around them, cloud water droplets are almost perfectly spherical. This means that Lorenz-Mie theory can accurately describe their absorption and scattering properties. The conventional representation of Lorenz-Mie extinction (total) and scattering cross-sections in the monodisperse case are

$$\mathtt{s}_{\mathrm{e,s}}(\lambda, r) = Q_{\mathrm{e,s}}(m_\lambda, 2\pi r/\lambda) \times \pi r^2 \tag{3.62}$$

where r is the droplet radius, and $2\pi r/\lambda$ is known as the "size parameter." The non-dimensional functions $Q_{\mathrm{e,s}}(x)$ are efficiency factors that also depend on wavelength through changes in the index of the real and imaginary parts of the refraction index of water m_λ. Absorption cross-section is obtained from $\mathtt{s}_{\mathrm{a}} = \mathtt{s}_{\mathrm{e}} - \mathtt{s}_{\mathrm{s}}$. A representation similar to (3.62) exists for the differential cross-section for scattering $\mathrm{d}\mathtt{s}_{\mathrm{s}}/\mathrm{d}\mathbf{\Omega}$ used to compute the phase function in (3.45).

For large $2\pi r/\lambda$ and no absorption, $Q_{\mathrm{e}} \approx Q_{\mathrm{s}}$ approaches 2. Recalling that droplet radii range from a few μm to a few tens of μm, this is not a bad approximation at non-absorbing wavelengths in the VIS/NIR spectrum. Cross-sections of scattering/absorbing spheres are complemented by empirical representations of polydisperse droplet populations $\mathrm{d}N(r)/\mathrm{d}r$, given typically in $\mathrm{cm}^{-3}\mu\mathrm{m}^{-1}$, to yield usable extinction-, scattering- and absorption coefficients:

$$\sigma_{\mathrm{s,a}}(\lambda) = \pi n \int\limits_{r_{\min}}^{r_{\max}} r^2 Q_{\mathrm{s,a}}(m_\lambda, 2\pi r/\lambda)\mathrm{d}\,\Pr(r), \tag{3.63}$$

where (total) droplet density n is the integral of $\mathrm{d}N(r)/\mathrm{d}r$ over all possible r values and $\mathrm{d}\,\Pr(r) = (\mathrm{d}N(r)/\mathrm{d}r) \times \mathrm{d}r/n$. In the approximation where $Q_{\mathrm{e}} = Q_{\mathrm{s}} \approx 2$, we have

$$\sigma = \sigma_{\mathrm{s}} \approx 2\pi \left\langle r^2 \right\rangle n, \tag{3.64}$$

as was already used in (3.37). Similar averaging over $\mathrm{d}\mathtt{s}_{\mathrm{s}}/\mathrm{d}\mathbf{\Omega}$ yields the Lorenz-Mie scattering phase function $p_{\mathrm{Mie}}(\mu_{\mathrm{s}})$ which the underlying EM theory naturally produces in terms of spherical harmonics.

Figure 3.9 shows, on the one hand, the natural outcome of Lorenz-Mie theory (values of the Legendre coefficients) in panel (a) and, on the other hand, the reconstruction of the phase function in angle space in panel (b). The droplet population is

the "C1" standard (Deirmendjian, 1969) and the wavelength is 1.064 μm. We note the relatively slow decay in Legendre coefficients. We also note the strong forward peak caused by diffraction; its width (in radians) is inversely proportional to the size parameter. In contrast with this inherently scalar or EM wave phenomenon, we also see a peak at the "rainbow" deflection angle that, for the most part, is explained by geometrical optics with one total internal reflection inside the droplet.

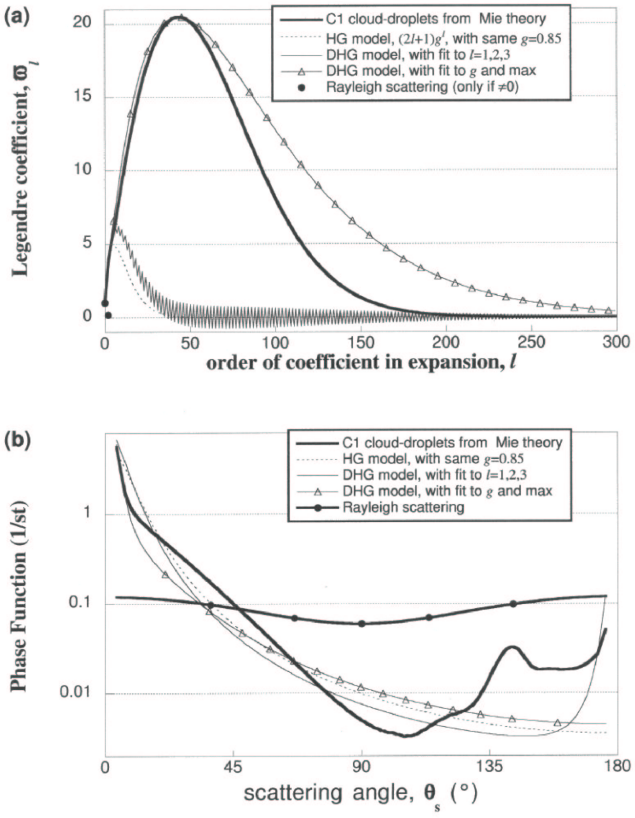

Fig. 3.9. Rayleigh (molecular) phase function and Lorenz- (cloud droplet) phase function with Henyey-Greenstein approximations. **(a)** Legendre coefficients in the $\omega_l = (2l+1)\eta_l$ representation that multiply the $P_l(\mu_s) \in [-1,+1]$. **(b)** Angular values. Notice the variation over 3+ orders-of-magnitude for the C1 phase function. As the scattering angle increases, we see: (1) the strong forward-scattering peak caused by diffraction at $\theta_s \lesssim 1/10$ rad and readily observed in the "silver lining" phenomenon; (2) the maximum causing the rainbow phenomenon at $\theta_s \approx 140\,\mathrm{deg}$; and (3) the backscattering peak responsible for the "glory" effect at θ_s close to $180\mathrm{deg}$, the anti-solar direction.

We have also plotted in Fig. 3.9 two approximations using the simple- and double HG models from (3.57) and (3.59) respectively. In the former case, we just set $g = 0.848$. In the later case, we can match the 2nd- and 3rd-order Legendre coefficients too; this leads to $g_{\rm f} = 0.879$, $g_{\rm b} = 0.9835$, and $f = 0.983$, with the result in Fig. 3.9b that the backscatter peak at $\theta_{\rm s} = \pi$ is captured on a relative scale. Alternatively, we can fit the height and position of the maximum in ω_l; this leads to $g_{\rm f} = 0.977$, $g_{\rm b} = -0.625$, and $f = 0.633$, with the result in Fig. 3.9b that the diffraction peak at $\theta_{\rm s} = 0$ is better reproduced by adding two forward H-Gs. There are of course other possibilities.

Scattering and Absorption by Non-Spherical Particles. Not all clouds are made of liquid droplets. Cirrus and mixed-phase clouds contain ice-particles with a myriad shapes. Some crystals inherit very regular geometry from the 6-fold symmetry induced by the hydrogen bond in ice; others are extremely random, and everything in between has been observed. It suffices to state here that scattering properties, especially phase functions, of distributions of large non-spherical particles are qualitatively different from Lorenz-Mie theoretical predictions using "equivalent sphere" assumptions. In the range of (very large) size-parameters relevant to solar and even to large extent thermal atmospheric RT, geometric optics has been used quite successfully to predict scattering properties of non-spherical particles (Liou, 2002). The volume by Mishchenko et al. (2000) is a recent and comprehensive source of information on single-scattering theory for non-spherical particles, ice crystals or other.

In the lower troposphere, aerosol particles play an important role in its optics and radiation budget. So do particulates injected by large volcanic eruptions into the swift circulations in the stratosphere. Because of its role in the microphysics and life-cycle of clouds, the climate community has developed a renewed interest in the anthropogenic component of the aerosol. In some regions/seasons, it is by far the dominant one with dramatic consequences on air quality as well as global and local climate (Ramanathan et al., 2002). Among man-made aerosol, black carbon is highly absorbing, hence very important for the solar radiation budget and how it is partitioned between the atmosphere and the surface. Black-carbon particles have notoriously convoluted shapes, best modeled as randomly aggregated fractal objects over a wide range of scales that includes the wavelength (at least in the early phases of the particle's life). Because these particles could dominate in nuclear winter scenarios, their scattering and absorption properties were computed quite a while ago by Berry and Percival (1986).

3.5 Propagation

We presented scattering as a random choice of new direction of propagation for the photon. After emission and between collisions (resulting in either a scattering or a final absorption) or escape, there is also an inherent randomness in photon propagation. We define here a few statistical quantities needed to characterize photon transport.

3.5.1 Photon Free-Path Distributions

From (3.32), but dropping the "0" subscripts for simplicity, we can derive *direct* transmission

$$T_{\rm dir}(s;\boldsymbol{x},\boldsymbol{\Omega}) = \exp[-\tau(s;\boldsymbol{x},\boldsymbol{\Omega})] = \Pr\{step \geq s|\boldsymbol{x},\boldsymbol{\Omega}\} \tag{3.65}$$

by taking the ratio $I_{\rm out}/I_{\rm in} = I(\cdot;s)/I(\cdot;0)$. This is the probability a photon does *not* suffer any kind of collision in an experiment over the *fixed* distance s, starting at $\boldsymbol{x}$ in direction $\boldsymbol{\Omega}$. Now think of the photon's free path or "step" to its next collision. As expressed above, $T_{\rm dir}(s;\boldsymbol{x},\boldsymbol{\Omega})$ is the probability that this random variable exceeds s. So, thinking now of s as the random step length, its PDF is defined by

$$p(s|\boldsymbol{x},\boldsymbol{\Omega})\mathrm{d}s = \mathrm{d}P(s|\boldsymbol{x},\boldsymbol{\Omega}) = \Pr\{s \leq step < s+\mathrm{d}s|\boldsymbol{x},\boldsymbol{\Omega}\}. \tag{3.66}$$

Using (3.65) and (3.30), this leads to

$$p(s|\boldsymbol{x},\boldsymbol{\Omega}) = \left(\frac{\mathrm{d}}{\mathrm{d}s}\right)P(s|\boldsymbol{x},\boldsymbol{\Omega}) = \sigma(\boldsymbol{x}+\boldsymbol{\Omega}s)\exp[-\tau(s;\boldsymbol{x},\boldsymbol{\Omega})]. \tag{3.67}$$

The above notation $p(\cdot)$ is not to be confused with the phase functions introduced in Sect. 3.4.1 above for volume scattering and Sect. 3.6.2 below for surface scattering (reflection). We note however that both free-path distributions and phase functions are PDFs that play closely interlaced roles in the photon transport process: here we move (propagate) photons to a new position while phase functions move them into a new direction (of propagation).

Consider the case of *uniform* extinction σ, the only quantity required in the problem at hand. The resulting free-path distribution is given by

$$p(s|\sigma) = \sigma \mathrm{e}^{-\sigma s}, \tag{3.68}$$

as follows directly from (3.67), or using Beer's exponential transmission law in (3.34).

3.5.2 Mean-Free-Path

A fundamental quantity in transport theory (for light quanta or any other type of particle) is the *mean free path* or "MFP"

$$\ell(\boldsymbol{x},\boldsymbol{\Omega}) = \mathcal{E}(s|\boldsymbol{x},\boldsymbol{\Omega}) = \int_0^\infty s\mathrm{d}P(s|\boldsymbol{x},\boldsymbol{\Omega}) \tag{3.69}$$

which, as indicated, will generally depend on the pair $\{\boldsymbol{x},\boldsymbol{\Omega}\}$ in the 3D case. Reconsidering the uniform-σ case in (3.68), we find

$$\ell(\sigma) = \mathcal{E}(s) = 1/\sigma. \tag{3.70}$$

So there is such a thing as *the* mean free path in homogeneous media, but not in 3D media. One can talk about $1/\sigma(\boldsymbol{x})$ as a *local* MFP in 3D media. However, at a given $\boldsymbol{x}$ it will only occasionally coincide with $\ell(\boldsymbol{x}, \boldsymbol{\Omega})$ in (3.69) for certain choices of $\boldsymbol{\Omega}$. We prefer to call this a 3D field of *pseudo*-MFP values. By averaging (3.69) over $\{\boldsymbol{x}, \boldsymbol{\Omega}\}$, on can define the *mean* mean free path, which is necessarily larger than the inverse of the mean extinction (e.g., Davis and Marshak, 2003).

Equation (3.70) provides us with a more descriptive interpretation of optical distance, at least for homogeneous media, as given in (3.33):

$$\tau = \sigma d = d/\ell, \tag{3.71}$$

is just physical distance d in units of MFPs. When d is equated with h, the thickness of (i.e., distance across) the media, we are looking at the ratio of the two fundamental scales in the RT problem. The solution of the problem will clearly reflect a different flavor of transport physics depending on whether τ is smaller or τ is larger than unity:

- if $\tau \ll 1$, photons will tend to "stream" (move ballistically along straight lines);
- if $\tau \gg 1$, photons will tend to "diffuse" (move along convoluted paths akin to random walks).

In 3D RT problems, there are regions where optical thickness is large and others where it is small, at least on a relative scale. Davis and Marshak (2001) show that this sets up horizontal fluxes in predictable patterns they recognize as "channeling" events (Cannon, 1970).

3.5.3 Other Moments of the Free-Path Distribution

Higher-order moments of the free-path distribution are also of interest:

$$\mathcal{E}(s^q|\boldsymbol{x}, \boldsymbol{\Omega}) = \int_0^\infty s^q \mathrm{d}P(s|\boldsymbol{x}, \boldsymbol{\Omega}). \tag{3.72}$$

Free-path moments of arbitrary order $q > -1$ can be computed from the exponential distribution in (3.68) for homogeneous media, and we find

$$\mathcal{E}(s^q) = \Gamma(q+1)/\sigma^q = \Gamma(q+1)\ell(\sigma)^q \tag{3.73}$$

where $\Gamma(\cdot)$ is Euler's Gamma function:

$$\Gamma(x) = \int_0^\infty t^{x-1}\mathrm{e}^{-t}\mathrm{d}t. \tag{3.74}$$

Recall that, for integer values, $\Gamma(n+1) = n!,\ n \geq 0$. So, in particular, the root-mean-square (RMS) free-path is

$$\sqrt{\mathcal{E}(s^2)} = \sqrt{2}/\sigma = \sqrt{2}\,\mathcal{E}(s). \tag{3.75}$$

It is larger than the MFP in (3.70), as required by Schwartz's inequality. Free-path variance $\mathcal{D}(s) = \mathcal{E}(s^2) - \mathcal{E}(s)^2$ is therefore equal to $\mathcal{E}(s)^2$, a characteristic of the exponential distribution. Davis and Marshak (2003) show that $\mathcal{E}(s^q) > \mathcal{E}(s)^q$ in general 3D media for any $q > 1$, implying that free-path distributions are always *wider* than the exponential one based on the MFP.

3.6 Sources

In this section, we introduce explicitly the dependence of all radiative quantities and most optical properties on wavelength λ or wavenumber $\nu = 1/\lambda$ (adopting spectroscopic usage) that has been implicit so far. Even if nothing else does, source terms will drive this dependence in atmospheric applications. A wide variety of sources are found in the bulk of optical media as well as on their boundaries. We call these *primary* sources. Furthermore, volume scattering and surface reflection are at once sinks and sources, depending on which beam one is talking about. We will call these *secondary* sources.

3.6.1 Volume Sources

General Definition. We return to Fig. 3.6 used already to define the extinction of I with no strict need for an incoming beam this time (i.e., $I = 0$ is a possibility); we focus however on the "+" sign in the exiting radiance. This describes a situation where photons are generated inside the sample volume, thus adding

$$\delta I_\nu \propto \delta s \tag{3.76}$$

to the existing population, if any. As usual, the proportionality constant has a name and an important role in RT theory. Define

$$Q_\nu(\boldsymbol{x}, \boldsymbol{\Omega}) = \lim_{\delta s \to 0} \frac{\delta I_\nu}{\delta s}, \text{ in } \mathrm{m}^{-3}\mathrm{s}^{-1}\mathrm{sr}^{-1}(\mathrm{cm}^{-1})^{-1} \text{ (or } \mathrm{W/m^3/sr/cm^{-1}}) \tag{3.77}$$

as the (volume) source term. [3] Two contrasting and important examples follow.

Solar Photon Injection. Rather than "incoming" at the upper boundary, we can use what we have learned about propagation and scattering in previous sections to model the "injection" of sunlight into the bulk of the medium after a first scattering or surface reflection; see Fig. 3.10. Note that in this case, the radiance field is split between the direct and diffuse components, and this source term feeds only the latter. We have

$$Q_{\odot\nu}(\boldsymbol{\Omega}_0; \boldsymbol{x}, \boldsymbol{\Omega}) = F_{0\nu}\ \exp[-\tau_\nu(\boldsymbol{x}_0(\boldsymbol{x}, \boldsymbol{\Omega}_0), \boldsymbol{x})]\, \sigma_\nu(\boldsymbol{x})\, \varpi_{0\nu}(\boldsymbol{x})\, p_\nu(\boldsymbol{x}, \boldsymbol{\Omega}_0 \to \boldsymbol{\Omega}) \tag{3.78}$$

[3] The reader will know from context how to distinguish the source term introduced here and the Lorenz-Mie efficiency factor $Q_{\mathrm{e,s,a}}$ introduced in Sect. 3.4.1.

where $F_{0\nu}$ is the spectral value of the solar constant and $\boldsymbol{x}_0(\boldsymbol{x}, \boldsymbol{\Omega}_0)$ is the point where the solar beam of interest starts at the TOA or cloud top. For a plane-parallel cloud $\{z \in \mathbb{R}^3 : 0 < z < h\}$ and solar rays coming in, as is often assumed, along the x-axis (negative-to-positive direction) we have $\boldsymbol{x}_0 = (x - (h - z)/\mu_0, y, h)^{\mathrm{T}}$ where $\mu_0 \in (0, 1]$ is the cosine of the sun angle. As similar expression as (3.78) can be written for a direct transmission through the atmosphere and a reflection of the lower boundary.

The relatively long expression in (3.78) is really just a sequence of probabilities. Given a solar $\{\boldsymbol{\Omega}_0, \nu\}$-photon impinging on the top of the cloudy layer, we have the following events in causal order:

- transmission from impact point $\boldsymbol{x}_0$ to $\boldsymbol{x}$;
- interception at point of interest $\boldsymbol{x}$;
- scattering (rather than absorption);
- scattering from solar beam direction $\boldsymbol{\Omega}_0$ into the beam of interest $\boldsymbol{\Omega}$.

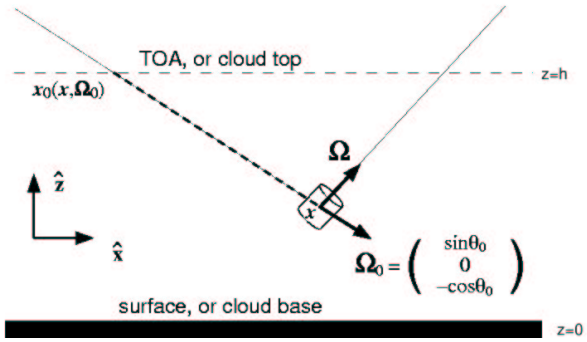

Fig. 3.10. Volume injection of solar flux in a plane-parallel medium.

Thermal Emission. In local thermal equilibrium (LTE), the rate of emission equals the rate of absorption (Kirchhoff's law). From there, we can write the source term for thermal emission:

$$Q_{\mathrm{T}\nu}(\boldsymbol{x}, \boldsymbol{\Omega}) = \sigma_{\mathrm{a}\nu}(\boldsymbol{x})\, B_\nu[T(\boldsymbol{x})],\ \forall \boldsymbol{\Omega}, \tag{3.79}$$

where $T(\boldsymbol{x})$ is the local absolute temperature and $B_\nu(T)$ is Planck's function.

We used these two examples of source term partially because of their contrasting mathematical expressions but also because of their importance in both remote sensing and climate applications. The Earth's climate system is essentially an engine that converts $Q_{\odot\nu}(\boldsymbol{\Omega}_0; \boldsymbol{x}, \boldsymbol{\Omega})$ as "fuel" into atmospheric, oceanic and all kinds of other motions, leaving $Q_{\mathrm{T}\nu}(\boldsymbol{x})$ as "exhaust." Notice that the solar photons intercepted by the Earth are high-energy and directed, hence low-entropy, while their

thermal counterparts emitted by the Earth are low-energy, hence more numerous, and isotropic. So they are carrying away the excess of entropy required to maintain the climate.

Multiple Scattering. Scattering, just like absorption, depletes a beam in terms of direct transmission. However, unlike absorption, the same scattering replenishes other beams. So it is productive to see scattering as a source of radiance. From (3.43), but in terms of scattered radiance, we have

$$\delta I_{\nu \mathrm{s}} \approx \delta F_{\nu \mathrm{s}} / \delta \boldsymbol{\Omega} \approx F_{0\nu} \sigma_{\mathrm{s}\nu}(\boldsymbol{x}) p_\nu(\boldsymbol{x}, \boldsymbol{\Omega}_0 \to \boldsymbol{\Omega}) \delta s. \tag{3.80}$$

Replacing F_0 by $I_\nu(\boldsymbol{x}, \boldsymbol{\Omega}_0)\mathrm{d}\boldsymbol{\Omega}_0$ and integrating over all incidence directions (denoted more traditionally as $\boldsymbol{\Omega}'$ rather than $\boldsymbol{\Omega}_0$), we obtain

$$S_\nu(\boldsymbol{x}, \boldsymbol{\Omega}) = \lim_{\delta s \to 0} \frac{\delta I_{\nu \mathrm{s}}}{\delta s} = \sigma_{\mathrm{s}\nu}(\boldsymbol{x}) \oint_{4\pi} p_\nu(\boldsymbol{x}, \boldsymbol{\Omega}' \to \boldsymbol{\Omega}) I_\nu(\boldsymbol{x}, \boldsymbol{\Omega}') \mathrm{d}\boldsymbol{\Omega}'. \tag{3.81}$$

This is known as the source *function* in multiple scattering theory. It is not to be confused with the (spectral) source *term* Q_ν in (3.77), especially since they have the same physical units.

3.6.2 Boundary Sources

General Definition. What if photons are emitted in direction $\boldsymbol{\Omega}$ from a boundary point $\boldsymbol{x}_{\mathrm{S}}$ with normal $\boldsymbol{n}(\boldsymbol{x}_{\mathrm{S}})$? We need a modified mathematical description of the photon creation at the surface of a medium, or at its interface with another medium. By reconsidering (3.76) and (3.77), we now have an addition to the existing photon population, if any, given by

$$\delta E_\nu \propto \nu \delta N_\nu \propto |\boldsymbol{n}(\boldsymbol{x}_{\mathrm{S}}) \bullet \boldsymbol{\Omega}| \delta A \delta t \delta \boldsymbol{\Omega} \tag{3.82}$$

where we have reverted to the elementary quantities used in Sect. 3.2 since there is no δs here to define a volume.

The proportionality constant again has a name and, furthermore, it has the same physical units as radiance. Define

$$f_\nu(\boldsymbol{x}_{\mathrm{S}}, \boldsymbol{\Omega}) = \lim_{\delta A, \delta t, \delta \boldsymbol{\Omega} \to 0} \frac{\delta N_\nu \text{ (or } \delta E_\nu)}{|\boldsymbol{n}(\boldsymbol{x}_{\mathrm{S}}) \bullet \boldsymbol{\Omega}| \delta A \delta t \delta \boldsymbol{\Omega}}, \text{ in } \mathrm{m}^{-2}\mathrm{s}^{-1}\mathrm{sr}^{-1} \text{ (or } \mathrm{W/m}^2\mathrm{sr}^{-1}) \tag{3.83}$$

as the surface source term. This field plays a critical role further on in the formulation of boundary conditions for the general 3D RT problem.

Example: Thermal Emission. By its definition, the spectral radiance coming from the surface of a *black* body at temperature T is (1) isotropic and (2) given by the Planck function $B_\nu(T)$. So $f(\boldsymbol{x}_{\mathrm{S}}, \boldsymbol{\Omega}) \equiv B_\nu[T(\boldsymbol{x}_{\mathrm{S}})]$ in (3.83). Most natural surfaces

are however not purely black: they are at least partially reflective in amounts that generally depend on wavenumber. In other words, they have specific spectral emissivities $\epsilon_\nu(\boldsymbol{x}_\mathrm{S})$, generally position-dependent, defined by

$$f_\nu(\boldsymbol{x}_\mathrm{S}, \boldsymbol{\Omega}) = \epsilon_\nu(\boldsymbol{x}_\mathrm{S}) B_\nu[T(\boldsymbol{x}_\mathrm{S})], \ \forall \boldsymbol{\Omega}. \tag{3.84}$$

By comparison of (3.84) above with (3.79) for bulk thermal emission, we see that (non-dimensional) emissivity is for surfaces what the absorption coefficient (in units of inverse length) is for volumes. This captures the fact that surface sources have the same units as radiance while volume sources are radiance "gained" per unit of length.

Surface emission is of course a powerful resource in thermal sensing of surface properties from aircraft or satellite. This exercise is however predicated on the detector- and/or algorithm-based ability for "$\epsilon - T$" separation, and the correction for atmospheric effects. Part of the "$\epsilon - T$" separation problem is that the "$\forall \boldsymbol{\Omega}$" in (3.84) is in fact an idealization and for even quite fine observation scales ϵ_ν is actually function of $\boldsymbol{\Omega}$ as well as of $\boldsymbol{x}_\mathrm{S}$. This non-thermodynamical dependence captures unresolved surface heterogeneity and roughness effects that can be modeled in full detail with 3D radiative transfer, as shown further on.

Bidirectional Reflectance Distribution Function, and Related Quantities. We now need to formulate mathematically what happens at the surface of a medium in the frequently encountered situation where it has a reflecting property. This is not a source of photons per se but, like the scattering process, it behaves as a sink for out-going beams ($\boldsymbol{\Omega} \bullet \boldsymbol{n}(\boldsymbol{x}_\mathrm{S}) \geq 0$) and a source for in-coming ones ($\boldsymbol{\Omega} \bullet \boldsymbol{n}(\boldsymbol{x}_\mathrm{S}) < 0$). The classic paper on textured surface radiometry is by Minnaert (1941) while the standard reference for definitions and nomenclature for reflecting surfaces is by Nicodemus et al. (1977).

The local bidirectional reflectance distribution function (or "BRDF") is defined as the ratio of reflected radiance per unit of incoming irradiance at a surface point $\boldsymbol{x}_\mathrm{S} \in \partial\mathrm{M}$. Consider a small area δA around $\boldsymbol{x}_\mathrm{S}$ and an element of solid angle $\delta\boldsymbol{\Omega}$ around the direction $\boldsymbol{\Omega}$ into which the photons are reflected. An amount δE_ref of radiant energy is detected, and we define the BRDF as:

$$\rho_\nu(\boldsymbol{x}_\mathrm{S}, \boldsymbol{\Omega}_0 \rightarrow \boldsymbol{\Omega}) = \lim_{\delta A, \delta t, \delta\boldsymbol{\Omega} \rightarrow 0} \frac{\delta E_\mathrm{ref}}{\mu_0 F_{0\nu} \delta A \delta t \delta\boldsymbol{\Omega}} = \frac{I_\nu(\boldsymbol{x}_\mathrm{S}, \boldsymbol{\Omega})}{\mu_0 F_{0\nu}}, \text{ in sr}^{-1} \tag{3.85}$$

where $F_{0\nu}$ is the incoming collimated flux and $\mu_0 = |\boldsymbol{n}(\boldsymbol{x}_\mathrm{S}) \bullet \boldsymbol{\Omega}_0|$ the associated cosine of the zenith angle. Assuming there are no sub-surface radiative fluxes, the BRDF obeys Helmholtz's reciprocity relation: $\rho_\nu(\boldsymbol{x}_\mathrm{S}, \boldsymbol{\Omega}_0 \rightarrow \boldsymbol{\Omega}) = \rho_\nu(\boldsymbol{x}_\mathrm{S}, -\boldsymbol{\Omega} \rightarrow -\boldsymbol{\Omega}_0)$, cf. Sect. 3.10.3.

In plane-parallel geometry $\boldsymbol{n}(\boldsymbol{x}_\mathrm{S}) = \hat{\mathbf{z}}$ and the BRF (bi-directional reflectance factor) in (3.19) is a non-dimensionalized BRDF for a specific reflection event, $\pi\rho_\nu(\boldsymbol{x}_\mathrm{S}, \boldsymbol{\Omega}_0 \rightarrow \hat{\mathbf{z}})$. The BRF can of course be defined for any reflection angle, not just towards the zenith:

$$\mathrm{BRF} = \frac{\pi I_\nu(\boldsymbol{x}_\mathrm{S}, \boldsymbol{\Omega})}{\mu_0 F_{0\nu}} = \pi\rho_\nu(\boldsymbol{x}_\mathrm{S}, \boldsymbol{\Omega}_0 \rightarrow \boldsymbol{\Omega}). \tag{3.86}$$

This quantity is becoming a standard product for a new generation of global imaging spectro-radiometers, such as the Polarization and Directionality of the Earth's Reflectance Instrument (POLDER), the Along-Track Scanning Radiometer-2 (ATSR-2), and the Multiangle Imaging Radiometer Spectro-Radiometer (MISR). These instruments have acquired and continue to acquire this angular signature of reflected radiation from individual scenes, with spatial resolutions ranging from several kilometers to a few meters Diner et al. (1999).

Spectral *planar* albedo α_ν, as the ratio of outgoing- to incoming-fluxes, is a non-dimensional quantity:

$$\alpha_\nu(\boldsymbol{x}_\mathrm{S}, \boldsymbol{\Omega}_0) = \int\limits_{\boldsymbol{n}(\boldsymbol{x}_\mathrm{S})\bullet\boldsymbol{\Omega}>0} \boldsymbol{n}(\boldsymbol{x}_\mathrm{S}) \bullet \boldsymbol{\Omega}\, \rho_\nu(\boldsymbol{x}_\mathrm{S}, \boldsymbol{\Omega}_0 \rightarrow \boldsymbol{\Omega})\, \mathrm{d}\boldsymbol{\Omega}, \tag{3.87}$$

where $\boldsymbol{n}(\boldsymbol{x}_\mathrm{S})\bullet\boldsymbol{\Omega} = \mu$ if the surface is horizontal ($\boldsymbol{n}(\boldsymbol{x}_\mathrm{S}) \equiv \hat{\boldsymbol{z}}$). For locally Lambertian surfaces, the BRF and BRDF are independent of both angles: $\rho_\nu(\boldsymbol{x}_\mathrm{S}, \boldsymbol{\Omega}_0 \rightarrow \boldsymbol{\Omega}) \equiv \alpha_\nu(\boldsymbol{x}_\mathrm{S})/\pi$. This makes the quantity $\pi\rho_\nu(\cdots)$ easy to interpret in the applications as the (non-dimensional) albedo a Lambertian reflector would have to possess in order to yield the same radiance under the same illumination conditions. For actual Lambertian surfaces, α_ν is of course independent of $\boldsymbol{\Omega}$.

Spectral *spherical* albedo a_ν is obtained by averaging the planar albedo over the hemisphere of possible irradiance angles weighted by $|\mu_0|$, as required by incoming photon flux conservation:

$$a_\nu(\boldsymbol{x}_\mathrm{S}) = \frac{1}{\pi} \int\limits_{\boldsymbol{n}(\boldsymbol{x}_\mathrm{S})\bullet\boldsymbol{\Omega}_0<0} |\boldsymbol{n}(\boldsymbol{x}_\mathrm{S}) \bullet \boldsymbol{\Omega}_0| \alpha_\nu(\boldsymbol{x}_\mathrm{S}, \boldsymbol{\Omega}_0) \mathrm{d}\boldsymbol{\Omega}_0, \tag{3.88}$$

where $\boldsymbol{n}(\boldsymbol{x}_\mathrm{S}) \bullet \boldsymbol{\Omega}_0 = \mu_0$ if the surface is horizontal. This is the ratio of reflected to incoming fluxes for an isotropic sky; equivalently, this is the overall albedo of a planet uniformly covered with the given planar albedo. Lambertian surfaces yield $a_\nu = \alpha_\nu$ which, in this case, is independent of the in-coming direction.

Kirchhoff's law of detailed balance (conservation) of radiation during surface-environment exchanges under local thermodynamical equilibrium tells us that $\epsilon_\nu(\boldsymbol{x}_\mathrm{S})$ defined in (3.84) is given by

$$\epsilon_\nu(\boldsymbol{x}_\mathrm{S}) = 1 - a_\nu(\boldsymbol{x}_\mathrm{S}) \tag{3.89}$$

for all ν in the thermal spectrum, and we will show in the next Section that strict thermal equilibrium precludes directional effects. "Black" bodies indeed get their name from the requirement that $a_\nu \equiv 0$ (absolutely no reflection) to obtain $\epsilon_\nu = 1$ for all ν. But, even for non-black materials, this applies only in the case of ideal micro-uniform surfaces. Natural surfaces have texture (roughness and heterogeneity) that is captured at scales of interest in remote sensing, even at the finest resolution, by assuming a local/directional surface emissivity model with $\epsilon_\nu(\boldsymbol{x}_\mathrm{S}, \boldsymbol{\Omega})$ for $\boldsymbol{n}(\boldsymbol{x}_\mathrm{S}) \bullet \boldsymbol{\Omega} > 0$. We can equate this with $1 - \alpha_\nu(\boldsymbol{x}_\mathrm{S}, -\boldsymbol{\Omega})$ in (3.87) by invoking reciprocity (exchanging the places of $\boldsymbol{\Omega}_0$ and $\boldsymbol{\Omega}$ while changing their signs). The

surface will reflect (hence not emit) a fraction $\alpha_\nu(\boldsymbol{x}_\mathrm{S}, -\boldsymbol{\Omega})$ of the incoming flux into direction $-\boldsymbol{\Omega}$ when subjected to an isotropic diffuse illumination, which is what a thermally-balanced environment would look like to the surface.

Reflection is sometimes called "surface scattering" and we can indeed draw a fruitful analogy here with the scattering phase function presented in Sect. 3.4.1, and then used in Sect. 3.6.1, for an elementary *volume*. We can similarly define a phase function for *surface* reflection or scattering using

$$I_\nu(\boldsymbol{x}_\mathrm{S}, \boldsymbol{\Omega}) = \alpha_\nu(\boldsymbol{x}_\mathrm{S}, \boldsymbol{\Omega}) \int\limits_{\boldsymbol{n}(\boldsymbol{x}_\mathrm{S})\bullet\boldsymbol{\Omega}'<0} p_{\mathrm{S}\nu}(\boldsymbol{x}_\mathrm{S}, \boldsymbol{\Omega}' \to \boldsymbol{\Omega}) I(\vec{x}, 0, \boldsymbol{\Omega}') \mathrm{d}\boldsymbol{\Omega}', \qquad (3.90)$$

for any $\boldsymbol{\Omega}$ such that $\boldsymbol{n}(\boldsymbol{x}_\mathrm{S}) \bullet \boldsymbol{\Omega} > 0$. Notice how $\alpha_\nu(\boldsymbol{x}_\mathrm{S}, \boldsymbol{\Omega})$ plays the role of the scattering probability $\sigma_{\mathrm{s}\nu}(\boldsymbol{x})$ in (3.81) or, better still, the non-dimensional single-scattering albedo $\varpi_{0\nu}$ since $\sigma_{\mathrm{s}\nu} = \varpi_{0\nu}\sigma_{\mathrm{e}\nu}$. Like scattering phase functions and BRDFs, $p_{\mathrm{S}\nu}(\boldsymbol{x}_\mathrm{S}, \boldsymbol{\Omega}' \to \boldsymbol{\Omega})$ is expressed in sr^{-1}. Comparing this definition with (3.85)-(3.87), we see that

$$p_{\mathrm{S}\nu}(\boldsymbol{x}_\mathrm{S}, \boldsymbol{\Omega}' \to \boldsymbol{\Omega}) = |\boldsymbol{n}(\boldsymbol{x}_\mathrm{S}) \bullet \boldsymbol{\Omega}'| \rho_\nu(\boldsymbol{x}_\mathrm{S}, \boldsymbol{\Omega}' \to \boldsymbol{\Omega}) / \alpha_\nu(\boldsymbol{x}_\mathrm{S}, \boldsymbol{\Omega}). \qquad (3.91)$$

To conserve fluxes, the integral of $p_{\mathrm{S}\nu}(\boldsymbol{x}_\mathrm{S}, \boldsymbol{\Omega}' \to \boldsymbol{\Omega})$ over the lower ($'$ed) hemisphere is required to be unity.

For illustration purposes, consider two extreme types of reflecting surface that we will assume uniform and horizontal for simplicity:

- Lambertian (diffuse, isotropic) reflection illustrated on the r.-h. side of Fig. 3.11b; this leads to
$$p_{\mathrm{S}\nu}(\boldsymbol{\Omega}' \to \boldsymbol{\Omega}) = |\mu'|/\pi. \qquad (3.92)$$
- Specular (metallic, mirror) reflection as on l.-h. side of Fig. 3.11b; this yields
$$p_{\mathrm{S}\nu}(\boldsymbol{\Omega}' \to \boldsymbol{\Omega}) = \delta(\mu' + \mu)\delta(\varphi' - \varphi). \qquad (3.93)$$

Steady Irradiance in Plane-Parallel Geometry: Collimated or Diffuse, Uniform or Localized. We introduce here the short-hand $\vec{x} = (x, y)^\mathrm{T}$ for Cartesian coordinates, hence

$$\boldsymbol{x} = \begin{pmatrix} \vec{x} \\ z \end{pmatrix}. \qquad (3.94)$$

The boundaries of the plane-parallel (or "slab") medium are set at $z = 0$ and $z = h$ and they can act as radiation sources.

We need to describe how the Sun excites incoming radiance at a cloud top, a collimated but spatially uniform irradiance, cf. Fig. 3.11a. Mathematically, we have

$$\left\{ \begin{array}{ll} I_\nu(\vec{x}, h, \boldsymbol{\Omega}) = F_{0\nu}\delta(\boldsymbol{\Omega} - \boldsymbol{\Omega}_0), & \mu < 0 \\ I_\nu(\vec{x}, 0, \boldsymbol{\Omega}) = 0, & \mu > 0 \end{array} \right\}, \forall \vec{x}. \qquad (3.95)$$

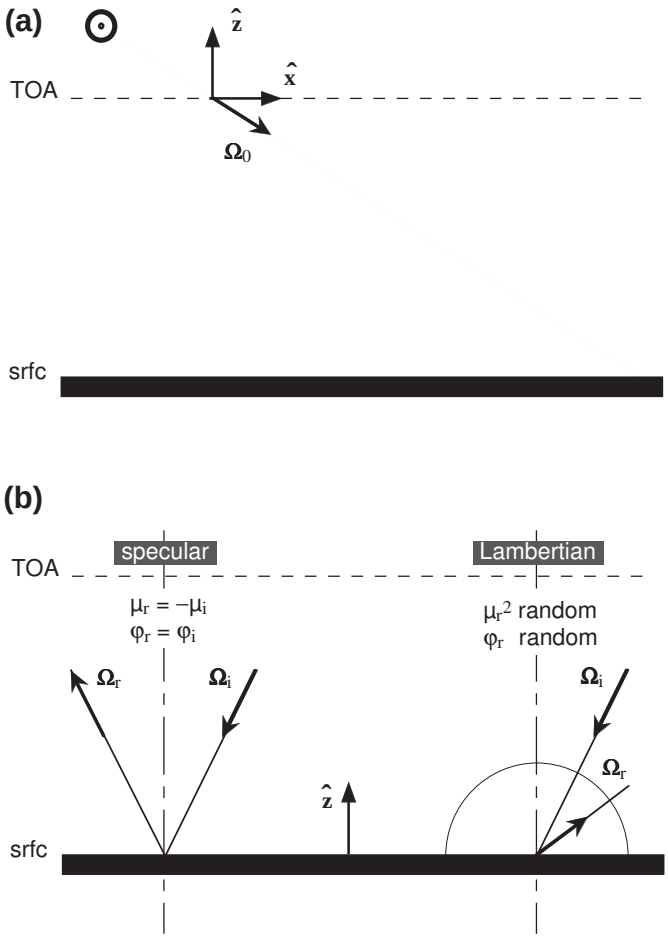

Fig. 3.11. Boundary sources for an infinite slab. **(a)** Irradiance by a (solar) collimated beam from above. **(b)** Reflective surface below, either specular (l.-h. side) or Lambertian (r.-h. side). Subscripts "i" designate the incident beams, and "r" for their reflected counterparts. Note that to generate random vectors uniformly distributed (isotropic) in the upper hemisphere, one exploits (3.92): the probability measure in φ is uniform over $[0, 2\pi)$ while in μ it is $2\mu d\mu = d\mu^2$ over $[0, 1]$.

This assumes that $I_\nu(\boldsymbol{x}, \boldsymbol{\Omega})$ is the *total* radiance field (not separated into diffuse and direct components). Note that the boundaries are still radiation sinks for out-going beams, as described in Sect. 3.3.

Another useful example is steady isotropic illumination from a localized source below at $\vec{x}_0$:

$$\begin{cases} I_\nu(\vec{x}, h, \mathbf{\Omega}) = 0, & \mu < 0, \forall \vec{x} \\ I_\nu(\vec{x}, 0, \mathbf{\Omega}) = F_{0\nu}\delta(\vec{x} - \vec{x}_0)\mu/\pi, & \mu > 0 \end{cases} \tag{3.96}$$

where, again, the boundaries are sinks for out-going radiation. We will see such sources in the theory of RT Green functions covered Sect. 3.10.1.

The interested reader can easily write descriptions for other combinations of boundary source properties: uniform and diffuse, localized and collimated, possibly moved to the opposite side.

Reflection in Plane-Parallel Geometry: Lambertian, Specular, or Otherwise. What happens at the *lower* boundary of a plane-parallel medium? Using the surface phase function in (3.90)-(3.91), we define

$$\begin{cases} I_\nu(\vec{x}, h, \mathbf{\Omega}) = 0, & \mu < 0, \forall \vec{x} \\ I_\nu(\vec{x}, 0, \mathbf{\Omega}) = \alpha_\nu(\boldsymbol{x}_\mathrm{S}, \mathbf{\Omega}) \int_{\mu' < 0} p_{\mathrm{S}\nu}(\vec{x}, \mathbf{\Omega}' \to \mathbf{\Omega}) I(\vec{x}, 0, \mathbf{\Omega}') \mathrm{d}\mathbf{\Omega}', & \mu > 0 \end{cases} . \tag{3.97}$$

Real surfaces are of course not pure cases of Lambertian or specular behavior used until now as examples. Combinations are possible and other types of BRDF can be introduced. A popular 3-parameter representation of the BRDF for many natural surfaces is given by Rahman et al. (1993).

Finally, the linearity of RT with respect to sources can be invoked to break down complex problems with boundary and/or volume sources and one or more reflecting surfaces into a non-trivial combination of problems with purely absorbing boundaries and others with properly chosen boundary sources. More details are provided in Sect. 3.10.1 and in Chap. ???.

3.7 Local Balance

Looking back, we have studied how photons are created (Q), transported (σ and $p(\mathbf{\Omega}' \to \mathbf{\Omega})$), destroyed ($\sigma_\mathrm{a}$) or lost ($\partial$M), and finally detected ($I, J, and \boldsymbol{F} \bullet \boldsymbol{n}$). We collect here the positive and negative contributions to the photon population in an elementary volume and thus obtain at last the RT equation or "RTE," in its basic integro-differential form. We then derive the continuity equation for radiant energy and pause for a few thoughts on radiative transfer in the greater scheme of things.

3.7.1 Integro-Differential Radiative Transfer Equation

Returning once more to Fig. 3.6, we see that position along the beam $\{\boldsymbol{x}, \mathbf{\Omega}\}$ can be represented in general as $\boldsymbol{x} + \mathbf{\Omega}s$ and positions infinitesimally close to $\boldsymbol{x}$ by $\boldsymbol{x} + \mathbf{\Omega}\delta s$ where $\delta s \to 0$. Therefore,

$$\lim_{\delta s \to 0} \frac{\delta I}{\delta s} = \mathbf{\Omega} \bullet \nabla I \tag{3.98}$$

in notations independent of any particular coordinate-system. This operator is known as a directional (or advective) derivative and quantifies change in $I(\boldsymbol{x}, \boldsymbol{\Omega})$ near $\boldsymbol{x}$ in direction $\boldsymbol{\Omega}$. In Cartesian coordinates, we have

$$\nabla = \left(\frac{\partial}{\partial x}, \frac{\partial}{\partial y}, \frac{\partial}{\partial z}\right)^{\mathrm{T}} = \begin{pmatrix} \partial_x \\ \partial_y \\ \partial_z \end{pmatrix}, \tag{3.99}$$

hence

$$\boldsymbol{\Omega} \bullet \nabla = \boldsymbol{\Omega}_x \frac{\partial}{\partial x} + \boldsymbol{\Omega}_y \frac{\partial}{\partial y} + \boldsymbol{\Omega}_z \frac{\partial}{\partial z}\,. \tag{3.100}$$

The steady-state radiative transfer equation (RTE) is

$$\boldsymbol{\Omega} \bullet \nabla I = -\sigma(\boldsymbol{x}) I(\boldsymbol{x}, \boldsymbol{\Omega}) + S(\boldsymbol{x}, \boldsymbol{\Omega}) + Q(\boldsymbol{x}, \boldsymbol{\Omega}) \tag{3.101}$$

where we have collected the r.-h. terms from Sections 3.3.3, 3.6.1 and 3.6.1 respectively, and given them the appropriate sign ($+$ for a gain, $-$ for a loss). Dependence on frequency ν is again made implicit since it is omnipresent. Note that we retrieve $I = constant$ along the beam if $\sigma \equiv 0$ which, in turn, implies $S \equiv 0$ as well as $Q \equiv 0$, at least for the common sources in the atmosphere described in the previous section.

Grouping all terms dependent on radiance I, we can write the RTE formally as

$$LI = Q \tag{3.102}$$

where

$$L = \boldsymbol{\Omega} \bullet \nabla + \sigma(\boldsymbol{x}) - \sigma_{\mathrm{s}}(\boldsymbol{x}) \oint_{4\pi} p(\boldsymbol{x}, \boldsymbol{\Omega}' \rightarrow \boldsymbol{\Omega})[\cdot]\mathrm{d}\boldsymbol{\Omega}' \tag{3.103}$$

is the integro-differential *linear* transport operator. The mathematical structure of the RTE is that of an infinite system of *coupled* 1st-order partial differential equations (PDEs) parameterized by $\boldsymbol{\Omega} \in \Xi$. The next chapter is entirely devoted to methods of numerical solution of the RTE complemented with boundary conditions to be described in the next Section.

When the phase function is azimuthally symmetric, it is often helpful to combine the two last terms of L into a single integral operator

$$L = \boldsymbol{\Omega} \bullet \nabla + \sigma(\boldsymbol{x}) \oint_{4\pi} \{\delta(\boldsymbol{\Omega}' - \boldsymbol{\Omega}) - \varpi_0(\boldsymbol{x}) p(\boldsymbol{x}, \boldsymbol{\Omega}' \bullet \boldsymbol{\Omega})\}[\cdot]\mathrm{d}\boldsymbol{\Omega}' \tag{3.104}$$

Both the "delta-M rescaling" used in spherical harmonics (Wiscombe, 1977) and the "maximum cross-section" method used in Monte Carlo (Marchuk et al., 1980) exploit this operator identity. These tricks are both invoked in the next chapter to improve numerical accuracy and/or computational efficiency. The angular kernel in the above equation has Legendre coefficients $1 - \varpi_0(\boldsymbol{x})\eta_l(\boldsymbol{x})$, $l \geq 0$, since those of a Dirac δ (phase function) centered on $\theta = 0$ are all unity in (3.50). A simple way to see this is to set $g = 1$ for the HG phase function in (3.58).

Consider the case where volume sources vanish ($Q \equiv 0$), and volume sinks also vanish ($\sigma = \sigma_s$, scattering is conservative). It is interesting to notice that it is the *non-isotropic* part of the radiance field that drives the spatial gradients. Indeed, if the radiance field I is independent of $\mathbf{\Omega}$, then the two last terms in (3.103) cancel, as does the r.-h. side of (3.102). So the directional gradients vanish identically. Conversely, if the directional gradients vanish, then I is a fixed point of the angular transform $I(\mathbf{\Omega}) \mapsto \oint_{4\pi} p(\mathbf{\Omega}' \to \mathbf{\Omega}) I(\mathbf{\Omega}') \mathrm{d}\mathbf{\Omega}'$ for *any* $\mathbf{\Omega}$; equivalently, it is in the null space of the angular integral transformation in (3.104). If $p(\mathbf{\Omega}' \to \mathbf{\Omega})$ is not $\delta(\mathbf{\Omega}' - \mathbf{\Omega})$, this implies that I is isotropic (independent of $\mathbf{\Omega}$).

As another example of this two-way connection between spatial gradients and non-isotropic radiance fields (hence net fluxes), consider *exact* thermodynamical equilibrium (TE), i.e., uniform temperature T. In this case, $I_\nu \equiv B_\nu(T)$ where we have restored the dependence on ν explicitly. Moreover, $Q_\nu = \sigma_{a\nu} B_\nu(T)$ and the isotropic radiance yields $S = \sigma_{s\nu} J_\nu / 4\pi = \sigma_{s\nu} B_\nu$. So, as expected, gradients vanish, and the RTE reduces to the identity $0 = \sigma_\nu (I_\nu - B_\nu)$ for any single-scattering albedo $\varpi_0 = \sigma_{s\nu}/\sigma_\nu$ and phase function under the important condition that $\sigma_\nu \neq 0$ (i.e., non-transparent matter is present). In *local* thermal equilibrium (LTE), we only require have $Q_\nu(\boldsymbol{x}) = \sigma_{a\nu} B_\nu(T(\boldsymbol{x}))$; so the gradients in T will generate an anisotropy in $I(\boldsymbol{x}, \mathbf{\Omega})$, and the fluctuations of $I(\boldsymbol{x}, \mathbf{\Omega})$ will not follow those of $B_\nu(T(\boldsymbol{x})$ exactly.

In summary, radiation transport per se results from a intricate balance of spatial and angular variability in $I(\boldsymbol{x}, \mathbf{\Omega})$ as controlled by the RTE.

3.7.2 Radiant Energy Conservation and Local Heating/Cooling Rates

By integrating (3.101) over all possible directions, we obtain an expression for the conservation of (as well as conversion to/from) radiant energy, irrespective of the direction it is traveling in. Explicitly, using definitions from Sect. 3.2.3, we have

$$\nabla \bullet \boldsymbol{F} = -\sigma_a(\boldsymbol{x}) J(\boldsymbol{x}) + q(\boldsymbol{x}) \tag{3.105}$$

where

$$\begin{aligned} q(\boldsymbol{x}) &= \oint_{4\pi} Q(\boldsymbol{x}, \mathbf{\Omega}) \mathrm{d}\mathbf{\Omega} \\ &= \begin{cases} 4\pi \sigma_a(\boldsymbol{x}) B_\nu(T(\boldsymbol{x})), & \text{for thermal emission} \\ \sigma_s(\boldsymbol{x}) \exp[-\tau(\boldsymbol{x}_0(\boldsymbol{x}, \mathbf{\Omega}_0), \boldsymbol{x})] F_0, & \text{for solar-beam injection} \end{cases} . \end{aligned} \tag{3.106}$$

Also, if $\{J, \boldsymbol{F}\}$ are only modeling the diffuse field, i.e., solar flux injection is modeled with $Q(\boldsymbol{x}, \mathbf{\Omega})$, then another term is needed to capture the energy absorbed from the directly transmitted beam. By direct evaluation of $J_{\mathrm{dir}}(\boldsymbol{x})$, we have

$$\nabla \bullet \boldsymbol{F}_{\mathrm{dir}} = -\sigma_a(\boldsymbol{x}) \exp[-\tau(\boldsymbol{x}_0(\boldsymbol{x}, \mathbf{\Omega}_0), \boldsymbol{x})] F_0. \tag{3.107}$$

There is a practical meaning for total radiative flux divergence in the computation of absorptance A in (3.26) for the source-free case and in the local energy

conservation law in (3.105): conversion to and from thermal energy. In other words, we get:

- cooling if $\nabla \bullet \boldsymbol{F} > 0$ as, e.g., in the LTE problem when $J(\boldsymbol{x}) < 4\pi B_\nu(T(\boldsymbol{x}))$ in (3.105)-(3.106); and
- heating if $\nabla \bullet \boldsymbol{F} < 0$ as, e.g., for $\boldsymbol{F}_{\mathrm{dir}}$ in (3.107).

The algebraically-valued *heating* rate is given by

$$\frac{\mathrm{d}T}{\mathrm{d}t} = \frac{1}{\rho C_{\mathrm{p}}}(-\nabla \bullet \boldsymbol{F}), \text{ in K/s (or } \times 3600 \text{ K/hr, or } \times 86400 \text{ K/day)} \qquad (3.108)$$

where ρ is the ambient mass density and C_{p} is the specific heat at constant pressure.

The heating/cooling rate in (3.108) is usually computed after full spectral integration, and only makes real physical sense as a time change in kinetic temperature if all non-radiative contributions to the local energy budget are included. However, it is conventional in climate science at least to divide $\mathrm{d}T/\mathrm{d}t$ into "shortwave" (solar) and "longwave" (thermal, terrestrial) components. In principle, one can preserve all the spectral information by leaving the "specific" /cm^{-1} units in F_ν and in B_ν (or the /μm units in F_λ and B_λ); these units will carry over to $(-\nabla \bullet \boldsymbol{F})$ and $\mathrm{d}T/\mathrm{d}t$. In practice, the simpler r.-h. side(s) of (3.105) (and of (3.107), as required) is (are) of course used to compute the flux divergence field(s) in (3.108).

The local rate of deposition of radiant energy, $(-\nabla \bullet \boldsymbol{F}) = \sigma_{\mathrm{a}}(\boldsymbol{x})J(\boldsymbol{x})$ in the absence of bulk sources, is used in (3.108) for a concern in climate or cloud-system dynamics. There are other important applications, especially in photochemistry where some judicious spectral sampling and integration is implied: ozone production, chlorophyll activity, etc. In vegetation remote sensing, it is commonly known as "FPAR," fraction of photosynthetically available radiation.

3.7.3 A Few Thoughts on Climate, Observations, and Beyond

At this point, we are about midway through the chapter and we have finally juxtaposed the two most fundamental elements of climate physics: solar heating and IR cooling in the Earth's thin but vital atmosphere. This is essentially all climate modelers want from RT, $-\nabla \bullet \boldsymbol{F}_\nu$ in (3.108) integrated across the solar-through-thermal spectrum. This radiative quantity — along with a few other energy exchange terms that the first law of thermodynamics tells us to look at — will tell the model(er)s what happens next in the evolution of climate system or some portion thereof, maybe a single cloud or a plant stand. This energy budget is assessed at the smallest spatial and temporal scales the model(er)s can or want to resolve. In turn, the climate system dynamics will modify the scenario given to the resident RT problem-solver: the changing temperature T appears in the thermal source term, the solar source $\mu_0 F_0$ is modulated by the diurnal cycle (shutting off completely at night), and the various density fields that determine the absorption and scattering properties in the RTE will also evolve. We are therefore trapped in an endless feed-back loop. There are many tools used in the difficult task of creating new knowledge about the climate system

in which we live. Modeling is one way, which computers have enhanced considerably over the past decades. Remote observations (radiance fields sampled in space, time, and across the EM spectrum) are another that has been considerably enhanced, at least in shear volume, by satellite technology.

This seems to be a good time to take a short pause from the science of radiative transfer and engage in some more lofty thoughts. It is interesting to note that when we finally touch the essence of a physical science like RT, we find principles that been articulated very clearly in a very different era and in an altogether different culture. Looking at Eq. (3.105) as would Capra (1991), we see the interaction of Brahma-the-Creator (q), of Vishnu-the-Preserver ($\nabla \bullet \boldsymbol{F}$), and of Shiva-the-Destroyer ($-\sigma_{\mathrm{a}} J$). This metaphor based on the core trinity from the Hindu pantheon applies even better to our deeper formulation of the RTE, augmented for the circumstances with possibly inelastic collisions: $L_\nu \, I_\nu \; = \; Q_\nu$ (Brahma, Creation), where I_ν is the full spectral range of an ever-moving pool of radiant energy (karma) and $L_\nu \; = \; \boldsymbol{\Omega} \bullet \nabla[\cdot]$ (Vishnu, Preservation) $+ \sigma_\nu[\cdot]$ (Shiva, Destruction) $- \sigma_{\mathrm{s}\nu} \int \oint p(\nu', \boldsymbol{\Omega}' \rightarrow \nu, \boldsymbol{\Omega})[\cdot] \mathrm{d}\nu' \mathrm{d}\boldsymbol{\Omega}'$ (again Shiva, who is also worshiped as the God of Transformation). As noted earlier in this section, Lord Shiva's Dance (intertwined processes of extinction/propagation and scattering/reflection) is what makes radiative transfer so interesting, and quite challenging in 3D.

It fascinating to see that we have a continuity equation in (3.105) that uses $J_\nu(\boldsymbol{x})$, the simplest radiation transport quantity that is what ultimately counts for the *material* universe, and that it derives from the full 3D radiative transfer equation in (3.102)-(3.103) for $I_\nu(\boldsymbol{x}, \boldsymbol{\Omega})$, the more subtle quantity that feeds our insatiable need to explore the universe. This exploration calls for all sorts of instruments that basically extend our senses. [4] The signals these instruments produce are ultimately distilled into new *knowledge*, often with the help of sophisticated inverse RT theory. By any standard, this is a more elevated plane than the physical one. When humans gain knowledge, they eventually take some *action*. This can be good or bad for their environment at large, including fellow human beings. As scientists, we stop at that threshold. As RT experts, it is our hope that judgment error can minimized by better estimations of $J(\boldsymbol{x})$ in complex multi-physics models that support far-reaching decisions, and by better physics-based interpretations of $I_\nu(\boldsymbol{x}, \boldsymbol{\Omega})$.

3.8 Global Balance

We cover the general boundary conditions (BCs) that are needed, beyond the RTE, to specify completely the radiance field $I(\boldsymbol{x}, \boldsymbol{\Omega})$. Our commitment to 3D RT requires us to consider non-plane-parallel media, that may or may not be internally homogeneous, in some detail. A natural and interesting counterpoint to BCs are "escaping" boundary fields because, on the one hand, they are all that can be observed remotely

[4] In Earth/planet observation as well as astronomy, "pixels" are in principle scanned by varying $\boldsymbol{\Omega}$ *from* the observer's position $\boldsymbol{x}_m athrmobs$ in space; often $Omvec$ is in a very small subregion of direction-space Ξ. In this case, it is convenient to think of $\boldsymbol{\Omega}$ as the constant direction *towards* the observer while $\boldsymbol{x}_m athrmpix$ scans the pixels in the image.

(a task for radiances) and, on the other hand, they control the radiation budget of the medium (a task for fluxes). Finally, we derive the *formal* solution of the RTE and the two widely-used integral formulations of the RTE (with BCs necessarily included).

3.8.1 Boundary Conditions

A complication arises in prescribing BCs if the medium M, defined as the domain where extinction $\sigma(\boldsymbol{x})$ is strictly positive, is not convex. That is because of re-entering rays, and we want to be able to say that we know we radiation is going *into* the medium a priori but generally do not know what is coming *out* of it. This issue is basically geometrical and is best dealt with simply by allowing for vanishing extinction $\sigma(\boldsymbol{x})$ and extending the definition of M to its "convex hull." That is what becomes of M if it is covered by an imaginary sheet of rubber. For instance, a doughnut-shaped medium is wrapped (not shrink-wrapped) in imaginary cellophane, and the resulting convex medium will have region of zero extinction where the hole used to be.

We can therefore always assume that M is an open convex subset of $\mathbb{R}^3$ and we denote the closed set of all its boundary points as in mathematical analysis by "∂M." We can now express the most general BC for the RTE as

$$I(\boldsymbol{x}, \boldsymbol{\Omega}) = f(\boldsymbol{x}, \boldsymbol{\Omega}),\ \boldsymbol{x} \in \partial\mathrm{M},\ \boldsymbol{\Omega} \bullet \boldsymbol{n}(\boldsymbol{x}) < 0. \tag{3.109}$$

Along with the RTE, including its own source term, this determines the radiance field uniquely. In some applications, we must also consider the boundaries (internal) reflection properties. This gives rise to constraints that couple various out-going and in-coming beams at the inside surface of ∂M, as described in Sect. 3.6.2. As already pointed out, surface reflection processes act formally like a special kind of scattering.

In Fig. 3.12, to which we will return for further discussion momentarily, we have illustrated the case of a smooth ∂M where $\boldsymbol{n}(\boldsymbol{x})$ exists everywhere. We address boundary points where $\boldsymbol{n}(\boldsymbol{x})$ does not exist further on. We only require that the "measure" of that set be zero, which basically means that they intercept vanishingly few incoming or outgoing photons.

Plane-Parallel Media: The Many Ways They can be Hosts to 3D Radiative Transfer. Section 3.6.2 on steady boundary sources describes typical BCs for slab geometry. They can be combined to have sources at both top and bottom, or none at all (so-called "absorbing" BCs). It suffices that the boundary or volume sources be spatially variable to necessitate the 3D RTE, internal variability of optical properties is not always a requirement. Sometimes it is necessary to consider surface reflection, as described in Sect. 3.6.2. Here again the properties of the bulk of the medium and the sources can be uniform and just variability of the surface reflectivity is enough to excite the horizontal gradients in the 3D RTE. These scenarios are germane to cloud lidar studies and aerosol adjacency effects respectively.

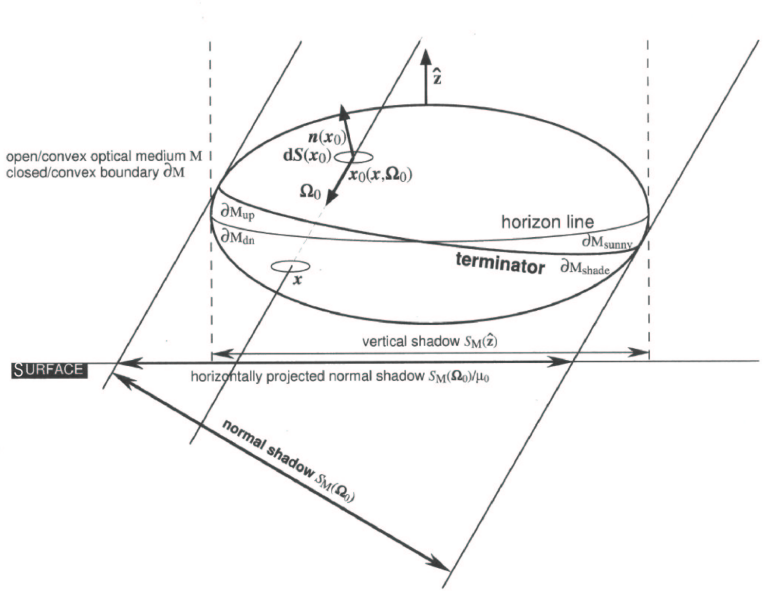

Fig. 3.12. Illumination of a horizontally finite medium with a collimated beam that may be oblique with respect to a surface.

So, the RTE in (3.101) and one of these BC scenarios entirely determine $I(\boldsymbol{x}, \boldsymbol{\Omega})$ in the plane-parallel medium

$$\mathrm{M} = \{\boldsymbol{x} \in \mathbb{R}^3 : \ 0 < z < h\} \tag{3.110}$$

described by given optical properties $\sigma(\boldsymbol{x})$, $\varpi_0(\boldsymbol{x})$, $p(\boldsymbol{x}, \boldsymbol{\Omega}' \bullet \boldsymbol{\Omega})$, and volume sources $Q(\boldsymbol{x}, \boldsymbol{\Omega})$. These quantities appear in the various terms on the r.-h. side of the RTE. Now, in practice, the variability of the optical properties is often specified only over a finite domain $[0, L_x) \otimes [0, L_y) \otimes [0, h)$. The vertical limits $z = 0, h$ receive the usual treatment, while "periodic" BCs are applied horizontally. Therefore, to determine radiance in the basic cell, we require

$$\mathrm{M} = \{\boldsymbol{x} \in \mathbb{R}^3 \ : \ 0 < x < L_x, \ 0 < y < L_y, \ 0 < z < h\} \tag{3.111}$$

by requiring

$$\left.\begin{array}{l} I(x, 0, z, \boldsymbol{\Omega}) = I(x, L_y, z, \boldsymbol{\Omega}), \ 0 \le x < L_x \\ I(0, y, z, \boldsymbol{\Omega}) = I(L_x, y, z, \boldsymbol{\Omega}), \ 0 \le y < L_y \end{array}\right\}, \ 0 < z < h, \ \forall \boldsymbol{\Omega} \tag{3.112}$$

inside the medium.

We often need to consider, at least formally, semi-infinite media, i.e., the limit $h \to \infty$ in (3.110). This is of course an idealization, albeit a useful one. In this case, we only need to specify BCs on the boundary at $z = 0$, which may be viewed as a top (e.g., of an ocean) or a bottom (e.g. of an extended atmosphere).

We can even think of the atmosphere-surface system as a stratified semi-infinite medium with its upper boundary being the TOA. This TOA can be set for convenience at a fixed altitude ($z = 0$ or h or whatever), with or without incoming radiation, and all the rest is about *internal* sources and scattering/reflection processes. From then on, surface emission is assimilated to an internal source confined to a manifold $z = z_{\rm S}(x, y)$ and directed toward the upward side of the said manifold while surface reflection is assimilated to a special kind of oriented scattering that occurs on the same manifold. Below the surface, extinction is formally viewed as infinite; so there is no need to go there, radiatively speaking. See Fig. 3.13. All we have excluded here is topologically complicated terrain that can not be modeled with an analytical or digital elevation model of the form $z_{\rm S}(x, y)$. We thus exclude overhangs, caves and tunnels since these would call for multi-valued functions $z_{\rm S}(x, y)$.

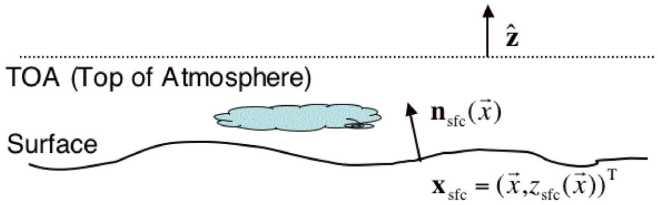

Fig. 3.13. A 3D radiative transfer problem in variable-altitude terrain with or without an atmosphere over overlying it, with or without horizontal variability (such as clouds) in it. This scenario is considered general enough for most present needs, including small-scale modeling of a rough surface's angular properties. Note that in the following subsection the finite cloud in this schematic will be considered in isolation.

The beauty of this formulation is that we are no longer limited to flat or even convex terrain. We have already accommodated in Sect. 3.6.2 the possibility of non-uniform reflectivity and emissivity properties for the special case $z_{\rm S}(\vec{x}) \equiv 0$ (under the assumption that TOA is at $z = h > 0$). For the more general situation, we only assume that the *inward* normal vector $\boldsymbol{n}(\vec{x})$ exists (almost everywhere) and that it is "open to the sky" (i.e., $\boldsymbol{n}(\vec{x}\bullet\hat{\mathbf{z}} > 0$ which follows directly from the single-valuedness of $z_{\rm S}(\vec{x})$). In summary, we have to solve the 3D RTE at all points in

$$M = \{\boldsymbol{x} = (\vec{x}, z_{\rm S}(\vec{x}))^{\rm T} \in \mathbb{R}^3 : \; z_{\rm S}(\vec{x}) < z < h\}. \tag{3.113}$$

subject to the constraints

$$\left.\begin{array}{l} f(\boldsymbol{x}, \boldsymbol{\Omega}) = \epsilon_\nu(\boldsymbol{x}, \boldsymbol{\Omega}) B_\nu[T(\boldsymbol{x})] \;\text{ in (3.109)} \\ I(\boldsymbol{x}, \boldsymbol{\Omega}) = \alpha_\nu(\boldsymbol{x}, \boldsymbol{\Omega}) \int_{\boldsymbol{n}(\vec{x})\bullet\boldsymbol{\Omega}'<0} p_{{\rm S}\nu}(\boldsymbol{x}, \boldsymbol{\Omega}' \to \boldsymbol{\Omega}) I(\boldsymbol{x}, \boldsymbol{\Omega}') {\rm d}\boldsymbol{\Omega}' \end{array}\right\}, \tag{3.114}$$
$$\forall \boldsymbol{x} = (\vec{x}, z_{\rm S}(\vec{x}))^{\rm T}, \; \forall \boldsymbol{\Omega} \text{ such that } \boldsymbol{\Omega} \bullet \boldsymbol{n}(\vec{x}) > 0.$$

Even though we require inward normal vectors to exist *almost everywhere*, there can be very many facets in the terrain model that quickly change their orientation

$\boldsymbol{n}(\vec{x})$ as well as their optical properties, $\epsilon, \alpha, p_{\rm S}$ in (3.114). So we now we have the possibility of modeling rough terrain that is fractal-like over a large range of scales.

This is a necessary complication in many important applications, some of them in planetary science where there is in fact no atmosphere at all. One application of 3D radiative transfer driven only by rough terrain effects is to compute, starting with a deterministic or stochastic description of a uniformly emissive but rough surface, the macroscopic angular dependence of the "effective" emissivity in (3.114). The resulting model for $\epsilon_\nu(\cdot, \boldsymbol{\Omega})$ could be used as a parameterization of unresolved variability in a subsequent flat-surface plane-parallel computation. The same remark applies to the macroscopic models for reflective properties of surfaces with complex internal structure (cf. Chap. ??? on vegetation canopies).

An example is given in Fig. 3.14 where we used a Monte Carlo technique to compute the angular dependence of the enhancement factor for effective emissivity, $f_\epsilon(\theta) = \epsilon_{\rm eff}(\theta)/\epsilon - 1$, caused by surface roughness. To illustrate this systematic effect of terrain variability, we used a surface made of an unresolved array of closely-packed hemispherical "craters" with a (power-law) size distribution such that they fill 2D space completely. The surface was maintained at a constant temperature and its *uniform* emissivity ϵ takes the three indicated values; we plot $f_\epsilon/(1-\epsilon)$ to emphasize the dominant linear trend in albedo $\alpha = 1 - \epsilon$ as well as the residual nonlinearity at lower ϵ (higher α). This ratio is, to a first approximation, the mean probability of being a photon to remain trapped in the cavity $p_{\rm trap}(\theta)$. Escape probability $1 - p_{\rm trap}(\theta)$ is defined as $1/2\pi$ times the solid-angle of open sky viewed from a point on the surface and averaged over that part of the crater that is seen from viewing angle θ. For $\theta \approx 90^\circ$, $p_{\rm trap}$, this ratio is $\approx 1/2$ because of the vertical ridges of the craters are all that contribute for grazing angles; for smaller values of θ, $p_{\rm trap}$ decreases. A more precise nonlinear model for $\epsilon_{\rm eff}(\theta)$ accounting for all orders of internal reflection is given by $(\epsilon/[1 - (1 - \epsilon)p_{\rm trap}(\theta)]$. Using this model, with $f_{.9375}(\theta)/.0625$ from Fig. 3.14b as an estimate for $p_{\rm trap}(\theta)$, predicts the other $f_\epsilon(\theta)$ values at better than 4% accuracy.

Generalization to Horizontally Finite Media. Another interesting class of 3D RT problems involve horizontally finite media that may or may not be internally variable. For instance, the popular case of rectangular parallelepipeds or "cuboids" would have M defined by (3.111) but without the lateral recycling of radiance described in (3.112). Geometrical — actually, topological — considerations are in order to specify BCs as well as partition the boundary fields further on. All of what is said here is general enough to contain the plane-parallel media treated above in the limit of infinite aspect ratio $h/\min L_x, L_y$, where M becomes the slab in (3.110).

If only volume sources are considered then $f(\boldsymbol{x}, \boldsymbol{\Omega}) = 0$ (absorbing BCs) while for a solar beam (not "injected" through the volume source term) with flux F_0 and incidence direction $\boldsymbol{\Omega}_0$, we have

$$f(\boldsymbol{x}, \boldsymbol{\Omega}) = F_0 \delta(\boldsymbol{\Omega} - \boldsymbol{\Omega}_0) 1_{\partial {\rm M}_{\rm sunny}(\boldsymbol{\Omega}_0)}(\boldsymbol{x}) \tag{3.115}$$

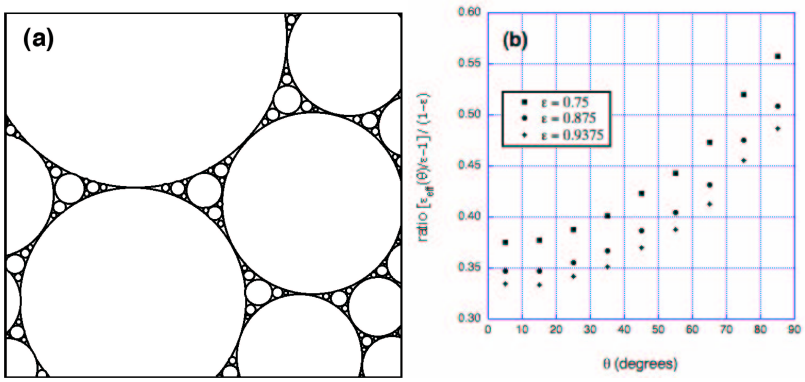

Fig. 3.14. Angular dependence of effective emissivity for a uniform but variable-height surface, an array of closely-packed hemispherical "craters." **(a)** A schematic of the unresolved variability modeled here. **(b)** Computations performed using a straightforward Monte Carlo ray-tracing technique with 3 values of ϵ. The effect is systematic and present at all viewing angles but large ones, looking at more shallow terrain are even more emissive (appear to be warmer) due to increased probability of escape after any number of partial reflections. The largest absolute change in emissivity is for $\epsilon = 0.75$ and $\theta \approx 90^\circ$: $\epsilon_{\rm eff} \approx 0.85$.

where $1_{\partial \mathrm{M}_{\rm sunny}(\boldsymbol{\Omega}_0)}(\boldsymbol{x})$ is the indicator function for the subset of ∂M where the solar rays enter M. We will call it the illuminated or "sunny" side of M.

Even if the solar beam source is modeled by "injection" in to the bulk of M, it is useful to define $\partial \mathrm{M}_{\rm sunny}(\boldsymbol{\Omega}_0)$. Specifically, we have

$$\partial \mathrm{M}_{\rm sunny}(\boldsymbol{\Omega}_0) = \underline{\{\boldsymbol{x} \in \partial \mathrm{M} : \ \boldsymbol{n}(\boldsymbol{x}) \bullet \boldsymbol{\Omega}_0 \leq 0\}}. \tag{3.116}$$

Notice the inclusion of $\boldsymbol{n}(\boldsymbol{x}) \bullet \boldsymbol{\Omega}_0 = 0$ here, which makes $\partial \mathrm{M}_{\rm sunny}$ a *closed* set, at least if $\boldsymbol{n}(\boldsymbol{x})$ exits everywhere (as in Fig. 3.12). If $\boldsymbol{n}(\boldsymbol{x})$ does not exist everywhere (as on the conspicuous edges that appear in Fig. 3.15), then we use the "closure" of the set, i.e., the set itself plus the limit points of all possible infinite sequences belonging to the set. We have used an underscore to designate the closure operation. Closure adds no new points in the everywhere smooth boundary case in Fig. 3.12). However, in cases like in Fig. 3.15) all points on edges from which there is a unobstructed view of the sun, even if at grazing angles, are added to $\{\boldsymbol{x} \in \partial \mathrm{M} : \ \boldsymbol{n}(\boldsymbol{x}) \bullet \boldsymbol{\Omega}_0 \leq 0\}$.

By extension, we have

$$\partial \mathrm{M}_{\rm shady}(\boldsymbol{\Omega}_0) = \{\boldsymbol{x} \in \partial \mathrm{M} : \ \boldsymbol{n}(\boldsymbol{x}) \bullet \boldsymbol{\Omega}_0 > 0\} = \partial \mathrm{M} \backslash \partial \mathrm{M}_{\rm sunny}(\boldsymbol{\Omega}_0), \tag{3.117}$$

an *open* set that is the non-illuminated or "shady" side of the boundary of M in Fig. 3.12. The direction of the asymmetry with respect to the points where $\boldsymbol{n}(\boldsymbol{x}) \bullet \boldsymbol{\Omega}_0 = 0$ is not arbitrary, and is justified physically further on. Convexity of M guarantees that $\partial \mathrm{M}_{\rm sunny}$ and $\partial \mathrm{M}_{\rm shady}$ are both singly connected.

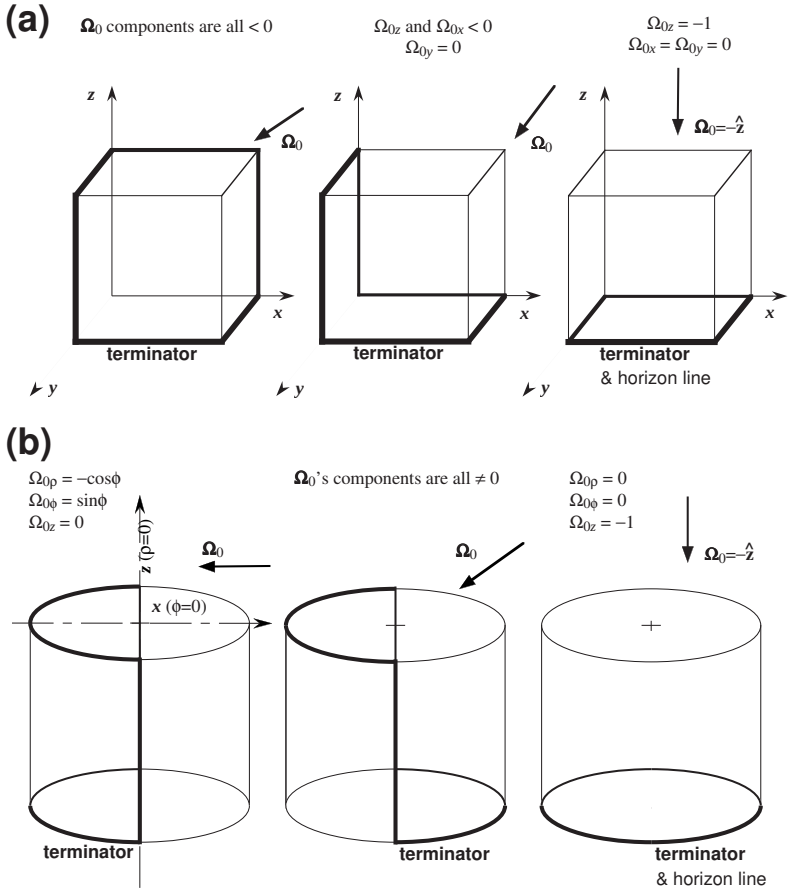

Fig. 3.15. Reflection versus transmission in isolated cloud models. **(a)** Cuboidal shapes. **(b)** Cylindrical shapes.

3.8.2 Exact and Formal Solutions of the 3D RTE

Suppose $S(\boldsymbol{x}, \boldsymbol{\Omega}) \equiv 0$ in (3.101), equivalently $\sigma_{\rm s}(\boldsymbol{x}) \equiv 0$ in (3.81), i.e., no scattering. The RTE is then a doubly infinite system of *independent* ODEs, one class for each $\boldsymbol{\Omega}$ in Ξ and then one for each two-dimensional (2D) vector $\vec{x} \in \mathrm{S}(\boldsymbol{\Omega})$, the associated 2D projection of M along $\boldsymbol{\Omega}$ (as used previously, e.g., in Fig. 3.12 to compute projected areas of finite clouds). Each of these ODEs can be written as

$$\frac{\mathrm{d}I}{\mathrm{d}s} = -\sigma(\boldsymbol{x})I + Q(\boldsymbol{x}, \boldsymbol{\Omega}) \tag{3.118}$$

where Q is the known volume source term. This ODE is immediately integrable, yielding

$$I(\boldsymbol{x},\boldsymbol{\Omega}) = f(\boldsymbol{x}_{\partial\mathrm{M}}(\boldsymbol{x},\boldsymbol{\Omega}),\boldsymbol{\Omega})\exp[-\tau(s_{\partial\mathrm{M}}(\boldsymbol{x},\boldsymbol{\Omega});\boldsymbol{x},-\boldsymbol{\Omega})] + \int_0^{s_{\partial\mathrm{M}}(\boldsymbol{x},\boldsymbol{\Omega})} Q(\boldsymbol{x}-\boldsymbol{\Omega}s,\boldsymbol{\Omega})\exp[-\tau(s;\boldsymbol{x},-\boldsymbol{\Omega})]\mathrm{d}s \tag{3.119}$$

where

- $\boldsymbol{x}_{\partial\mathrm{M}}(\boldsymbol{x},\boldsymbol{\Omega})$ is the (unique) piercing point of the beam $\{\boldsymbol{x},-\boldsymbol{\Omega}\}$ with the (convex) boundary ∂M, and
- $s_{\partial\mathrm{M}}(\boldsymbol{x},\boldsymbol{\Omega}) = \|\boldsymbol{x}-\boldsymbol{x}_{\partial\mathrm{M}}(\boldsymbol{x},\boldsymbol{\Omega})\|$ is the distance from $\boldsymbol{x}$ to ∂M along $-\boldsymbol{\Omega}$.

The first term is thus a given BC in (3.109) followed by direct transmission to $\boldsymbol{x}$ (cf. Sect. 3.3.3) and, in the second term, $\tau(s;\boldsymbol{x},-\boldsymbol{\Omega})$ is the optical distance through the 3D medium from $\boldsymbol{x}$ to a *backwards* running point $\boldsymbol{x}-\boldsymbol{\Omega}s$ again from (3.30).

The steady-state 3D RT problem in absence of scattering is therefore reduced to a numerical implementation of (3.119). We can also formally equate the source *term* Q in (3.118) to the source *function* S which in fact depends on the unknown $I(\boldsymbol{x},\boldsymbol{\Omega})$. Then (3.119) is called the "formal" solution of the RTE.

3.8.3 Integral Radiative Transfer Equations

By substituting the expression in (3.81) for S into the formal solution (3.119) where we also make the substitution $Q \mapsto S+Q$, we find

$$I(\boldsymbol{x},\boldsymbol{\Omega}) = I_{fQ}(\boldsymbol{x},\boldsymbol{\Omega}) + \int_0^{s_{\partial\mathrm{M}}(\boldsymbol{x},\boldsymbol{\Omega})} \sigma_{\mathrm{s}}(\boldsymbol{x}-\boldsymbol{\Omega}s)\exp[-\tau(s;\boldsymbol{x},-\boldsymbol{\Omega})]\mathrm{d}s \times \oint_{\Xi} p(\boldsymbol{x}-\boldsymbol{\Omega}s,\boldsymbol{\Omega}'\to\boldsymbol{\Omega})I(\boldsymbol{x}-\boldsymbol{\Omega}s,\boldsymbol{\Omega}')\mathrm{d}\boldsymbol{\Omega}' \tag{3.120}$$

where $I_{fQ}(\boldsymbol{x},\boldsymbol{\Omega})$ is the boundary-and/or-volume "forcing" term given by (3.119) as it stands. This defines the integral form of the RTE where we recognize the cumulative contributions of "up-stream" elements: the positional argument is $-\boldsymbol{\Omega}s$ and scattering is into the beam of interest.

We have thus obtained a self-contained integral equation for the general radiative transfer problem which can however be written more simply at the cost of making the 3-dimensional integral in (3.120) look as if it was 5-dimensional. Specifically, one makes use of

$$\mathrm{d}\boldsymbol{x}' = s^2\mathrm{d}s\mathrm{d}\boldsymbol{\Omega}' \tag{3.121}$$

to convert the resulting double (line and angle) integral(s) over $\mathrm{d}s\mathrm{d}\boldsymbol{\Omega}'$ into a volume integral over M. Then, noting that $s=\|\boldsymbol{x}'-\boldsymbol{x}\|$ and using the identity

$$\int_{\mathrm{M}}[\cdot]d\boldsymbol{x}' = \oint_{\Xi}\int_{\mathrm{M}}[\cdot]\,\delta\left(\boldsymbol{\Omega}'-\frac{\boldsymbol{x}'-\boldsymbol{x}}{\|\boldsymbol{x}'-\boldsymbol{x}\|}\right)\mathrm{d}\boldsymbol{x}'\mathrm{d}\boldsymbol{\Omega}', \tag{3.122}$$

we obtain

$$I(\boldsymbol{x},\boldsymbol{\Omega}) = \oint\limits_{\Xi}\int\limits_{\mathrm{M}} \mathcal{K}_I(\boldsymbol{x}',\boldsymbol{\Omega}'\to\boldsymbol{x},\boldsymbol{\Omega}) I(\boldsymbol{x}',\boldsymbol{\Omega}')\mathrm{d}\boldsymbol{x}'\mathrm{d}\boldsymbol{\Omega}' + I_{fQ}(\boldsymbol{x},\boldsymbol{\Omega}) \tag{3.123}$$

where the 5-dimensional transport kernel is

$$\mathcal{K}_I(\boldsymbol{x}',\boldsymbol{\Omega}'\to\boldsymbol{x},\boldsymbol{\Omega}) = \sigma_{\mathrm{s}}(\boldsymbol{x}')\, p(\boldsymbol{x}',\boldsymbol{\Omega}'\to\boldsymbol{\Omega})\, \delta\!\left(\boldsymbol{\Omega}' - \frac{\boldsymbol{x}'-\boldsymbol{x}}{\|\boldsymbol{x}'-\boldsymbol{x}\|}\right) \frac{\exp[-\tau(\boldsymbol{x}',\boldsymbol{x})]}{\|\boldsymbol{x}'-\boldsymbol{x}\|^2}. \tag{3.124}$$

For numerical implementation, (3.120) is of course the only route.

Of course, if S is actually known, then (3.119), again with the substitution $Q \mapsto S + Q$, can be used to infer I. Hence the idea of formulating another integral equation, this time for the source function $S(\boldsymbol{x},\boldsymbol{\Omega})$ by performing the reverse substitution of (3.119) into (3.81). Through similar manipulations as above, this leads to the so-called "ancillary" equation which reads as

$$\begin{aligned} S(\boldsymbol{x},\boldsymbol{\Omega}) = S_{fQ}(\boldsymbol{x},\boldsymbol{\Omega}) + \sigma_{\mathrm{s}}(\boldsymbol{x}) \oint\limits_{\Xi} p(\boldsymbol{x},\boldsymbol{\Omega}'\to\boldsymbol{\Omega})\mathrm{d}\boldsymbol{\Omega}' \\ \times \int\limits_0^{s_{\partial\mathrm{M}}(\boldsymbol{x},\boldsymbol{\Omega})} \exp[-\tau(s;\boldsymbol{x},-\boldsymbol{\Omega})] S(\boldsymbol{x}-\boldsymbol{\Omega}s,\boldsymbol{\Omega}')\mathrm{d}s \end{aligned} \tag{3.125}$$

where

$$S_{fQ}(\boldsymbol{x},\boldsymbol{\Omega}) = \sigma_{\mathrm{s}}(\boldsymbol{x}) \oint\limits_{4\pi} p(\boldsymbol{x},\boldsymbol{\Omega}'\to\boldsymbol{\Omega}) I_{fQ}(\boldsymbol{x},\boldsymbol{\Omega}')\mathrm{d}\boldsymbol{\Omega}'. \tag{3.126}$$

is the known forcing term. Again we see in (3.125) the up-stream integration but with far fewer terms in the spatial integral. This turns out to be significant advantage in numerical implementations and the relatively minor price to pay is that, after $S(\boldsymbol{x},\boldsymbol{\Omega})$ is obtained, there is one last application of the formal solution (3.119) to derive $I(\boldsymbol{x},\boldsymbol{\Omega})$.

Here again, a more compact rewriting of (3.125) is possible:

$$S(\boldsymbol{x},\boldsymbol{\Omega}) = \oint\limits_{\Xi}\int\limits_{\mathrm{M}} \mathcal{K}_S(\boldsymbol{x}',\boldsymbol{\Omega}'\to\boldsymbol{x},\boldsymbol{\Omega}) S(\boldsymbol{x}',\boldsymbol{\Omega}')\mathrm{d}\boldsymbol{x}'\mathrm{d}\boldsymbol{\Omega}' + S_{fQ}(\boldsymbol{x},\boldsymbol{\Omega}) \tag{3.127}$$

where the transport kernel is now

$$\mathcal{K}_S(\boldsymbol{x}',\boldsymbol{\Omega}'\to\boldsymbol{x},\boldsymbol{\Omega}) = \sigma_{\mathrm{s}}(\boldsymbol{x})\, p(\boldsymbol{x},\boldsymbol{\Omega}'\to\boldsymbol{\Omega})\, \delta\!\left(\boldsymbol{\Omega}' - \frac{\boldsymbol{x}'-\boldsymbol{x}}{\|\boldsymbol{x}'-\boldsymbol{x}\|}\right) \frac{\exp[-\tau(\boldsymbol{x}',\boldsymbol{x})]}{\|\boldsymbol{x}'-\boldsymbol{x}\|^2}. \tag{3.128}$$

The only difference between the kernels $\mathcal{K}_S$ and $\mathcal{K}_I$ is the dependence of the scattering properties on the ending point rather than the starting point of the displacement modeled by the kernels, cf. $\tau(\boldsymbol{x}',\boldsymbol{x})$. Both the Spherical-Harmonic Discrete-Ordinate

Method (SHDOM) and the backward Monte Carlo method described in the following chapter capitalize on this remark.

Finally, we note that the full 5-dimensional formalism used in the above integral equations is primarily useful in theoretical considerations (existence and analytical properties of solutions, etc.). 3-dimensional formulations are used in numerical implementations. Indeed, the identity in (3.122) can be used to get rid of the angular integral it was used to create. Pre-scattering direction $\boldsymbol{\Omega}'$ then becomes a simple function of $\boldsymbol{x}' - \boldsymbol{x}$, namely, its direction in Ξ, and $\boldsymbol{\Omega} \in \Xi$ becomes essentially a control parameter for the fields and the kernels while the 3D integration is done (and probably iterated) over $\boldsymbol{x}'$.

3.9 Outgoing Radiation

The photon population that leaves an optical medium through its outer boundary is of particular interest. This is in part because it offers a means of assessing the radiant energy budget of the medium; recall the arguments given in Sect. 3.3.1 where we were considering an arbitrary region, not necessarily the whole medium. This is in at least as large a part because escaping radiation can be detected remotely and it tells us volumes about the structure and properties of the medium at some significant stand-off distance; in fact, all of observational astrophysics and remote sensing is predicated on this simple fact.

3.9.1 Plane-Parallel Media with Horizontally Variable Structure and/or Sources.

Varying radiances and fluxes at the boundaries are of special interest in 3D RT. For the plane-parallel medium in (3.110), we are looking at the up- and down-welling radiances

$$\left\{\begin{matrix}\pi I(\vec{x}, h, \boldsymbol{\Omega}(\mu, \varphi))/\mu_0 F_0,\, \mu \geq 0 \\ \pi I(\vec{x}, 0, \boldsymbol{\Omega}(\mu, \varphi))/\mu_0 F_0,\, \mu \leq 0\end{matrix}\right\},\ \forall \vec{x}, \tag{3.129}$$

given here in the natural non-dimensional representation introduced in (3.19). In this standard normalization, radiance is represented as the non-dimensional BRF in (3.19) and, more generally, Eq. (3.86) in Sect. 3.6.2). This interpretation works similarly for transmittance if one thinks of a *bi*-Lambertian surface, i.e., that reflects *and* transmits isotropically. For fluxes, we are interested in

$$\left\{\begin{matrix}R(\vec{x}) = F_z^{(+)}(\vec{x}, h)/\mu_0 F_0, & \text{reflectance field} \\ T(\vec{x}) = F_z^{(+)}(\vec{x}, 0)/\mu_0 F_0, & \text{transmittance field}\end{matrix}\right\}, \forall \vec{x}, \tag{3.130}$$

recalling from (3.15) that the normal vectors are always oriented outward from M, hence the "(+)" subscripts assigned to *both* hemispherical fluxes. They are relative to the local normal and not the absolute upward z-axis.

Analogous definitions apply to the periodically replicated media in (3.111). In that case at least, it is easy to define the domain-average quantities:

$$\begin{cases} R = \overline{R(\vec{x})} = \int\limits_{[0,L_x)\otimes[0,L_y)} R(\vec{x})\mathrm{d}\vec{x}/L_xL_y, & \text{(mean) reflectance} \\ T = \overline{T(\vec{x})} = \int\limits_{[0,L_x)\otimes[0,L_y)} T(\vec{x})\mathrm{d}\vec{x}/L_xL_y, & \text{(mean) transmittance} \end{cases}. \quad (3.131)$$

where we use the overscore to designate a spatial average of a field. The above definitions naturally extend to the case of an infinite domain by taking the limit of arbitrarily large L_x and/or L_y.

3.9.2 Generalization to Horizontally Finite Media.

"R/T" Partition by Illumination and Position at Escape: The simplest plane-parallel definition to emulate here is in (3.130). We thus define the *normalized* flux fields

$$\begin{cases} R(\boldsymbol{x}) = F^{(+)}_{\boldsymbol{n}(\boldsymbol{x})}(\boldsymbol{x})/|\boldsymbol{n}(\boldsymbol{x}) \bullet \boldsymbol{\Omega}_0|F_0,\ \boldsymbol{x} \in \partial\mathrm{M}_{\mathrm{sunny}}(\boldsymbol{\Omega}_0), & \text{for reflectance} \\ T(\boldsymbol{x}) = F^{(+)}_{\boldsymbol{n}(\boldsymbol{x})}(\boldsymbol{x})/|\boldsymbol{n}(\boldsymbol{x}_0(\boldsymbol{x},\boldsymbol{\Omega}_0)) \bullet \boldsymbol{\Omega}_0|F_0,\ \boldsymbol{x} \in \partial\mathrm{M}_{\mathrm{shady}}(\boldsymbol{\Omega}_0), & \text{for transmittance} \end{cases} \quad (3.132)$$

where $\boldsymbol{x}_0(\boldsymbol{x},\boldsymbol{\Omega}_0)$ is defined, in analogy with Sect. 3.6.1 for the plane-parallel medium, as the unique point on the sunny side of the cloud where the beam $\{\boldsymbol{x}, -\boldsymbol{\Omega}_0\}$ pierces $\partial\mathrm{M}_{\mathrm{sunny}}(\boldsymbol{\Omega}_0)$, cf. Fig. 3.12.

The overall responses to boundary (or otherwise modeled mono-directional) illumination are

$$\begin{cases} R = \int\limits_{\partial\mathrm{M}_{\mathrm{sunny}}(\boldsymbol{\Omega}_0)} F^{(+)}_{\boldsymbol{n}(\boldsymbol{x})}(\boldsymbol{x})\mathrm{d}S(\boldsymbol{x}) \ / \ F_0 S_{\mathrm{M}}(\boldsymbol{\Omega}_0), & \text{for reflectance} \\ T = \int\limits_{\partial\mathrm{M}_{\mathrm{shady}}(\boldsymbol{\Omega}_0)} F^{(+)}_{\boldsymbol{n}(\boldsymbol{x})}(\boldsymbol{x})\mathrm{d}S(\boldsymbol{x}) \ / \ F_0 S_{\mathrm{M}}(\boldsymbol{\Omega}_0), & \text{for transmittance} \end{cases} \quad (3.133)$$

where

$$S_{\mathrm{M}}(\boldsymbol{\Omega}_0) = \boldsymbol{\Omega}_0 \bullet \int\limits_{\partial\mathrm{M}_{\mathrm{shady}}(\boldsymbol{\Omega}_0)} \boldsymbol{n}(\boldsymbol{x})\mathrm{d}S(\boldsymbol{x}) = -\boldsymbol{\Omega}_0 \bullet \int\limits_{\partial\mathrm{M}_{\mathrm{sunny}}(\boldsymbol{\Omega}_0)} \boldsymbol{n}(\boldsymbol{x})\mathrm{d}S(\boldsymbol{x}) \quad (3.134)$$

is the area of the *normal* geometrical shadow of the medium M under collimated illumination from $\boldsymbol{\Omega}_0$, as illustrated in Fig. 3.12. Notice that, in contrast with the $\{R, T\}$ pair in (3.131), the one in (3.133) is not made of straightforward averages of the fields in (3.132). They are weighted averages using local solar irradiance (i.e., the denominators in (3.132)) so that the spatial integral is, as indicated, in non-normalized fluxes; then the totals are properly normalized by the integral of the weights in (3.134).

In Fig. 3.16a, we illustrate the quantities in (3.133) using spherical media $M = \{\boldsymbol{x} \in \mathbb{R}^3 :\ x^2+y^2+z^2 < r^2\}$. No absorption was assumed so we have $R+T = 1$ by

conservation and this suggests that we only need to study the ratio R/T to determine both quantities. Both isotropic and forward ($g = 0.85$ Henyey-Greenstein) scattering phase functions were used in the computations. Also the boundary sources were either collimated along $\mathbf{\Omega}_0$ or diffuse (isotropic), but always with relative strength given by $|\boldsymbol{n}(\boldsymbol{x}) \bullet \mathbf{\Omega}_0|$. Optical thickness measured across the diameter of the sphere $\tau_{\rm diam} = 2\sigma r$ is varied by factors of 2 from 0.125 to 64 (for $g = 0$) or 512 (for $g = 0.85$).

Davis (2002) derives an exact diffusion theoretical expression for R/T for such purely scattering spherical media that goes as $(1-g)\tau_{\rm diam}$ with a numerical prefactor between 0.70 to 0.86. (It is precisely $1/2\chi$, the inverse of $2\times$ the "extrapolation length" expressed in "transport" MFPs.) Photon diffusion theory (cf. Chap. ???) is an approximation that is expected to work well in the bulk of opaque highly scattering ($1-\varpi_0 \ll 1$) media, i.e., at more that a couple of transport MFPs $1/(1-\varpi_0 g)\sigma$ from boundaries and/or sources. This prediction is clearly confirmed by the numerical solutions of the RTE plotted in Fig. 3.16a for large optical thicknesses. Indeed, the vertical axis is R/T divided by the "rescaled" optical diameter $(1-g)\tau_{\rm diam}$ and it goes to the anticipated value as $\tau_{\rm diam}$ increases without bound. This is irrespective of the angular pattern of the illumination or the phase function; at most, the forward-scattering media under collimated-beam illumination converge to a slightly larger value (still well within the accepted range for the extrapolation length factor χ). The collapse of the curves for $g = 0$ and $g = 0.85$ is particularly good for the isotropic source cases, as is expected in this more clearly diffusive situation, and fully consistent with the way Davis (2002) set up his BCs and sources. Since $R \to 1$ in this limit, we have $T \propto 1/(1-g)\tau_{\rm diam}$. As noted by Davis (2002), this law does not seem to be sensitive to cloud geometry: a similar law is indeed obtained in slab geometry. This robustness with respect to outer cloud geometry is exploited further on.

We have also highlighted in Fig. 3.16a the locus of points where $R = T = 1/2$. In the optically thin limit ($\tau_{\rm diam} \ll 1/(1-g)$), we see that the two angular models for the sources give very different results, both easily explained. Diffuse sources appropriately distributed on the upper boundary yield $R \approx T \approx 1/2$ in spherical geometry because scattering is no longer a concern, only ballistic trajectories matter. In contrast, the collimated beam scenario crosses the $R = T$ line at $\tau_{\rm diam} \approx 2.5$ and R/T goes to another limit determined by the opposite approximation of diffusion, single-scattering and quasi-linear transmission laws. In this latter approximation, we indeed expect $R = 1 - T \propto \tau_{\rm diam}$ with a prefactor that will be sensitive to the phase function as well as to cloud geometry.

In the above natural enough definitions, we have used only the solar direction to partition the boundary fields according to the position on the boundary where the light emerges. Thus, introducing a ground surface and the associated vertical direction, "reflected" light can reach the ground and "transmitted" light can return to space, even if the Sun is at zenith. This is an essential feature of isolated (horizontally finite) clouds, and a topological impossibility in plane-parallel geometry. The important demarcation line is not so much the "horizon" line in Fig. 3.12 as the

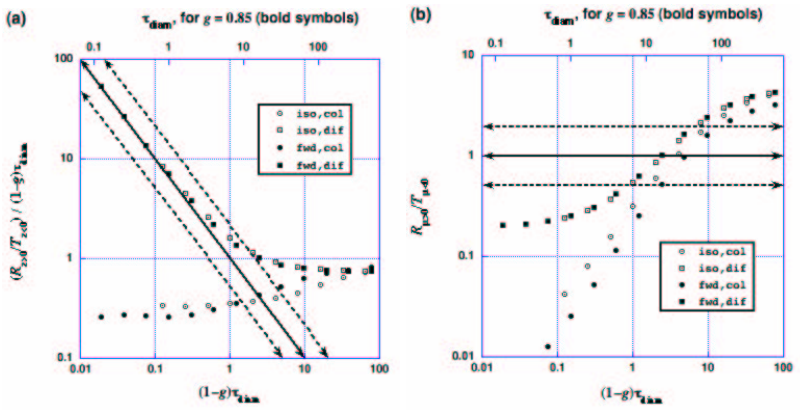

Fig. 3.16. Reflection and transmission of spherical cloud models. A Monte Carlo technique (cf. Chap. ???) was used with 10^5 histories for each case. **(a)** Partition of R and T according to position at escape (hence the subscripts describing the sign of z). **(b)** Partition of R and T according to direction at escape (hence the subscripts describing the sign of μ). In both partitions, the thick/solid double-arrowed line indicates where $R = T = 1/2$ (since $R+T = 1$ here); the dashed lines on either side indicate where $R/T = 2^{\pm 1}$, hence $R = 1/3$ or $R = 2/3$ and conversely for T.

"terminator," a terminology we borrow from planetary astronomy. It is defined as the closed set intersection

$$\partial \mathrm{M}_{\mathrm{term}}(\boldsymbol{\Omega}_0) = \underline{\partial \mathrm{M}_{\mathrm{shady}}(\boldsymbol{\Omega}_0)} \cap \partial \mathrm{M}_{\mathrm{sunny}}(\boldsymbol{\Omega}_0). \tag{3.135}$$

This definition is preferable to

$$\partial \mathrm{M}_{\perp}(\boldsymbol{\Omega}_0) = \{\boldsymbol{x} \in \partial M : \ \boldsymbol{n}(\boldsymbol{x}) \bullet \boldsymbol{\Omega}_0 = 0\} \tag{3.136}$$

because of possible degeneracy, that is, situations where whole facets with finite areas are part of the proposed demarcation set. If this is the case, then some of the out-going flux is then neither reflected nor transmitted — it is quite literally "side-leaked." This is a popular notion but unfortunately it can be quantified precisely only in very special cloud/Sun geometries where $\partial \mathrm{M}_{\perp}$ has a finite area. These special illumination conditions that "resonate" with outer cloud geometry may have received more attention because they happen to be attractive simplifications for the RT modeling.

An often-used but pathological geometry for cloud modeling is the popular cuboidal medium. The cuboid's pathology results from the possibility of solar rays grazing finite areas on its surface. The resolution of its terminator according to (3.135) under all possible illuminations is illustrated in Fig. 3.15a, while finite cylinders are treated in Fig. 3.15b. Note that the sunny/shady asymmetry in (3.116)-(3.117) is chosen so that, when present, side-leakage is grouped with reflectance. This is physically justified in order to minimize the number of low-order scatterings

binned as transmission. Indeed, physical intuition tells us that significant contributions from low orders-of-scattering is the hallmark of reflectance. Another physical reason for including $\partial \mathrm{M}_{\perp}(\boldsymbol{\Omega}_0)$ (when it is finite) with $\partial \mathrm{M}_{\mathrm{sunny}}(\boldsymbol{\Omega}_0)$, hence side-leakage (when it exists) with reflection, is obtained by slightly perturbing the illumination direction from the special (resonant) case that endows $\partial \mathrm{M}_{\perp}(\boldsymbol{\Omega}_0)$ with a finite area. That will generally collapse $\partial \mathrm{M}_{\perp}(\boldsymbol{\Omega}_0)$ onto $\partial \mathrm{M}_{\mathrm{term}}(\boldsymbol{\Omega}_0)$ as defined in (3.135), and put its area into that of $\partial \mathrm{M}_{\mathrm{sunny}}(\boldsymbol{\Omega}_0)$.

In summary, our manipulation of set-topological concepts (consequences of where we assign the $=$) support the physics of RT because topology is about point "proximity" and "connectedness." Spatial connection is also what transport theory is very much about.

The motivation behind discussions of side-leakage is to find a simple mechanistic model for an obvious effect of 3D geometry. Partially because the notion of side-leakage cannot be transmuted into a mathematically robust construct, Davis and Marshak (2001) have advocated the more physical concept of photon "channeling" as a better way to describe the elementary interaction between a steady, initially uniform photon flow and a spatial disturbance. Channeling is based on flow (i.e., vector-flux field) geometry rather than boundary geometry and therefore applies equally to internally variable media and to homogeneous media that are not plane-parallel if their horizontal extent is finite.

***"R/T"* Partition by Horizontal Orientation and Direction at Escape:** As if the above complications were not enough, definitions of reflection and transmission direction based on direction $\boldsymbol{\Omega}$ rather than position $\boldsymbol{x}$ are also possible and natural for horizontally finite (as well as infinite) media. Furthermore, these definitions are more likely to use the vertical rather than solar direction because of surface radiation budget considerations, as well as remote sensing. Unlike in plane-parallel geometry, the results are not the same here. Referring again to Fig. 3.12 and looking down along $-\hat{\mathbf{z}}$ at the scene from far above, we can define

$$\partial \mathrm{M}_{\mathrm{up}} = \partial \mathrm{M}_{\mathrm{sunny}}(\boldsymbol{\Omega}_0 = -\hat{\mathbf{z}}) \tag{3.137}$$

and corresponding $\partial \mathrm{M}_{\mathrm{shady}}$ is $\partial \mathrm{M}_{\mathrm{dn}}$, while $\partial \mathrm{M}_{\mathrm{term}}$ in (3.135) becomes $\partial \mathrm{M}_{\mathrm{horizon}}$. From this specific vantage point, we have

$$\begin{cases} \pi I(\boldsymbol{x}, +\hat{\mathbf{z}})/\mu_0 F_0, & \boldsymbol{x} \in \partial \mathrm{M}_{\mathrm{up}} \cap \partial \mathrm{M}_{\mathrm{sunny}}, \quad \text{nadir radiance from illuminated part} \\ \pi I(\boldsymbol{x}, +\hat{\mathbf{z}})/\mu_0 F_0, & \boldsymbol{x} \in \partial \mathrm{M}_{\mathrm{up}} \cap \partial \mathrm{M}_{\mathrm{shady}}, \quad \text{nadir radiance from shadowed part} \end{cases}, \tag{3.138}$$

the second case being impossible in slab geometry. A similar two-way partition will exist for zenith radiance

$$\pi I(\boldsymbol{x}, -\hat{\mathbf{z}})/\mu_0 F_0, \boldsymbol{x} \in \partial \mathrm{M}_{\mathrm{dn}}; \tag{3.139}$$

a sub-sample of this field along a line could be interpreted as the sequence of readings of vertically-pointing ground-based radiometer as the mean wind advects the cloud by. Analogous definitions can be spelled out for all other directions.

Encouraged by the apparent robustness of the thick-cloud limiting behavior of R/T with respect to cloud geometry, Davis (2002) applies his result for spherical non-absorbing clouds to the remote determination of the optical thickness of real-world finite clouds observed in ultra-high (5 m) resolution satellite imagery. At a purely scattering solar wavelength, all that is required is an estimate of the mean-flux ratio R/T to infer at least a rough (or "effective") value of $(1-g)\tau_{\rm diam}$.[5] This estimation of R/T is easily achieved for opaque isolated or broken cumulus clouds, especially viewed obliquely with respect to the Sun. As shown in Fig. 3.17, it is not hard to find the terminator in high-resolution images, being the relatively sharp transition between bright (reflective) and dark (transmissive) sides of the cloud. Then, since we are interested in highly scattered photons for both R and T, a Lambertian assumption that links radiance in any particular direction and flux from the corresponding surface (in this case, a cloud boundary) is not unreasonable. Therefore a radiance ratio can be equated with R/T. The ensuing (high-enough) values of $\tau_{\rm diam}$, taking as usual $g = 0.85$, are quite realistic for the type of cloud present in the scene.

Boundary radiances given for all positions and directions can be used collectively to define overall responses to collimated illumination with respect to the zenith direction: How much radiation reaches the ground (even if it is coming from the illuminated side of the cloud)? How much goes back to space (even if coming from the shaded side of the cloud)? The answers are

$$\begin{cases} R_{\uparrow} = \int\limits_{0}^{+1} \mu \mathrm{d}\mu \int\limits_{0}^{2\pi} \mathrm{d}\varphi \int\limits_{\boldsymbol{n}(\boldsymbol{x})\bullet\boldsymbol{\Omega}(\mu,\varphi)\geq 0} I(\boldsymbol{x},\boldsymbol{\Omega}(\mu,\varphi))\mathrm{d}S(\boldsymbol{x}) \;/\; [F_0 S_{\rm M}(\boldsymbol{\Omega}_0)] \\ T_{\downarrow} = \int\limits_{-1}^{0} |\mu| \mathrm{d}\mu \int\limits_{0}^{2\pi} \mathrm{d}\varphi \int\limits_{\boldsymbol{n}(\boldsymbol{x})\bullet\boldsymbol{\Omega}(\mu,\varphi)>0} I(\boldsymbol{x},\boldsymbol{\Omega}(\mu,\varphi))\mathrm{d}S(\boldsymbol{x}) \;/\; [F_0 S_{\rm M}(\boldsymbol{\Omega}_0)] \end{cases} , \tag{3.140}$$

respectively for reflection back to space and for transmission to the surface. The denominators are simplified expressions for the incoming flux $\mu_0 F_0$ measured along the vertical times the projection along the horizontal of the illuminated boundary $S_{\rm M}(\boldsymbol{\Omega}_0)/\mu_0$.

Figure 3.16b illustrates the definitions in (3.140) for the same four sequences of spherical clouds described above in connection with the companion figure under the simple assumption that $\boldsymbol{\Omega}_0 = -\hat{\mathbf{z}}$. Note that in this partition of R versus T, we have no a priori reason to divide the ratio $R_{\uparrow}/T_{\downarrow}$ by the optical thickness, but we of course still have $R_{\uparrow} + T_{\downarrow} = 1$ by conservation. We observe the same excellent collapse of the curves for $g = 0$ and $g = 0.85$ when plotted against $(1-g)\tau_{\rm diam}$ as in Fig. 3.16a. However, this only occurs when the spatially-modulated boundary sources are generated diffusely. Logically, the *isotropic* scattering media under collimated illumination merge with their isotropically illuminated counterparts in the large $\tau_{\rm diam}$ limit. However, this is clearly not the case for forward scattering media;

[5] One should say this is for the *equivalent* homogeneous sphere but that caveat is almost always omitted in descriptions of operational cloud remote sensing when applying standard plane-parallel theory to clouds that are more-or-less stratiform.

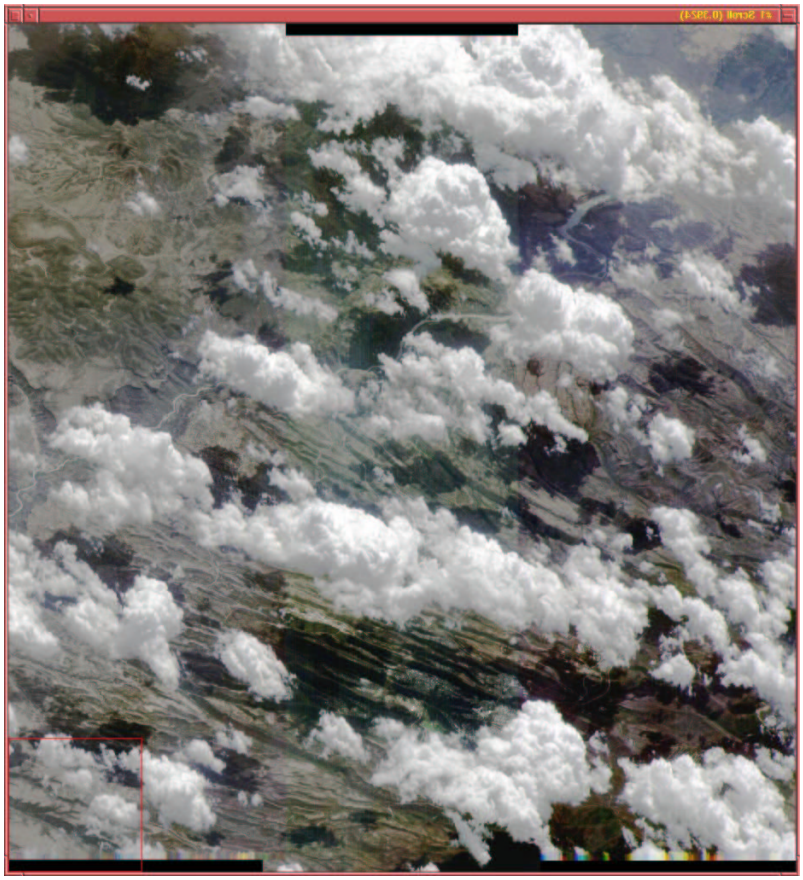

Fig. 3.17. Los Alamos (NM) scene with broken clouds captured with the Multispectral Thermal Imager (MTI) from a viewing angle of about 60°. This grey-scale image was produced from a true-color rendering of the scene based on 3 narrow channels at 484, 558, 650 nm. General characteristics of the MTI instrument and orbit are given by Weber et al. (1999). For a determination of mean optical thicknesses for three selected clouds with different outer sizes, see Davis (2002).

we attribute this to systematic reduction (enhancement) of $R_\uparrow$ ($T_\downarrow$) by low-orders of scattering that are always present in reflected light but dominate in the periphery (near-terminator) of the cloud. The small $\tau_{\rm diam}$ behavior here is exactly the same as for R/T according to position at escape in Fig. 3.16a, only without dividing by the independent variable $\tau_{\rm diam}$.

Discussion: It is physically obvious (and rigorously proven by reversing the angular and surface integrals) that absorptions computed from $1-R-T$ in (3.133) and $1-R_\uparrow-T_\downarrow$ in (3.140) are equal. The main point here is that solar sources

in finite clouds yield only two kinds of light: reflected and transmitted, just as in plane-parallel geometry. Transmitted light comes from the boundary points *far* from the sources and, at least for optically thick media, is characterized by high orders-of-scattering and accordingly low radiance levels. Reflected light comes from the boundary points *close* to the sources and, for optically thick media, is characterized by a broad distribution of orders-of-scattering (from a single scattering to at least as many as it typically takes to be transmitted); this circumstance will naturally correlate with relatively high levels of radiance. If the definitions of transmission and reflection are predicated on direction with respect to the vertical direction rather than boundary topology and source direction, then they will be mixtures of the above more physical definition based on position. This is true even if the axis of symmetry of the finite cloud (if it exists) is aligned with the vertical. Only in plane-parallel geometry do the definitions coincide.

A far-reaching consequence of the physics-based partition of escaping radiation by connection to the source is that, apart from a set of photon beams of measure 0 (propagating exactly horizontally), there is no such thing as "side-leakage" from a finite cloud. There is only reflected and transmitted light. However, transmitted photons may be traveling downward or upward, thus possibly misleading satellite remote-sensing algorithms that are hard-coded to think that clouds have to be bright. Similarly, reflected photons may be traveling upward or downward, thus contributing possibly very strongly to surface fluxes. To illustrate this last effect, Fig. 3.18 uses time-series two days long of the direct broad-band (BB) solar flux, measured normal to the beam, and the total BB down-welling surface flux collected in Boulder (Co); the diffuse down-welling flux was also detected. The first day (July 10, 2003) was clear, the next day ended with an episode of broken cloudiness. We first note in panel (a) that in the presence of broken clouds the total vertical flux can vastly exceed its clear-sky counterpart and even the direct flux measured perpendicular to the beam (i.e., without the μ_0 factor). Panel (b) shows, on the one hand, how the diffuse down-welling flux is driven almost linearly by the direct solar flux (single scattering dominates and optical distances are small enough to set $\exp(-\tau) \approx 1 - \tau$) and, on the other hand, how much the diffuse BB component is non-linearly enhanced by broken clouds. At non-absorbed VIS-NIR wavelengths, scattering by clouds can cause total transmittance to exceed unity.

Finite clouds in spherical refractive atmospheres open up even more interesting paradoxes with direct illumination of cloud base. This is a frequent and often spectacular display of radiance for ground-based observers located near the terminator of planet Earth, locally identified as sunset and sunrise.

3.10 Green Functions to Reciprocity via Adjoint Transport

We cover formal Green function theory for the RTE and relate it to the adjoint RT problem, both are essential to a number of applications and numerical techniques in 3D RT. This also provides the natural framework for introducing the *reciprocity*

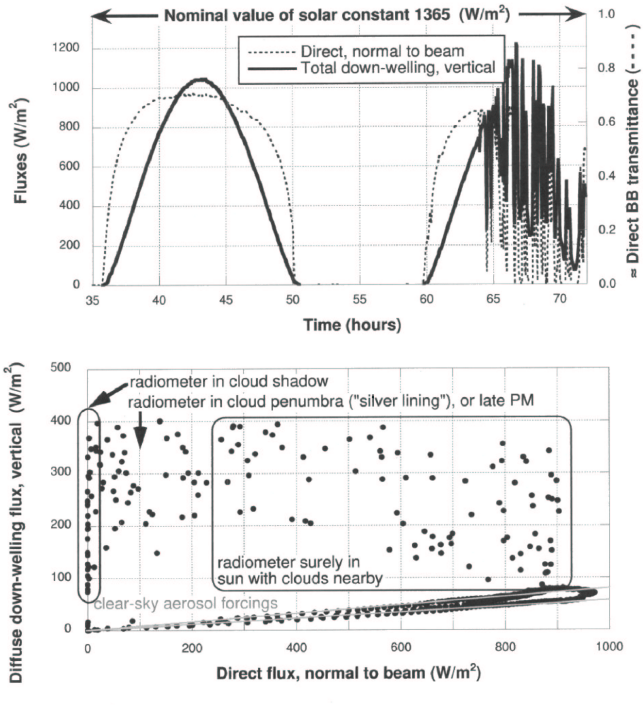

Fig. 3.18. Broken clouds enhance total down-welling surface flux far beyond the clear-sky direct contribution. **(upper)** The total vertical down-welling flux can vastly exceed the direct flux normal to the beam. **(lower)** A rough partition of the scatter plot of diffuse/vertical vs. direct/normal fluxes from upper panel. The data, courtesy of John Augustine and Gary Hodges from NOAA, was collected in Boulder (Co) on July 10-11, 2003.

principle which may or may not apply in a given 3D atmosphere-surface system depending on its inherent properties and the conditions surrounding the observations.

3.10.1 Green Functions in Radiative Transfer Theory

Definitions. Consider a 3D absorbing and scattering medium M bounded by a non-reflecting and non-emitting boundary ∂M. The *volume* Green function $G_{\mathrm{V}}(\boldsymbol{x}, \boldsymbol{\Omega}; \boldsymbol{x}', \boldsymbol{\Omega}')$ is the radiative response of M at a point $\boldsymbol{x}$, in direction $\boldsymbol{\Omega}$, to a monodirectional point-source located at a *given* point $\boldsymbol{x}'$ in M, continuously emitting photons in a *given* direction $\boldsymbol{\Omega}'$. The volume Green function satisfies the RTE

(3.102)-(3.103) with δ function source term Q, i.e.,

$$\begin{aligned}\boldsymbol{\Omega}\bullet\nabla G_{\mathrm{V}}(\boldsymbol{x},\boldsymbol{\Omega};\boldsymbol{x}',\boldsymbol{\Omega}')+\sigma(\boldsymbol{x})G_{\mathrm{V}}(\boldsymbol{x},\boldsymbol{\Omega};\boldsymbol{x}',\boldsymbol{\Omega}')\\ =\sigma_s(\boldsymbol{x})\oint_{\Xi}p(\boldsymbol{x},\boldsymbol{\Omega}''\rightarrow\boldsymbol{\Omega})G_{\mathrm{V}}(\boldsymbol{x},\boldsymbol{\Omega}'';\boldsymbol{x}',\boldsymbol{\Omega}')\mathrm{d}\boldsymbol{\Omega}''\\ +\delta_{\mathrm{V}}(\boldsymbol{x}-\boldsymbol{x}')\delta(\boldsymbol{\Omega}-\boldsymbol{\Omega}')\end{aligned}\tag{3.141}$$

with homogeneous (no entering radiance) BCs. Here $\delta(\boldsymbol{\Omega}-\boldsymbol{\Omega}')$, in sr^{-1}, and $\delta_{\mathrm{V}}(\boldsymbol{x}-\boldsymbol{x}')$, in m^{-3}, are Dirac delta-functions. Note that $\delta_{\mathrm{V}}(\boldsymbol{x}-\boldsymbol{x}')\delta(\boldsymbol{\Omega}-\boldsymbol{\Omega}')$ is a volume source normalized by its power. The volume Green function, therefore, is expressed in $\mathrm{m}^{-2}\mathrm{sr}^{-1}$. It should be also noted that the point $\boldsymbol{x}'$ and the direction of the monodirectional source $\boldsymbol{\Omega}'$ are *parameters* in the RTE; that is, the determination of the complete Green function requires to solve (3.142) for each and every point $\boldsymbol{x}'\in\mathrm{M}$ and direction $\boldsymbol{\Omega}'\in\Xi$.

In the "operator" language introduced in (3.102)-(3.103), (3.142) can be written simply as $L\,G_{\mathrm{V}}=\delta$ where the δ-function source term takes care of all the photon state-variables of immediate interest (position, direction). After performing a spherical harmonic decomposition in angle space and a 3D Fourier transform in position space (i.e., a continuous decomposition on harmonic functions), this concise formulation becomes $\tilde{L}\,\tilde{G}_{\mathrm{V}}=1$ where the tilde designates a transformed entity. So, it is not surprising that in some literatures the Green function is denoted $G_{\mathrm{V}}=L^{-1}$, i.e., as the inverse of a linear operator. This expresses the fact that knowing G_{V} or knowing L (including knowledge of the spatial distribution of the optical properties in M) are formally equivalent. The Green function is therefore called the "fundamental" solution or "resolvant" of the problem at hand, in this case, the RT problem. In this operator formalism, the solution to the general linear transport problem, $L\,I=Q$ (subject to homogeneous BCs), is $I=L^{-1}Q=G_{\mathrm{V}}Q$ which is short-hand for a 5-dimensional integral over the source positions and directions.

In the case of purely absorbing media ($\sigma_{\mathrm{s}}(\boldsymbol{x})\equiv 0$), the solution to (3.142) already derived in Sect. 3.8.2 can by given in explicit form using the volume GF (Case and Zweifel, 1967). Bearing in mind that it is designed to be the kernel of 5-dimensional integral, the Green function is best written as

$$G_{\mathrm{V}}(\boldsymbol{x},\boldsymbol{\Omega};\boldsymbol{x}',\boldsymbol{\Omega}')=\frac{\exp[-\tau(\boldsymbol{x}',\boldsymbol{x})]}{\|\boldsymbol{x}'-\boldsymbol{x}\|^2}\delta(\boldsymbol{\Omega}'-\boldsymbol{\Omega})\delta\left(\frac{\boldsymbol{x}'-\boldsymbol{x}}{\|\boldsymbol{x}'-\boldsymbol{x}\|}-\boldsymbol{\Omega}\right).\tag{3.142}$$

This follows from the exact "no-scattering" solution in (3.119) with no boundary sources ($f(\cdot)\equiv 0$ on ∂M) and using the identities in (3.121)-(3.122). The resemblance of the GF in (3.142) with the kernels (3.124) and (3.128) of the integral forms of the RTE covered in the previous section is not accidental: the scattering quantities $\sigma_{\mathrm{s}}p(\boldsymbol{\Omega}'\rightarrow\boldsymbol{\Omega})$ are replaced by $\delta(\boldsymbol{\Omega}'-\boldsymbol{\Omega})$. Also, and contrary to the ones used previously in this section, the last δ-function is non-dimensional. Indeed, it is paired with $\mathrm{d}\boldsymbol{x}'$ (in m^{-3}) and, in its argument, $\boldsymbol{x}'$ is divided by the distance $\|\boldsymbol{x}'-\boldsymbol{x}\|$. Finally, the $\|\boldsymbol{x}'-\boldsymbol{x}\|^{-2}$ term does *not* express an algebraic decay (in addition to $\tau(\boldsymbol{x}',\boldsymbol{x})$ is constant). The source is indeed monodirectional, in which case we know from previous sections that it is only affected by extinction term $\exp[-\tau(\boldsymbol{x}',\boldsymbol{x})]$. Rather, this

algebraic term comes from the Jacobian required to go from the one-dimensional integral in $s = \|\boldsymbol{x}' - \boldsymbol{x}\|$, as mandated by the directional derivative in (3.142), to a three-dimensional integral in $\mathrm{d}\boldsymbol{x}'$ by bringing in a solid angle integral in $\mathrm{d}\boldsymbol{\Omega}$.

The *surface* Green function, $G_{\mathrm{S}}(\boldsymbol{x}, \boldsymbol{\Omega}; \boldsymbol{x}_{\mathrm{S}}, \boldsymbol{\Omega}')$, is the solution to the transport equation in (3.142) but without the volume source term. However, radiation is penetrating into the medium through the surface $\partial\mathrm{M}$ as given by the inhomogeneous BC

$$G_{\mathrm{S}}(\boldsymbol{x}, \boldsymbol{\Omega}; \boldsymbol{x}_{\mathrm{S}}, \boldsymbol{\Omega}') = \delta_{\mathrm{S}}(\boldsymbol{x} - \boldsymbol{x}_{\mathrm{S}})\delta(\boldsymbol{\Omega} - \boldsymbol{\Omega}'),\ \boldsymbol{x} \in \partial\mathrm{M},\ \boldsymbol{\Omega} \bullet \boldsymbol{n}(\boldsymbol{x}) < 0, \qquad (3.143)$$

i.e., a point source at $\boldsymbol{x}_{\mathrm{S}} \in \partial\mathrm{M}$ emitting with unitary power in the direction $\boldsymbol{\Omega}'$. Here $\delta_{\mathrm{S}}(\cdot)$ is a two-dimensional δ function (in m^{-2}). Thus, $G_{\mathrm{S}}(\boldsymbol{x}, \boldsymbol{\Omega}; \boldsymbol{x}_{\mathrm{S}}, \boldsymbol{\Omega}')$ is the radiative response of the medium M at a point $\boldsymbol{x}$, in direction $\boldsymbol{\Omega}$, to a collimated boundary source. Because sources can be located on the boundary, the volume and surface Green functions are related:

$$G_{\mathrm{S}}(\boldsymbol{x}, \boldsymbol{\Omega}; \boldsymbol{x}_{\mathrm{S}}, \boldsymbol{\Omega}') = |\boldsymbol{n}(\boldsymbol{x}_{\mathrm{S}}) \bullet \boldsymbol{\Omega}'\,| G_{\mathrm{V}}(\boldsymbol{x}, \boldsymbol{\Omega}; \boldsymbol{x}_{\mathrm{S}}, \boldsymbol{\Omega}'), \qquad (3.144)$$

as is shown further on.

In terms of these two Green functions, we may write the general solution to the RTE (3.101) with arbitrary volume source $Q(\boldsymbol{x}, \boldsymbol{\Omega})$ and BCs (3.109) with sources given by $f(\boldsymbol{x}_{\mathrm{S}}, \boldsymbol{\Omega})$. We obtain

$$\begin{aligned} I(\boldsymbol{x}, \boldsymbol{\Omega}) = &\int_{\mathrm{M}} \oint_{\Xi} G_{\mathrm{V}}(\boldsymbol{x}, \boldsymbol{\Omega}; \boldsymbol{x}', \boldsymbol{\Omega}') Q(\boldsymbol{x}', \boldsymbol{\Omega}') \mathrm{d}\boldsymbol{x}' \mathrm{d}\boldsymbol{\Omega}' \\ &+ \int_{\boldsymbol{x}_{\mathrm{S}} \in \partial\mathrm{M}} \mathrm{d}S(\boldsymbol{x}_{\mathrm{S}}) \int_{\boldsymbol{n}(\boldsymbol{x}_{\mathrm{S}}) \bullet \boldsymbol{\Omega} < 0} G_{\mathrm{S}}(\boldsymbol{x}, \boldsymbol{\Omega}; \boldsymbol{x}_{\mathrm{S}}, \boldsymbol{\Omega}') f(\boldsymbol{x}_{\mathrm{S}}, \boldsymbol{\Omega}') \mathrm{d}\boldsymbol{\Omega}'. \end{aligned} \qquad (3.145)$$

The first term in (3.145) is the solution of the 3D transport equation with the volume sources $Q(\boldsymbol{x}, \boldsymbol{\Omega})$ and no incoming radiance. The second term describes the 3D radiation field in M generated by the sources $f(\boldsymbol{x}, \boldsymbol{\Omega})$ distributed over the boundary $\partial\mathrm{M}$.

The Green function concept was originally developed in neutron transport theory several decades ago (Bell and Glasstone, 1970). It has enabled the reformulation of the radiative transfer problems in terms of some "basic" subproblems and to express the solution to the transport equation with arbitrary sources and boundary conditions as a superposition of the solutions of the basic subproblems. We now demonstrate with a relevant example.

Illustration with Cloud-Surface Interaction. Consider a cloudy or aerosol layer bounded from below by a non-uniform Lambertian surface. This is a problem of considerable interest in satellite remote sensing of surface properties (Lyapustin and Knyazikhin, 2002) as well as ground-based remote sensing of clouds (Marshak et al., 2000). Photon-cloud-surface interaction can be described by the RTE with zero

volume sources and BCs given in Sect. 3.6.2. The intensity $I(\boldsymbol{x}, \boldsymbol{\Omega})$ can be represented as a sum of two components: the radiation calculated for a "black" surface, $I_{\rm blk}(\boldsymbol{x}, \boldsymbol{\Omega})$, and the remaining radiation, $I_{\rm rem}(\boldsymbol{x}, \boldsymbol{\Omega})$; that is,

$$I(\boldsymbol{x}, \boldsymbol{\Omega}) = I_{\rm blk}(\boldsymbol{x}, \boldsymbol{\Omega}) + I_{\rm rem}(\boldsymbol{x}, \boldsymbol{\Omega}). \tag{3.146}$$

In (3.146), the second component accounts for the radiation field excited by multiple surface-cloud interactions. It satisfies $LI_{\rm rem} = 0$, with a homogeneous (zero-incoming radiance) BC on the upper boundary, and

$$I_{\rm rem}(\boldsymbol{x}_{\rm S}, \boldsymbol{\Omega}) = \pi^{-1} \alpha(\boldsymbol{x}_{\rm S}) F(\boldsymbol{x}_{\rm S}) \tag{3.147}$$

at the lower boundary $z = 0$ where $\alpha(\boldsymbol{x}_{\rm S})$ is the variable surface albedo, assumed Lambertian, and $F(\boldsymbol{x}_{\rm S})$ is a variable down-welling hemispherical flux assumed, for the moment, to be prescribed. Note that since the geometry of this medium is plane-parallel, as in Sect. 3.6.2, we could use the "split" notation $\boldsymbol{x}_{\rm S} = (\vec{x}_{\rm S}, z_{\rm S})^{\rm T}$ here, but we will continue to use notation that applies to the most general medium geometry.

The remaining radiation can be expressed through the surface Green function as

$$I_{\rm rem}(\boldsymbol{x}, \boldsymbol{\Omega}) = \frac{1}{\pi} \int\limits_{z_{\rm S}=0} \alpha(\boldsymbol{x}_{\rm S}) F(\boldsymbol{x}_{\rm S}) [\int\limits_{\mu'<0} G_{\rm S}(\boldsymbol{x}, \boldsymbol{\Omega}; \boldsymbol{x}_{\rm S}, \boldsymbol{\Omega}') {\rm d}\boldsymbol{\Omega}'] \, {\rm d}S(\boldsymbol{x}_{\rm S}). \tag{3.148}$$

In (3.148), the integral over upward directions describes the radiation field in M generated by an isotropic point-source $\pi^{-1}\delta(\boldsymbol{x} - \boldsymbol{x}_{\rm S})$ located at the point $\boldsymbol{x}_{\rm S} \in \partial{\rm M}$. Given the downward flux field $F(\boldsymbol{x}_{\rm S})$ at the lower boundary, the remaining radiance $I_{\rm rem}$ can be evaluated from (3.148). The field $F(\boldsymbol{x}_{\rm S})$ itself depends on $I_{\rm rem}$ and thus (3.148) alone provides a full description of surface-cloud interactions. Combining (3.146) and (3.148), one obtains a *two*-dimensional integral equation for the unknown total flux $F_z^{(-)}(\boldsymbol{x}_{\rm S})$ for $\boldsymbol{x}_{\rm S} \in \partial{\rm M}$ (meaning here the plane $z = 0$):

$$F_z^{(-)}(\boldsymbol{x}) = \int\limits_{z_{\rm S}=0} \alpha(\boldsymbol{x}'_{\rm S}) R(\boldsymbol{x}_{\rm S}, \boldsymbol{x}'_{\rm S}) F_z^{(-)}(\boldsymbol{x}'_{\rm S}) {\rm d}S(\boldsymbol{x}'_{\rm S}) + F_{z,{\rm blk}}^{(-)}(\boldsymbol{x}). \tag{3.149}$$

This unknown flux accounts for what the cloud transmits as well as all the multiple surface-cloud interactions. Here $F_{z,{\rm blk}}^{(-)}$ is the downward flux at the bottom of the medium calculated for the "black" surface problem and acts as a source term in the integral equation. $R(\boldsymbol{x}_{\rm S}, \boldsymbol{x}'_{\rm S})$ is the downward flux at $\boldsymbol{x}_{\rm S} \in \partial{\rm M}$ generated by the point-wise and isotropic source $\pi^{-1}\delta(\boldsymbol{x}_{\rm S} - \boldsymbol{x}'_{\rm S})$ located at $\boldsymbol{x}_{\rm S} \in \partial{\rm M}$ and it acts as a kernel for the integral equation in (3.149). In turn, this kernel is given by an integral of the surface Green function:

$$R(\boldsymbol{x}_{\rm S}, \boldsymbol{x}'_{\rm S}) = \int\limits_{\mu>0} \mu {\rm d}\boldsymbol{\Omega} \int\limits_{\mu'<0} \pi^{-1} G_{\rm S}(\boldsymbol{x}_{\rm S}, \boldsymbol{\Omega}; \boldsymbol{x}'_{\rm S}, \boldsymbol{\Omega}') {\rm d}\boldsymbol{\Omega}', \tag{3.150}$$

for any pair of surface points $(\boldsymbol{x}_{\rm S}, \boldsymbol{x}'_{\rm S})$. Notice that we are preserving angular symmetry between the isotropic source at $\boldsymbol{x}'_{\rm S}$ and the resulting field at $\boldsymbol{x}_{\rm S}$. If moreover

the atmosphere is horizontally uniform, then we are sure that the GF in (3.150) will depend only on $||\boldsymbol{x}_{\rm S} - \boldsymbol{x}'_{\rm S}||$. This makes the integral in (3.149) a straightforward convolution product.

We now return to the aerosol "adjacency" and cloud remote sensing problems that motivated this exercise. Because the above horizontally uniformity assumption is viable for aerosol atmosphere, we have reduced the full 3D RT problem of assessing the mixture of albedo values $\alpha(\boldsymbol{x}_{\rm S})$ in the observations $I(\boldsymbol{x}, \boldsymbol{\Omega})$, e.g., from space, to an integral equation that is easily solved in Fourier space. For more details about this adjacency mitigation strategy in remote sensing, including generalization to non-Lambertian ground, we refer to the paper by Lyapustin and Knyazikhin (2002). In the case of clouds, the same horizontally uniformity assumption is of course highly questionable. Nonetheless, by working with two wavelengths that where the clouds have similar scattering properties, but the ground's reflection properties not, one can minimize the impact of 3D RT effects in the observations and apply 1D RT theory locally to infer cloud properties. More details about this mitigation technique in the paper by Marshak et al. (2000).

Inverse Problems. Green functions play an important role in developing algorithms for retrieving coefficients in the RTE from radiation leaving a medium, in other words, performing an optical tomography. Choulli and Stefanov (1996) and Antyufeev and Bondarenko (1996) reported that, under quite general conditions on the sources, the 3D fields of *total* cross-section (per unit of length), $\sigma(\boldsymbol{x})$, and the *differential* scattering cross-section, $\sigma_{\rm s}(\boldsymbol{x})p(\boldsymbol{x}, \boldsymbol{\Omega} \rightarrow \boldsymbol{\Omega}')$, can be uniquely retrieved from boundary-field measurements. This result indicates that there is a one-to-one correspondence between the complex 3D structure of a given domain M of space bounded by a non-reflecting surface ∂M and the outgoing boundary radiation field $I(\boldsymbol{x}_{\rm S}, \boldsymbol{\Omega})$, $\boldsymbol{x}_{\rm S} \in \partial$M, $\boldsymbol{n}(\boldsymbol{x}_{\rm S}) \bullet \boldsymbol{\Omega} > 0$. The following interpretation of the Green function underlies the derivation of this property.

The volume and surface Green functions describe the radiative response of the medium M to a source concentrated at an isolated spatial point and emitting photons in one direction. A Dirac δ function is naturally used to describe such a source. The theory of distributions developed by Laurent Schwartz (Schwartz, 1950) justifies the use of such functions in describing and solving physical problems. Since the boundary condition is expressed in terms of a Schwartz distribution, the solution to the transport equation is a distribution too. Schwartz's theory distinguishes two types of functions, "regular" and "singular" distributions.

There is a one-to-one correspondence between usual functions (with a well-defined value for each value of its argument) and regular distributions; thus, an ordinary function can be regarded as a special case of a distribution. The Dirac δ-function is the simplest example of a singular distribution. No usual function can be identified with it and it is only defined under integral operations.

Generally speaking, the solution of the RTE can be expressed as a sum of regular and singular distributions. The singular component must be treated separately because numerical techniques cannot deal with bone fide distributions. A technique to

separate the singular components from (3.142) is based on the following result (Germogenova, 1986; Choulli and Stefanov, 1996; Antyufeev and Bondarenko, 1996). For a 3D medium, the radiances due to uncollided and single-scattered photons from a point-wise mono-directional source, denoted respectively G_0 and G_1, are singular distributions while the remaining multiply-scattered field is described by a regular distribution $G_{\rm ms}$. The Green function is therefore the sum of two singular and one regular component:

$$G = G_0 + G_1 + G_{\rm ms}. \tag{3.151}$$

The singular components make the above mentioned one-to-one correspondence between observable radiance fields and optical properties possible. This generalizes the classic idea of tomographic reconstruction based only on the uncollided (a.k.a. directly-transmitted) radiance in G_0 and opens the possibility of using reflected radiance to perform 3D reconstruction. Application of this technique to describe radiation regimes in clouds and vegetation canopies are discussed respectively by Knyazikhin et al. (2002) and Zhang et al. (2002). More on this will be found in Chap. ???.

We can anticipate that in optically-dense weakly-absorbing media $G_{\rm ms}$ will generally be the dominant term and its removal from the measurements of boundary radiances can leave estimates of the singular component $G_0 + G_1$ at par with the instrumental noise level. In this situation, radically different techniques that capitalize on $G_{\rm ms}$ and photon "diffusion-wave" theory can be invoked (Yodh and Chance, 1995, and references therein). Here exact 3D reconstruction is of course not an option, but large-enough and strong-enough inhomogeneities can be detected.

3.10.2 Adjoint Radiative Transfer

Definitions. Adjoint equations and their solutions play an important role in radiative transfer theory. Adjoint functions are, in a very real sense, orthogonal to the solutions of the radiative transfer equation. For this and other reasons, they are widely used in perturbation theory and variational calculations relating to the behavior of 3D optical media. The properties of the solutions of the adjoint RTE are also used in the development of effective Monte Carlo calculations (Marchuk et al., 1980).

The adjoint RTE can be written formally as

$$L^* I^* = Q^*, \tag{3.152}$$

where L^* is the adjoint integro-differential linear transport operator,

$$L^* = -\mathbf{\Omega} \bullet \nabla + \sigma(\boldsymbol{x}) - \sigma_{\rm s}(\boldsymbol{x}) \oint\limits_{\Xi} p(\boldsymbol{x}, \mathbf{\Omega} \to \mathbf{\Omega}')[\cdot] {\rm d}\mathbf{\Omega}'. \tag{3.153}$$

The following differences should be noted between L^* in (3.153) and L in (3.103):

1. the Lagrangian derivative has the opposite sign, and
2. the incident and scattering directions have been interchanged, i.e., $\mathbf{\Omega}' \to \mathbf{\Omega}$ in (3.103) becomes $\mathbf{\Omega} \to \mathbf{\Omega}'$ in (3.153).

Physically, we are considering here the time-reversed photon flow. This gives us the hint that adjoint sources Q^* describe the position of detectors while the adjoint transport operator L^* takes them backwards in time to actual sources. This makes the space-angle distribution I^* of adjoint "photons" an estimate of how much a given position-direction matters for a given radiometric observation (often in a remote region) modeled by Q^*. We are thus looking for the solution of (3.153) satisfying the adjoint BCs, namely,

$$I^*(\boldsymbol{x}, \boldsymbol{\Omega}) = f^*(\boldsymbol{x}, \boldsymbol{\Omega}),\ \boldsymbol{x} \in \partial \mathrm{M},\ \boldsymbol{\Omega} \bullet \boldsymbol{n}(\boldsymbol{x}) > 0. \tag{3.154}$$

Note that this boundary condition is formulated for *outgoing* directions. This makes physical sense if there are detectors at the boundaries. If there are not ($f^* \equiv 0$), then escaping photons will no longer influence detectors inside the medium (where $Q^* \neq 0$).

To capture the notions of weight and influence used here to give physical meaning to the adjoint radiance field, some authors (Marchuk, 1964) have came to call I^* "importance." Adjoint equations are used many fields of dynamical modeling to analyze nonlinear tele-connections. In meteorology, this can be done by looking at the clusters of backwards trajectories which, in turn, has influenced data assimilation methodology. In 3D RT, one can think of the 3D "component" of the radiance field as response to a perturbation of uniformity in extinction. It is therefore not surprising that adjoint RT theory — and indeed adjoint GFs introduced below — play a key role in the perturbative approach to 3D RT (Box et al., 1989; Polonsky and Davis, 2003).

Some Useful Identities. To describe the relationship between solutions of the standard (or "forward") and adjoint radiative transfer equations, the "inner" product of two RT functions $f(\boldsymbol{x}, \boldsymbol{\Omega})$ and $g(\boldsymbol{x}, \boldsymbol{\Omega})$ is introduced:

$$< f, g > = \int\limits_{\mathrm{M}} \oint\limits_{\Xi} f(\boldsymbol{x}, \boldsymbol{\Omega}) g(\boldsymbol{x}, \boldsymbol{\Omega}) \mathrm{d}\boldsymbol{\Omega} \mathrm{d}\boldsymbol{x}. \tag{3.155}$$

Now let $I(\boldsymbol{x}, \boldsymbol{\Omega})$ be the solution of the forward problem, i.e., I satisfies the RTE $LI = Q$ and the generic BCs in (3.109). This equation is now multiplied by I^* and (3.152) by I; the resulting expressions are subtracted and the difference is integrated over M and Ξ. Taking into account the identity

$$< \boldsymbol{\Omega} \bullet \nabla I, I^* > = - < I, \boldsymbol{\Omega} \bullet \nabla I^* > + \int\limits_{\partial \mathrm{M}} \mathrm{d}S(\boldsymbol{x}) \oint\limits_{\Xi} \boldsymbol{n}(\boldsymbol{x}) \bullet \boldsymbol{\Omega} I(\boldsymbol{x}, \boldsymbol{\Omega}) I^*(\boldsymbol{x}, \boldsymbol{\Omega}) \mathrm{d}\boldsymbol{\Omega}, \tag{3.156}$$

one obtains the basic relationship between solutions of the forward and adjoint RTE, namely,

$$< Q, I^* > - < I, Q^* > = \int\limits_{\partial \mathrm{M}} \mathrm{d}S(\boldsymbol{x}) \int\limits_{\boldsymbol{n}(\boldsymbol{x})\bullet\boldsymbol{\Omega}>0} \boldsymbol{n}(\boldsymbol{x})\bullet\boldsymbol{\Omega} I(\boldsymbol{x},\boldsymbol{\Omega}) f^*(\boldsymbol{x},\boldsymbol{\Omega})\mathrm{d}\boldsymbol{\Omega}$$
$$- \int\limits_{\partial \mathrm{M}} \mathrm{d}S(\boldsymbol{x}) \int\limits_{\boldsymbol{n}(\boldsymbol{x})\bullet\boldsymbol{\Omega}<0} |\boldsymbol{n}(\boldsymbol{x})\bullet\boldsymbol{\Omega}| f(\boldsymbol{x},\boldsymbol{\Omega}) I^*(\boldsymbol{x},\boldsymbol{\Omega})\mathrm{d}\boldsymbol{\Omega}. \tag{3.157}$$

In the case of the homogeneous BCs, no incoming photons ($f \equiv 0$) and no outgoing adjoint flux ($f^* \equiv 0$), (3.157) can be simplified to $< Q, I^* > = < I, Q^* >$, or explicitly

$$\int\limits_{\mathrm{M}} \oint\limits_{\Xi} Q(\boldsymbol{x},\boldsymbol{\Omega}) I^*(\boldsymbol{x},\boldsymbol{\Omega})\mathrm{d}\boldsymbol{x}\mathrm{d}\boldsymbol{\Omega} = \int\limits_{\mathrm{M}} \oint\limits_{\Xi} Q^*(\boldsymbol{x},\boldsymbol{\Omega}) I(\boldsymbol{x},\boldsymbol{\Omega})\mathrm{d}\boldsymbol{x}\mathrm{d}\boldsymbol{\Omega}. \tag{3.158}$$

Connection with Green Functions. By substituting $Q(\boldsymbol{x},\boldsymbol{\Omega}) = \delta_{\mathrm{V}}(\boldsymbol{x}-\boldsymbol{x}_1)\delta(\boldsymbol{\Omega}-\boldsymbol{\Omega}_1)$ in (3.158), hence $I(\boldsymbol{x},\boldsymbol{\Omega}) \equiv G_{\mathrm{V}}(\boldsymbol{x},\boldsymbol{\Omega};\boldsymbol{x}_1,\boldsymbol{\Omega}_1)$, one obtains

$$I^*(\boldsymbol{x}_1,\boldsymbol{\Omega}_1) = \int\limits_{\mathrm{M}} \oint\limits_{\Xi} Q^*(\boldsymbol{x},\boldsymbol{\Omega}) G_{\mathrm{V}}(\boldsymbol{x},\boldsymbol{\Omega};\boldsymbol{x}_1,\boldsymbol{\Omega}_1)\mathrm{d}\boldsymbol{x}\mathrm{d}\boldsymbol{\Omega}. \tag{3.159}$$

Thus, $I^*(\boldsymbol{x}_1,\boldsymbol{\Omega}_1)$ is a Q^*-weighted integral response of the medium to a monodirectional point-source. In other words, the adjoint solution $I^*(\boldsymbol{x}_1,\boldsymbol{\Omega}_1)$ is a measure of the "importance" for the medium's response of a photon leaving from $(\boldsymbol{x},\boldsymbol{\Omega})$. For example, it follows from the adjoint BCs (3.154) with $f^* \equiv 0$ that a photon at the non-reflecting boundary of the medium M and about to leave it has no importance whatsoever since it cannot return. By further substituting $Q^*(\boldsymbol{x},\boldsymbol{\Omega}) = \delta_{\mathrm{V}}(\boldsymbol{x}-\boldsymbol{x}_2)\delta(\boldsymbol{\Omega}-\boldsymbol{\Omega}_2)$ into (3.159), the relation between the forward and adjoint volume Green functions is obtained:

$$G_{\mathrm{V}}(\boldsymbol{x}_2,\boldsymbol{\Omega}_2;\boldsymbol{x}_1,\boldsymbol{\Omega}_1) = G^*_{\mathrm{V}}(\boldsymbol{x}_1,\boldsymbol{\Omega}_1;\boldsymbol{x}_2,\boldsymbol{\Omega}_2). \tag{3.160}$$

This symmetry makes sense since one goes from the linear transport operator in (3.103) to its adjoint counterpart in (3.150) by reversing the Lagrangian flow.

Equation (3.157) yields a useful result when the solution of the forward problem is a volume Green function, and that of the adjoint problem is a surface Green function. We set $Q(\boldsymbol{x},\boldsymbol{\Omega}) = \delta_{\mathrm{V}}(\boldsymbol{x}-\boldsymbol{x}_1)\delta(\boldsymbol{\Omega}-\boldsymbol{\Omega}_1)$ and $f \equiv 0$ for the forward problem, and $Q^* \equiv 0$, $f^*(\boldsymbol{x},\boldsymbol{\Omega}) = \delta_{\mathrm{S}}(\boldsymbol{x}-\boldsymbol{x}_{\mathrm{S}})\delta(\boldsymbol{\Omega}-\boldsymbol{\Omega}_2)$, $\boldsymbol{x}_{\mathrm{S}} \in \partial\mathrm{M}$, $\boldsymbol{n}(\boldsymbol{x}_{\mathrm{S}})\bullet\boldsymbol{\Omega}_2 > 0$, for the adjoint problem. Substituting these into (3.157) results in

$$G^*_{\mathrm{S}}(\boldsymbol{x}_1,\boldsymbol{\Omega}_1;\boldsymbol{x}_{\mathrm{S}},\boldsymbol{\Omega}_2) = \boldsymbol{n}(\boldsymbol{x}_{\mathrm{S}})\bullet\boldsymbol{\Omega}_2\; G_{\mathrm{V}}(\boldsymbol{x}_{\mathrm{S}},\boldsymbol{\Omega}_2;\boldsymbol{x}_1,\boldsymbol{\Omega}_1) \tag{3.161}$$

where $\boldsymbol{x}_{\mathrm{S}}$ is on the boundary. Using (3.159), this leads to (3.144) since $\boldsymbol{\Omega}'$ in the forward problem is equated with $-\boldsymbol{\Omega}_2$ in the adjoint problem. A relationship between the surface Green function and its adjoint can be derived from (3.157) in a similar manner.

3.10.3 Reciprocity Principle

Formulation with Green Functions. Intensity $G(\boldsymbol{x}_2, \boldsymbol{\Omega}_2; \boldsymbol{x}_1, \boldsymbol{\Omega}_1)$ at $\boldsymbol{x}_2$ in direction $\boldsymbol{\Omega}_2$ due to a point source at $\boldsymbol{x}_1$ emitting in direction $\boldsymbol{\Omega}_1$ can be related to the intensity at $\boldsymbol{x}_1$ in direction $-\boldsymbol{\Omega}_1$ due to a source at $\boldsymbol{x}_2$ emitting in direction $-\boldsymbol{\Omega}_2$ by means of the RTE. Such reciprocity relations often prove useful in relating the solution of a particular problem to that of a simpler problem or to one for which the solution is known. The adjoint RTE can be used to derive reciprocity relations. In this following, we will assume that

$$p(\boldsymbol{x}, -\boldsymbol{\Omega}' \to -\boldsymbol{\Omega}) = p(\boldsymbol{x}, \boldsymbol{\Omega} \to \boldsymbol{\Omega}'), \tag{3.162}$$

which is certainly the case if the scattering phase function depends only on the scattering angle $\cos^{-1}(\boldsymbol{\Omega} \bullet \boldsymbol{\Omega}')$. This is a reasonable assumption in most atmospheric applications. It should be noted, however, that this property does not generally hold true in the case of radiative transfer in vegetation canopies; see Chap. ???.

Consider a 3D absorbing and scattering medium M bounded by a non-reflecting surface ∂M. Let Q and f be the volume and boundary sources, respectively. Intensity $I(\boldsymbol{x}, \boldsymbol{\Omega})$ of the 3D radiation field satisfies the RTE (3.101) and general BCs (3.109). If a function I^* is defined such that $I^*(\boldsymbol{x}, \boldsymbol{\Omega}) = I(\boldsymbol{x}, -\boldsymbol{\Omega})$, then $I^*(\boldsymbol{x}, \boldsymbol{\Omega})$ satisfies the adjoint RTE (3.152) with volume and boundary sources defined as (Bell and Glasstone, 1970)

$$Q^*(\boldsymbol{x}, \boldsymbol{\Omega}) = Q(\boldsymbol{x}, -\boldsymbol{\Omega}) \text{ and } f^*(\boldsymbol{x}, \boldsymbol{\Omega}) = f(\boldsymbol{x}, -\boldsymbol{\Omega}). \tag{3.163}$$

In the case of the "free-surface" boundary condition of no incoming photons ($f \equiv 0$) and no outgoing adjoint flux ($f^* \equiv 0$), the right-hand side of (3.160) can be replaced by
$G_{\mathrm{V}}(\boldsymbol{x}_1, -\boldsymbol{\Omega}_1; \boldsymbol{x}_2, -\boldsymbol{\Omega}_2)$, i.e.,

$$G_{\mathrm{V}}(\boldsymbol{x}_2, \boldsymbol{\Omega}_2; \boldsymbol{x}_1, \boldsymbol{\Omega}_1) = G_{\mathrm{V}}(\boldsymbol{x}_1, -\boldsymbol{\Omega}_1; \boldsymbol{x}_2, -\boldsymbol{\Omega}_2). \tag{3.164}$$

This states that the intensity $I(\boldsymbol{x}_2, \boldsymbol{\Omega}_2)$ at $\boldsymbol{x}_2$ in the direction $\boldsymbol{\Omega}_2$ due to a point source at $\boldsymbol{x}_1$ emitting in direction $\boldsymbol{\Omega}_1$ is the same as the intensity $I(\boldsymbol{x}_1, \boldsymbol{\Omega}_1)$ at $\boldsymbol{x}_1$ in the direction $-\boldsymbol{\Omega}_1$ due to a point source at $\boldsymbol{x}_2$ emitting in direction $-\boldsymbol{\Omega}_2$. Thus, according to (3.164), the intensity is the same in two situations depicted in Fig. 3.19. The relation in the form of (3.164) is referred to as the *optical reciprocity theorem* (Bell and Glasstone, 1970).

By virtue of (3.144), we also have a reciprocity in the surface Green functions:

$$G_{\mathrm{S}}(\boldsymbol{x}_{\mathrm{S}2}, \boldsymbol{\Omega}_2; \boldsymbol{x}_{\mathrm{S}1}, \boldsymbol{\Omega}_1) = G_{\mathrm{S}}(\boldsymbol{x}_{\mathrm{S}1}, -\boldsymbol{\Omega}_1; \boldsymbol{x}_{\mathrm{S}2}, -\boldsymbol{\Omega}_2) \tag{3.165}$$

for any two points on ∂M. Note that the source directions in the second argument pair are oriented inward (e.g., $\boldsymbol{n}(\boldsymbol{x}_{\mathrm{S}1}) \bullet \boldsymbol{\Omega}_1 < 0$) while the detection directions in the first argument pair are oriented outward (e.g., $\boldsymbol{n}(\boldsymbol{x}_{\mathrm{S}2}) \bullet \boldsymbol{\Omega}_2 > 0$).

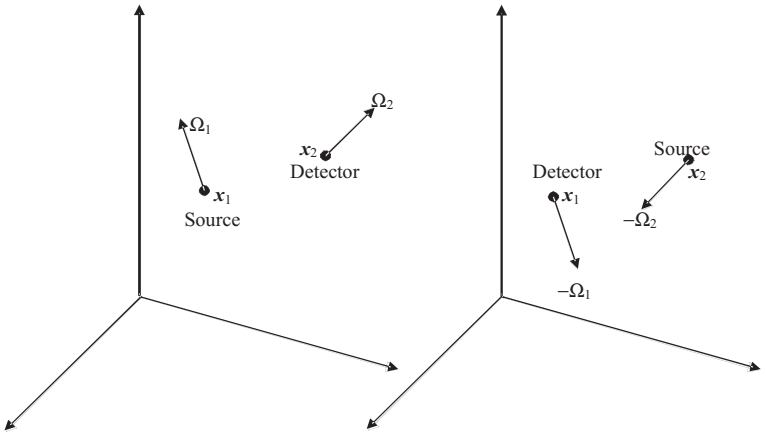

Fig. 3.19. The reciprocity principle. As expressed in (3.164), switching detector and source and inverting the directions of propagation yield the same result for the Green function.

Illustration with an Atmosphere-Surface System. Consider again the problem of a cloudy or aerosol layer bounded from below by a non-uniform and non-Lambertian reflecting surface at $z = 0$. In this situation, a fraction of the radiation can be reflected back into the layer by the ground according to some spatially varying BRDF, $\rho(\boldsymbol{x}_{\rm S}, \boldsymbol{\Omega}' \to \boldsymbol{\Omega})$, where $\boldsymbol{\Omega}'$ is in the downward hemisphere and $\boldsymbol{\Omega}$ is in the upward one. Going back to (3.90)-(3.91), the BRDF is normalized in such a way that

$$I(\boldsymbol{x}_{\rm S}, \boldsymbol{\Omega}) = \int\limits_{\mu'<0} \rho(\boldsymbol{x}_{\rm S}, \boldsymbol{\Omega}' \to \boldsymbol{\Omega}) |\mu'| I(\boldsymbol{x}_{\rm S}, \boldsymbol{\Omega}') {\rm d}\boldsymbol{\Omega}', \tag{3.166}$$

for all $\boldsymbol{x}_{\rm S}$ in the plane $z = 0$ and all $\mu > 0$. Under what conditions on ρ does the optical reciprocity theorem apply to such a composite atmosphere-surface medium? First, the right-hand side of (3.157) should vanish in order to obtain (3.158) and, as a consequence, the relation (3.160) hence (3.164). Second, the conditions (3.163) should be imposed to obtain the relationship $I(\boldsymbol{x}, -\boldsymbol{\Omega}) = I^*(\boldsymbol{x}, \boldsymbol{\Omega})$ between solutions of the forward and adjoint RTE. The former condition is satisfied if the solution of the adjoint RTE satisfies the following BC (Germogenova, 1986)

$$I^*(\boldsymbol{x}_{\rm S}, \boldsymbol{\Omega}) = \int\limits_{\mu'>0} \rho(\boldsymbol{x}_{\rm S}, \boldsymbol{\Omega} \to \boldsymbol{\Omega}') I^*(\boldsymbol{x}_{\rm S}, \boldsymbol{\Omega}') |\mu'| {\rm d}\boldsymbol{\Omega}', \tag{3.167}$$

for all $\boldsymbol{x}_{\rm S}$ and $\mu > 0$. In our example, the functions f and f^* are given by the right-hand sides of (3.166) and (3.167), respectively. Therefore, the equality $f^*(\boldsymbol{x}, -\boldsymbol{\Omega}) =$

$f(\boldsymbol{x}, \boldsymbol{\Omega})$ takes place if and only if

$$\int\limits_{\mu'<0} \rho(\boldsymbol{x}_{\mathrm{S}}, -\boldsymbol{\Omega} \rightarrow -\boldsymbol{\Omega}') I^*(\boldsymbol{x}_{\mathrm{S}}, -\boldsymbol{\Omega}') |\mu'| \mathrm{d}\boldsymbol{\Omega}' = \int\limits_{\mu'<0} \rho(\boldsymbol{x}_{\mathrm{S}}, \boldsymbol{\Omega}' \rightarrow \boldsymbol{\Omega}) I(\boldsymbol{x}_{\mathrm{S}}, \boldsymbol{\Omega}') |\mu'| \mathrm{d}\boldsymbol{\Omega}'. \tag{3.168}$$

Under this condition, $I(\boldsymbol{x}_{\mathrm{S}}, \boldsymbol{\Omega}) = I^*(\boldsymbol{x}_{\mathrm{S}}, -\boldsymbol{\Omega})$ and, therefore, the identity (3.168) holds true if

$$\rho(\boldsymbol{x}_{\mathrm{S}}, -\boldsymbol{\Omega} \rightarrow -\boldsymbol{\Omega}') = \rho(\boldsymbol{x}_{\mathrm{S}}, \boldsymbol{\Omega}' \rightarrow \boldsymbol{\Omega}). \tag{3.169}$$

which is similar to our assumption in (3.162) about the scattering phase function.

Thus, the condition (3.169) should be imposed on the BRDF to extend the validity of the reciprocity principle to media with reflecting boundaries. Note that the scattering phase function that appears in the RTE for vegetation canopies is not, as a rule, rotationally invariant. Besides, this function is generally asymmetric, i.e., $\rho(\boldsymbol{x}, -\boldsymbol{\Omega}' \rightarrow -\boldsymbol{\Omega}) \neq \rho(\boldsymbol{x}, \boldsymbol{\Omega} \rightarrow \boldsymbol{\Omega}')$. The BRDF of vegetation canopies, therefore, does not necessarily follow (3.169). This means that the reciprocity principle may not be applicable in the case of an atmosphere/vegetation-canopy system.

Violation of Directional Reciprocity over Finite Domains. Ultimately, the general reciprocity relations we have uncovered in Green functions are traceable to the microscopic reversibility of each and every reflection and scattering event. If, at a given locale, a certain change of propagation direction $\boldsymbol{\Omega}_1 \rightarrow \boldsymbol{\Omega}_2$ can occur then so can $\boldsymbol{\Omega}_2 \rightarrow \boldsymbol{\Omega}_1$, with equal probability. That is the meaning of the conditions (3.162) and (3.169) for reciprocity. In this respect, the 3D RT reciprocity relations we uncovered are special cases of Onsager's general relations for kinetic systems, not necessarily in equilibrium.

This also opens up the question of purely directional reciprocity as more symmetry is imposed on the system, or as the wealth of information in the Green function is selectively degraded. For instance, if the (cloud-surface) medium is plane-parallel and horizontally homogeneous, then the surface Green functions in (3.165) depend only on $\boldsymbol{x}_1 - \boldsymbol{x}_2$. If, furthermore, the source direction is normal to the surface ($\boldsymbol{\Omega}_2 = (0, 0, -1)^{\mathrm{T}}$) or, generally speaking, an axi-symmetric illumination pattern then only the modulus $||\boldsymbol{x}_1 - \boldsymbol{x}_2||$ matters. This of course includes isotropic illumination, equivalently, an average Green function for all possible incoming directions. One can also integrate the surface Green function in (3.165) over one spatial variable and then average the result over the other; more precisely, one carries this average over a finite domain which is gradually extended to infinity (unless periodic BCs are encountered first). Assuming $\boldsymbol{x}_1$ and $\boldsymbol{x}_2$ were on the same side, this yields

$$R(\boldsymbol{\Omega}_1; \boldsymbol{\Omega}_2) = R(-\boldsymbol{\Omega}_2; -\boldsymbol{\Omega}_1) \tag{3.170}$$

in natural notations, where $\boldsymbol{\Omega}_2$ is inward-oriented at the source and $\boldsymbol{\Omega}_1$ is outward-oriented at the detector. We thus recover Chandrasekhar's angular reciprocity relations for homogeneous plane-parallel media as a special case.

It was once believed that the reciprocity relation in (3.170) could be used in the real 3D atmosphere-surface system. The motivation was to faster build "angular

models" which are used to infer hemispheric TOA fluxes from observed radiances in ERBE/CERES [6] -like missions that monitor the Earth's radiation budget. Di Girolamo et al. (1998) showed beyond any doubt that this is not a good idea since in a 3D system reciprocity applies either for infinitesimal areas around the two points, or for the domain averages, but not for the intermediate pixel-scale which is just an attribute of the observation system.

3.11 Summary and Outlook

We have surveyed the definitions of the fundamental quantities used in general — that is, three-dimensional — radiative transfer from the standpoint of classical particle transport theory. We have looked at how these quantities relate to one another, including reciprocity relations and how they break down in 3D media over finite domains. We have shown how the key quantities are constrained by radiant energy conservation in the steady-state radiative transfer equation under various guises, along with its associated boundary conditions. Green functions are introduced and illustrated by showing how the general (and highly relevant) atmosphere/surface problem can be reduced to the two simpler problems of an atmosphere over an absorbing surface and a convolution using a Green function kernel.

We have thus introduced the basic tools used in the remainder of this volume. In mathematical short-hand, they compactly contain all the necessary information about the systematic biases that the 3D world inflicts upon forward and inverse radiative transfer based on 1D modeling. Bearing in mind the historical background painted in broad strokes in Sect. 3.1, these biases have been documented extensively over the past three or more decades. Many of these biases will be discussed in the following chapters. Several exciting developments in the fundamental aspects of 3D radiative transfer, some with tutorial value, have occurred over the same period. For lack of space, they were not included here, nor will they be covered anywhere in this volume. A non-exhaustive list based largely, but not entirely, on our own research is:

- scale-separation conditions for the applicability of the radiative transfer equation and its connection to scalar- and vector-wave optics;
- critical examination of the applicability of an "ensemble" distribution of droplet sizes motivated by the real-world observation that the largest droplets are so rare one may not be able to define a density for them;
- introduction of a new term into the radiative transfer equation to account for the rare encounters of photons with the very large cloud droplets that do not have a well-defined density;
- various derivations of Fick's law for photon diffusion from the 3D radiative transfer equation, leading to the powerful 3D diffusion approximation;

[6] ERBE: Earth Radiation Budget Experiment; CERES: Clouds and the Earth's Radiant Energy System.

- multiple forward scattering recast as a random walk on the sphere (of propagation directions) and derivation of Eddington's rescaling of extinction without diffusion or asymptotic theory;
- proof that effective (or "mean-field") transport kernels in random 3D media are *never* exactly exponential and, in the relevant case of spatially correlated media, that they have longer-than-exponential tails;
- criteria that predict the onset of strong 3D effects on the scale of the *actual* mean-free-path which can be considerably larger than the inverse of the mean extinction.
- definition of the elementary interaction of the steady-state photon flow with a spatial disturbance in a scattering medium as a "channeling" event, and its application to domain-average biases;
- derivation of a general expression for mean photon path length as volume-angle integral of the temporal Green function used in Chap. ???;
- asymptotic and exact diffusion theoretical formulas for the spatial and temporal characteristics of diffusely reflected and transmitted light on cloud parameters;
- extension of classic/Gaussian diffusion theory to highly variable media using Lévy-stable distributions and transport by "anomalous" diffusion.

Some of this material could be forged into a more advanced appraisal of the fundamentals of 3D radiative transfer that could in turn become the backbone of a phenomenology of 3D effects in photon transport, in other words, a framework from which better informed strategies can be articulated in computational or observational projects. The reader is therefore encouraged to use the suggested reading list below to further his/her awareness of the fundamental issues in 3D radiative transfer. The present authors have always found added-value for their institutional research assignments in remote sensing and/or radiation budget estimation by revisiting the fundamentals.

As an example, in Sect. 3.10.1 we remarked that the decomposition of the Green function into its singular components (0th- and 1st-order scattering fields) and its regular component (higher-order scattered photons) has proved useful in tomography. That breakdown of the Green function has recently been applied to the characterization of radiative transfer regimes in 3D clouds (Knyazikhin et al., 2002) as well as in 3D vegetation canopies (Zhang et al., 2002).

To further illustrate this process of information percolating from the fundamentals to applied radiative transfer, we gave special attention here to the radical departures from plane-parallel geometry embodied by horizontally finite clouds in isolation. We were thus forced to revisit the conventional partition of escaping solar radiation. In particular, we do away with the notion of "side-leakage" in favor of reflection since a cloud "side" can only be identified unambiguously in very special shape/illumination configurations and, even when it can be identified, topology of (i.e., proximity to) sources will cause it to be crossed by a significant population of escaping photons that have undergone relatively few orders-of-scattering. This indeed mimics the behavior of cloud top, the undisputed source of reflection. The conceptual cost here is to accept that *reflected* photons can reach the surface (i.e.,

for all climatic purposes, be "transmitted"). This is in fact an everyday observation: visualize the bright side of a cumulus under fair weather conditions or a distant cumulonimbus generated by deep convection. Similarly, we need to recognize that some of the highly scattered photons *transmitted* through the dimmer side of a finite cloud will eventually reach space (i.e., be "reflected"). This again is a frequent observation by Earth-monitoring satellites that can resolve small broken or isolated clouds, often from sun-synchronous orbits that exclude exactly overhead Sun. Pixel-by-pixel processing of such imagery would probably misidentify a pixel from the shady side of a cloud for lack of brightness. If (e.g., by using thermal emittance), the pixel was properly classified as cloudy, then the optical depth would be vastly underestimated. The simpler "reflection-or-transmission" partition of solar photon fate proposed here was successfully put into application by one of us (Davis, 2002) to infer optical depths of cumulus clouds from high-resolution satellite images. In short, this somewhat rude reminder of common-sense observation of our 3D world populated with finite-sized clouds — and support from elementary considerations in set topology — has clarified the role of these clouds in the Earth's radiation energetics and taught us how to better interpret satellite data.

This is just one example of why the fundamentals of radiative transfer are still a vibrant area of research. An area that is indeed pressured to advance by the climate community as well as the remote sensing community. Anticipating on the topics of Chaps. ??? and ???, we conclude by assessing the needs of these two major stakeholders of radiative transfer theory:

- *Climate Science.* It is commonplace to state that clouds are a major source of uncertainty in current climate system models. About all we know for sure is that low/warm/opaque clouds cool the climate (solar effects dominate) and therefore mitigate the global greenhouse effect, especially if they are as extensive as typical marine stratocumulus systems, while their high/cold/semi-transparent counterparts trap heat (thermal effects dominate) and therefore contribute to the global greenhouse effect. Cirrus layers fulfill all the conditions for the latter effect and are also very pervasive at all latitudes. So, interestingly, the net effect of clouds on the global climate is small but strong regional effects can be expected. This underscores the importance of accurate representations of clouds and of their radiative properties in Global Climate Models (GCMs). It is fair to say that, along with the most common tri-atomic molecules (and some more complex ones), clouds regulate the climate system's vast heat reservoirs (oceans, land masses, and cryosphere). As part of this mechanism, clouds are active participants in the complex dynamics of the hydrological cycle that may be stressed anthropogenically in ways we very poorly understand. Paradoxically, clouds are *never* plane-parallel and homogeneous in Nature but *always* plane-parallel and homogeneous in climate models, even the most current ones, simply because this makes them amenable to the 2-stream model (or one of its numerous variants). One wonders why clouds are not mentioned as often as aerosols, let alone greenhouse gases, as a source of concern in "big" climate science, at the IPCC level where research priorities are formulated. It is true that clouds are an inher-

ent part of the climate system rather than a "forcing" that one has (in principle) a handle on. But another part of the explanation surely comes from the necessity to "tune" GCMs to the climatologies of out-going long- and short-wave fluxes obtained from satellites. These datasets are constantly being improved by NASA's ERBE and CERES programs and by initiatives from other agencies worldwide. Since cloud-radiation interactions are essentially the first and last lines of defense in the Earth's climate system as it interacts radiatively with the rest of the Universe, the corresponding parameterizations are the obvious candidates for dialing the "right" CERES/ERBE-like fluxes. Indeed cloud optical properties can be used to obtain essentially any answer: unlike aerosols for instance, they give climate modelers a full dynamical range. Now the tuning of cloud optical depth is justified primarily by uncertainty in the parameterization of cloud physics rather than that of the radiative transfer. This state of affairs is nonetheless rather discouraging for the cloud-radiation modeling community because one of its poorest representations of clouds can still be used to yield the desired answer. What would happen if an independently validated, hence fundamentally non-tunable, cloud-radiation scheme were delivered to the GCM community?

- *Remote Sensing Science.* The 2-stream particle transport model, first developed and solved analytically by Schuster (1905), will soon be celebrating its first 100 years, and the first computationally viable multi-stream solution for homogeneous slab geometry was obtained well over 50 years ago by Chandrasekhar and co-workers using discrete ordinates. These solutions for plane-parallel optical media are still the workhorses in GCM-based climate modeling and in operational remote sensing of cloud properties respectively. New photon properties such as polarization and total path (in lidar or O_2 spectroscopy) are being explored at the same time as usage of the more familiar ones, wavelength and direction/pixel-space, is being pushed to new heights. Indeed, hyperspectral is superceding multispectral sampling of wavelength and sub-meter resolutions are now available, at least commercially. The increasing cost of space assets — by shear numbers if not by the unit — demands ever more *realistic* end-to-end modeling of existing and future observation systems. This modeling activity will undoubtedly usher in an entirely new class of physics-based algorithms for remote sensing that exploit rather than neglect spatial variability of the atmosphere/surface system. If nothing else, the harsh economics of programmatic investment in space-based Earth science will force the horizontally homogeneous plane-parallel atmosphere/cloud/surface model into retirement because new theory is very inexpensive compared to new hardware.

We again encourage the reader to delve into the suggested reading listed below with a running commentary. Some of the entries offer damage mitigation strategies for the widespread use of 1D standard models in applied radiative transfer (including "effective" properties and other corrections). Others offer outright alternatives in the form of new transport equations. Yet others describe new instrumental designs

using both passive and active modalities that exploit rather than neglect the effects 3D radiative transfer.

Acknowledgments

The authors acknowledge financial support from DOE's Atmospheric Radiation Measurement (ARM) and Multispectral Thermal Imager (MTI) programs, and NASA's Earth Observing System and Radiation Sciences programs. Fruitful discussions with numerous colleagues, associates, and students have helped us clarify our own understanding of the fundamentals of 3D RT and bring them to bear on our everyday problems. We thank them collectively.

References

Aida, M. (1977a). Reflection of solar radiation from an array of cumuli. *J. Met. Soc. Japan*, **55**, 174–181.

Aida, M. (1977b). Scattering of solar radiation as a function of cloud dimensions and orientation. *J. Quant. Spectrosc. Rad. Transf.*, **17**, 303–310.

Antyufeev, V.S. and A.N. Bondarenko (1996). X-ray tomography in scattering media. *SIAM J. Appl. Math.*, **56**, 573–587.

Avaste, O.A. and G.M. Vainikko (1973). Solar radiative transfer in broken clouds. *Izv. Acad. Sci. USSR Atmos. Oceanic Phys.*, **10**, 1054–1061.

Barkstrom, B.R. and R.F. Arduini (1977), Bolle, H.-J., editor, *The effect of finite size of clouds upon the visual albedo of the earth*, pages 188–190. Science Press, Princeton (NJ).

Bell, G.I. and S. Glasstone (1970). *Nuclear Reactor Theory*. Van Nostrand Reinholt, New York (NY).

Berry, M.V. and I.C. Percival (1986). Optics of fractal clusters such as smoke. *Optica Acta*, **33**, 577–591.

Bohren, C.F., J.R. Linskens, and M.E. Churma (1995). At what optical thickness does a cloud completely obscure the sun? *J. Atmos. Sci.*, **52**, 1257–1259.

Box, M.A., S.A.W. Gerstl, and C. Simmer (1989). Computation of atmospheric radiative effects via perturbation theory. *Beitr. Phys. Atmosph.*, **62**, 193–199.

Cannon, C.J. (1970). Line transfer in two dimensions. *Astrophys. J.*, **161**, 255–264.

Capra, F. (1991). *The Tao of Physics*. Shambhala Publ., Boston (MA), 3rd edition.

Case, K.M. and P.F. Zweifel (1967). *Linear Transport Theory*. Addison-Wesley, Reading (MA).

Chandrasekhar, S. (1958). On the diffuse reflection of a pencil of radiation by a plane-parallel atmosphere. *Proc. Natl. Acad. Sci. U.S.A.*, **44**, 933–940.

Chandrasekhar, S. (1960). *Radiative Transfer*. Dover Publications, New York (NY).

Choulli, M. and P. Stefanov (1996). Reconstruction of the coefficient of the stationary transport equation from boundary measurements. *Inverse Problems*, **12**, L19–L23.

Davies, R. (1978). The effect of finite geometry on the three-dimensional transfer of solar irradiance in clouds. *J. Atmos. Sci.*, **35**, 1712–1725.

Davies, R. and J.A. Weinman (1977), Bolle, H.-J., editor, *Results from two models of the three dimensional transfer of solar radiation in finite clouds*, pages 225–227. Science Press, Princeton (NJ).

Davis, A.B. (2002). Cloud remote sensing with sideways-looks: Theory and first results using Multispectral Thermal Imager (MTI) data. *SPIE Proceedings*, **4725**, 397–405.

Davis, A.B. and A. Marshak (2001). Multiple scattering in clouds: Insights from three-dimensional diffusion/P_1 theory. *Nuclear Sci. and Engin.*, **137**, 251–280.

Davis, A.B. and A. Marshak (2002). Space-Time characteristics of light transmitted through dense clouds. *J. Atmos. Sci.*, **59**, 2714–2728.

Davis, A.B. and A. Marshak (2003). Photon propagation in heterogeneous optical media with spatial correlations: Enhanced mean-free-paths and wider-than-exponential free-path distributions. *J. Quant. Spectrosc. Rad. Transf.*, in press.

Deirmendjian, D. (1969). *Electromagnetic Scattering on Spherical Polydispersions*. Elsevier, New York (NY).

Di Girolamo, L., T. Várnai, and R. Davies (1998). Apparent breakdown of reciprocity in reflected solar radiances. *J. Geophys. Res.*, **103**, 8795–8803.

Diner, D.J., G.P. Asner, R. Davies, Y. Knyazikhin, J.P. Muller, A.W. Nolin, B. Pinty, C. B. Schaaf, and J. Stroeve (1999). New directions in Earth observing: Scientific application of multi-angle remote sensing. *Bull. Amer. Meteorol. Soc.*, **80**, 2209–2228.

Germogenova, T.A. (1986). *The Local Properties of the Solution of the Transport Equation (in Russian)*. Nauka, Moscow, Russia.

Giovanelli, R.G. (1959). Radiative transfer in non-uniform media. *Aust. J. Phys.*, **12**, 164–170.

Giovanelli, R.G. and J.T. Jefferies (1956). Radiative transfer with distributed sources. *Lond. Phys. Soc. Proc.*, **69**, 1077–1084.

Henyey, L.C. and J.L. Greenstein (1941). Diffuse radiation in the galaxy. *Astrophys. J.*, **93**, 70–83.

Ishimaru, A. (1975). Correlations functions of a wave in a random distribution of stationary and moving scatterers. *Radio Science*, **10**, 45–52.

Kaufman, Y.J. (1979). Effect of the Earth's atmosphere on contrast for zenith observation. *J. Geophys. Res.*, **84**, 3165–3172.

Knyazikhin, Y., A. Marshak, W.J. Wiscombe, J. Martonchik, and R.B. Myneni (2002). A missing solution to the transport equation and its effect on estimation of cloud absorptive properties. *J. Atmos. Sci.*, **59**, 3572–3585.

Liou, K.-N. (2002). *An Introduction to Atmospheric Radiation*. Academic Press, San Diego, CA.

Lyapustin, A. and Y. Knyazikhin (2002). Green's function method for the radiative transfer problem. 2. Spatially heterogeneous anisotropic surface. *Applied Optics*, **41**, 5600–5606.

Marchuk, G. (1964). Eqaution for the value of information from weather satellites and formulation of inverse problems. *Kosm. Issled.*, **2**, 462–477.

Marchuk, G., G. Mikhailov, M. Nazaraliev, R. Darbinjan, B. Kargin, and B. Elepov (1980). *The Monte Carlo Methods in Atmospheric Optics*. Springer-Verlag, New York (NY).

Marshak, A., Yu. Knyazikhin, A.B. Davis, W.J. Wiscombe, and P. Pilewskie (2000). Cloud - vegetation interaction: Use of normalized difference cloud index for estimation of cloud optical thickness. *Geophys. Res. Lett.*, **27**, 1695–1698.

McKee, T.B. (1976). Simulated radiance patterns for finite cubic clouds. *J. Atmos. Sci.*, **33**, 2014–2020.

McKee, T.B. and S.K. Cox (1974). Scattering of visible radiation by finite clouds. *J. Atmos. Sci.*, **31**, 1885–1892.

Mihalas, D. (1979). *Stellar Atmospheres*. Freeman, San Francisco (CA), second edition.

Minnaert, M. (1941). The reciprocity principle in lunar photometry. *Astrophys. J.*, **93**, 403–410.

Mishchenko, M.I., J.W. Hovenier, and L.D. Travis (2000). *Light Scattering by Non-Sperical Particles*. Academic Press, San Diego (CA).

Mullamaa, Y. et al. (1972). Stochastic structure of cloud and radiation fields. Technical Report TT F-822, NASA Technical Translation.

Nicodemus, F.E., J.C. Richmond, J.J. Hsia, I.W. Ginsberg, and T. Limperis (1977). Geometrical considerations and nomenclature for reflectance. Technical Report NBS Monograph No. 160, National Bureau of Standards.

Odell, A.P. and J.A. Weinman (1975). The effect of atmospheric haze on images of the Earth's surface. *J. Geophys. Res.*, **80**, 5035–5040.

Otterman, J. and R.S. Fraser (1979). Adjacency effects on imaging by surface reflection and atmospheric scattering: Cross radiance zenith. *Appl. Opt.*, **18**, 2852–2860.

Polonsky, I.N. and A.B. Davis (2003). Exponential tails in lidar returns from dense clouds: A theoretical proof and the dependence on physical parameters. *SPIE Proceedings*, **5059**, 15–20.

Rahman, H., B. Pinty, and M.M. Verstraete (1993). Coupled surface-atmosphere reflectance (CSAR) model. 2. Semiempirical surface model usable with NOAA Advanced Very High Resolution Radiometer data. *J. Geophys. Res.*, **98**, 20,791–20,801.

Ramanathan, V., P.J. Crutzen, A.P. Mitra, and D. Sikka (2002). The INDian Ocean EXperiment and the Asian brown cloud. *Curr. Sci.*, **83**, 947–955.

Richards, P.I. (1956). Scattering from a point-source in plane clouds. *J. Opt. Soc. Am.*, **46**, 927–934.

Romanova, L.M. (1968a). Light field in the boundary layer of a turbid medium with strongly anisotropic scattering illuminated by a narrow beam. *Izv. Acad. Sci. USSR Atmos. Oceanic Phys.*, **4**, 1185–1196 (in Russian), 679–685 (English translation).

Romanova, L.M. (1968b). The light field in deep layers of a turbid medium illuminated by a narrow beam. *Izv. Acad. Sci. USSR Atmos. Oceanic Phys.*, **4**, 311–320 (in Russian), 175–179 (English translation).

Romanova, L.M. (1971a). Effective size of the light spot on the boundaries of a thick turbid medium illuminated by a narrow beam. *Izv. Acad. Sci. USSR Atmos. Oceanic Phys.*, **7**, 410–420 (in Russian), 270–277 (English translation).

Romanova, L.M. (1971b). Some characteristics of the light field generated by a point-collimated stationary light source in clouds and fog. *Izv. Acad. Sci. USSR Atmos. Oceanic Phys.*, **7**, 1153–1164 (in Russian), 758–764 (English translation).

Romanova, L.M. (1975). Radiative transfer in a horizontally inhomogeneous scattering medium. *Izv. Acad. Sci. USSR Atmos. Oceanic Phys.*, **11**, 509–513.

Ronnholm, K., M. Baker, and H. Harrison (1980). Radiation transfer through media with uncertain or random parameters. *J. Atmos. Sci.*, **37**, 1279–1290.

Schuster, A. (1905). Radiation through a foggy atmosphere. *Astrophys. J.*, **21**, 1–22.

Schwartz, L. (1950). *Théorie des Distributions*, volume 1 and 2. Hermann, Paris, France.

van Blerkom, D.J. (1971). Diffuse reflection from clouds with horizontal inhomogeneities. *Astrophys. J.*, **166**, 235–242.

Weber, P.G., B.C. Brock, A.J. Garrett, B.W. Smith, C.C. Borel, W.B. Clodius, S.C. Bender, R. Rex Kay, and M.L. Decker (1999). Multispectral Thermal Imager mission overview. *SPIE Proceedings*, **3753**, 340–346.

Weinman, J.A. and P.N. Swartztrauber (1968). Albedo of a striated medium of isotropically scattering particles. *J. Atmos. Sci.*, **34**, 642–650.

Wendling, P. (1977). Albedo and reflected radiance of horizontally inhomogeneous clouds. *J. Atmos. Sci.*, **34**.

Wiscombe, W.J. (1977). The delta-M method: Rapid yet accurate radiative flux calculations for strongly asymmetric phase functions. *J. Atmos. Sci.*, **34**, 1408–1422.

Wolf, E. (1976). New theory of radiative energy transfer in free electromagnetic fields. *Phys. Rev. D*, **13**, 869–886.

Yodh, A. and B. Chance (1995). Spectroscopy/imaging with diffusing light. *Phys. Today*, **48**, 34–40.

Zhang, Y., N. Shabanov, Y. Knyazikhin, and R.B. Myneni (2002). Assessing the information content of multiangle satellite data for mapping biomes. II. Theory. *Remote Sens. Environ.*, **80**, 435–446.

Suggested Reading

This selected bibliography has been sorted into a few broad categories at the cost of some repetitions between them and with the above reference list (quoted in the main text).

(1) *Books:* There now many excellent volumes on atmospheric radiation but they tend to treat only plane-parallel media when multiple scattering is included. For our 3D RT purposes, they remain a resource for all matters of radiation interaction with the gases and particulates that compose the Earth's atmosphere. We also list here a few classic monographies and two-author books that cover the fundamentals of

RT, or particle transport generally speaking, in more detail than typical atmospheric radiation volumes and treat at least one geometry other than plane-parallel, even if it remains highly symmetric. By chronological order).

Chandrasekhar, S. (1950). *Radiative Transfer*. 393 pp., Oxford University Press, London (UK).; reprinted by Dover (1960), New York (NY).

Davison, B. (1958). *Neutron Transport Theory*. 450 pp., Oxford University Press, London (UK).

Vladimirov, V.S. (1963). *Mathematical Problems in the One-Velocity Theory of Particle Transport*, Tech. Rep. AECL-1661, At. Energy of Can. Ltd., Chalk River, Ontario.

Case, K.M. and P.F. Zweifel (1967). *Linear Transport Theory*. Addison-Wesley Publ. Co., Reading (MA).

Bell, G.I. and S. Glasstone (1970). *Nuclear Reactor Theory*. 619 pp., Van Nostrand Reinholt, New York (NY).

Pomraning, G.C. (1973). *The Equations of Radiation Hydrodynamics*. 288 pp., Oxford-Pergamon Press, New York (NY).

Preisendorfer, R.W. (1978). *Hydrological Optics*, NOAA-PMEL, Hawaii.

Ishimaru, A. (1978). *Wave Propagation and Scattering in Random Media*. 2 vols., Academic, New York (NY).

Mihalas, D. (1979). *Stellar Atmospheres*. 2nd ed., xvii+632 pp., Freeman, San Francisco (CA).

van de Hulst, H.C. (1980). *Multiple Light Scattering: Tables, Formulas, and Applications*. 2 vols., Academic Press, San Diego (CA).

Siegel, R. and J.R. Howell (1981). *Thermal Radiation Heat Transfer*. 2nd ed., xvi + 862 pp., McGraw-Hill, New York (NY).

Bohren, C.F. and Huffman, D.R. (1983). *Absorption and Scattering of Light by Small Particles*, xiv+530 pp., Wiley, New York (NY).

Germogenova, T.A. (1986). *The Local Properties of the Solution of the Transport Equation* (in Russian). 272 pp., Nauka, Moscow.

Goody, R.M. and Y.L. Yung (1989). *Atmospheric Radiation: Theoretical Basis*. xiii+519 pp., Oxford University Press, New York (NY).

Lewis, E.E. and W.F. Miller, Jr. (1993). *Computational Methods of Neutron Transport*. xvi+401 pp., American Nuclear Society, La Grange Park (Ill).

Stephens, G.L. (1994). *Remote Sensing of the Lower Atmosphere: An Introduction*. xvi+523 pp., Oxford University Press, New York (NY).

Thomas, G.E. and K. Stamnes (1999). *Radiative Transfer in the Atmosphere and Ocean*. 546 pp., Cambridge University Press, New York (NY).

Liou, K.N. (2002). *An Introduction to Atmospheric Radiation*, xiv+583 pp., Academic Press, San Diego (CA).

(2) *RT in the time-domain:* Particle transport, even with steady sources and sinks, unfolds by its very definition in time. Although time-dependence is out of the scope of the present chapter it is used at least implicitly in Chaps. ??? (on net horizontal transport) and ??? (on O_2 A-band studies of solar photon path statistics).

Time/pathlength-based radiometry, whether time-resolved or via fine-resolution spectroscopy, has such tremendous potential for remote-sensing and climate diagnostics that we confidently predict it will become routine in the relatively near future. The following publications in this broad category are grouped as theoretical, O_2-oriented, lidar-oriented, lightning-oriented, and then listed chronologically. The avid reader is also encouraged to search the bio-medical imaging literature for pathlength-based methods of probing soft tissue with diffusing NIR photons; he/she will find interesting parallels with the multiple-scattering cloud lidar techniques.

Theory:

Irvine, W.M. (1964). The formation of absorption bands and the distribution of photon optical paths in a scattering atmosphere. *Bull. Astron. Inst. Neth.*, **17**, 266–279.

Ivanov, V.V. and S.D. Gutshabash (1974). Propagation of brightness wave in an optically thick atmosphere. *Physika Atmosphery i Okeana*, **10**, 851–863.

Davis, A. and A. Marshak (1997). Lévy kinetics in slab geometry: Scaling of transmission probability. In *Fractal Frontiers*, M.M. Novak and T.G. Dewey (Eds.), World Scientific, Singapore, pp. 63–72.

Davis, A.B. and A. Marshak (2001). Multiple scattering in clouds, Insights from three-dimensional diffusion/P_1 theory. *Nucl. Sci. Eng.*, **137**, 251–288.

Platnick, S. (2001). A superposition technique for deriving photon scattering statistics in plane-parallel cloudy atmospheres. *J. Quant. Spectrosc. Radiat. Transfer*, **68**, 57–73.

Davis, A.B. and A. Marshak (2002). Space-time characteristics of light transmitted by dense clouds, A Green function analysis. *J. Atmos. Sci.*, **59**, 2713–2727.

Oxygen-band/line spectroscopy:

Pfeilsticker, K., F. Erle, O. Funk, H. Veitel, and U. Platt (1998). First geometrical pathlength distribution measurements of skylight using the oxygen A-band absorption technique - I, Measurement technique, atmospheric observations, and model calculations. *J. Geophys. Res.*, **103**, 11483–11504.

Pfeilsticker, K. (1999). First geometrical pathlength distribution measurements of skylight using the oxygen A-band absorption technique - II, Derivation of the Lévy-index for skylight transmitted by mid-latitude clouds. *J. Geophys. Res.*, **104**, 4101–4116.

Min, Q.-L. and L.C. Harrison (1999). Joint statistics of photon pathlength and cloud optical depth. *Geophys. Res. Lett.*, **26**, 1425–1428.

Stephens, G.L. and A. Heidinger (2000). Molecular line absorption in a scattering atmosphere - Part I: Theory. *J. Atmos. Sci.*, **57**, 1599–1614.

Heidinger, A. and G.L. Stephens (2000). Molecular line absorption in a scattering atmosphere - Part II: Application to remote-sensing in the O_2 A-Band. *J. Atmos. Sci.*, **57**, 1615–1634.

Portman, R.W., S. Solomon, R.W. Sanders, J.S. Daniels, and E.G. Dutton (2001). Cloud modulation of zenith sky oxygen photon path lengths over Boulder: Measurement versus model. *J. Geophys. Res.*, **106**, 1139–1155.

Heidinger, A. and G.L. Stephens (2002). Molecular line absorption in a scattering atmosphere - Part III: Path length characteristics and the effects of spatially heterogeneous clouds. *J. Atmos. Sci.*, **59**, 1641–1654.

Multiple-scattering in lidar signals from clouds (beyond the small-angle approximation:

Winker, D.M. and L.R. Poole (1995). Monte-Carlo calculations of cloud returns for ground-based and space-based LIDARs. *Applied Physics B - Lasers and Optics*, **B60**, 341–344.

Winker, D.M., R.H. Couch, and M.P. McCormick (1996). An overview of LITE: NASA's Lidar In-space Technology Experiment. *Proc. IEEE*, **84**, 164–180.

Miller, S.D. and G.L. Stephens (1999). Multiple scattering effects in the lidar pulse stretching problem. *J. Geophys. Res.*, **104**, 22205–22219.

Davis, A.B., R.F. Cahalan, J.D. Spinhirne, M.J. McGill, and S.P. Love (1999). Off-beam lidar: An emerging technique in cloud remote sensing based on radiative Green-function theory in the diffusion domain. *Phys. Chem. Earth (B)*, **24**, 757–765.

Davis, A.B., D.M. Winker, and M.A. Vaughan (2001). First Retrievals of Dense Cloud Properties from Off-Beam/Multiple-Scattering Lidar Data Collected in Space. In *Laser Remote Sensing of the Atmosphere: Selected Papers from the 20th International Conference on Laser Radar*, A. Dabas and J. Pelon (Eds.), École Polytechnique, Palaiseau (France), pp. 35–38.

Kotchenova, S.Y., N.V. Shabanov, Y. Knyazikhin, A.B. Davis, R. Dubayah, and R.B. Myneni (2003). Modeling lidar waveforms with time-dependent stochastic radiative transfer theory for remote estimations of forest biomass. *J. Geophys. Res.*, **108**(D15), 4484, doi:1029/2002JD003288.

Evans, K.F., R.P. Lawson, P. Zmarzly, D. O'Connor, and W.J. Wiscombe (2003). In situ cloud sensing with multiple scattering lidar: Simulations and demonstration. *J. Atmos. and Oceanic Tech.*, **20**, 1505–1522.

Optical lightning studies:

Thomason, L.W. and E.P. Krider (1982). The effects of clouds on the light produced by lightning. *J. Atmos. Sci.*, **39**, 2051–2065.

Koshak, W.J., R.J. Solakiewicz, D.D. Phanord, and R.J. Blakeslee (1994). Diffusion model for lightning radiative transfer. *J. Geophys. Res.*, **99**, 14361–14371.

Suszcynsky, D.M., M.W. Kirkland, A.R. Jacobson, R.C. Franz, S.O. Knox, J.L.L. Guillen, and J.L. Green (2000). FORTÉ observations of simultaneous VHF and optical emissions from lightning: Basic phenomenology. *J. Geophys. Res.*, **105**, 2191–2201.

Light, T.E., D.M. Suszcynsky, M.W. Kirkland, and A.R. Jacobson, 2001). Simulations of lightning optical waveforms as seen through clouds by satellites. *J. Geophys. Res.*, **106**, 17103–17114.

(3) *Lateral photon transport:* For more ease, we have made separate lists for optically thin and thick media, with applications respectively to dense clouds and aerosol layers.

Transmission through optically thin medium over a reflecting surface: We list a few investigations of the so-called aerosol "adjacency" effect that appeared in the 80s or thereafter. Earlier references are listed in the main text on the closely related problem of transmission through optically thin media.

Mekler, Y. and Y.J. Kaufman (1980). The effect of Earth's atmosphere on contrast reduction for a nonuniform surface albedo and "two-halves" field. *J. Geophys. Res.*, **85**, 4067–4083.

Otterman, J., S. Ungar, Y. Kaufman, and M. Podolak (1980). Atmospheric effects on radiometric imaging from satellites under low optical thickness conditions. *Remote Sens. Environ.*, **9**, 115–129.

Tanré, D., M. Herman, and P.-Y. Deschamps (1981). Influence of the background contribution upon space measurements of ground reflectance. *Appl. Opt.*, **20**, 3676–3684.

Kaufman, Y.J. (1982). Solution of the equation of radiative-transfer for remote-sensing over nonuniform surface reflectivity. *J. Geophys. Res.*, **87**, 4137–4147.

Diner, D.J. and J.V. Martonchik (1984). Atmospheric transfer of radiation above an inhomogeneous non-Lambertian ground: 1 - Theory. *J. Quant. Spectrosc. Radiat. Transfer*, **31**, 97–125.

Diner, D.J. and J.V. Martonchik (1984). Atmospheric transfer of radiation above an inhomogeneous non-Lambertian ground: 2 - Computational considerations and results. *J. Quant. Spectrosc. Radiat. Transfer*, **31**, 279–304.

Takashima, T. and K. Masuda (1992). Simulation of atmospheric effects on the emergent radiation over a checkerboard type of terrain. *Astrophysics and Space Science*, **198**, 253–263

Reinersman, P.N. and K.L. Carder (1995). Monte Carlo simulation of the atmospheric point-spread function with an application to correction for the adjacency effect. *Appl. Opt.*, **34**, 4453–4471.

Lyapustin, A.I. (2001). Three-dimensional effects in the remote sensing of surface albedo. *IEEE Trans. Geosc. and Remote Sens.*, **39**, 254–263.

Lyapustin, A.I. and Y. Kaufman (2001). Role of adjacency effect in the remote sensing of aerosol. *J. Geophys. Res.*, **106**, 11909–11916.

Lyapustin, A.I. and Y. Knyazikhin (2002). Green's function method for the radiative transfer problem. II. Spatially heterogeneous anisotropic surface. *Appl. Opt.*, **41**, 5600–5606.

Reflection and transmission by optically thick media: Chapter ??? is largely devoted to this case of lateral transport in clouds and, here again, there is fruitful search to be done in the medical optics literature that will reveal interesting parallels with independent atmospheric endeavors.

Weinman, J.A. and M. Masutani (1987). Radiative transfer models of the appearance of city lights obscured by clouds observed in nocturnal satellite images. *J. Geophys. Res.*, **92**, 5565–5572.

Stephens, G.L. (1986). Radiative transfer in spatially heterogeneous, two-dimensional anisotropically scattering media, *J. Quant. Spectrosc. Radiat. Transfer*, **36**, 51–67.

Stephens, G.L. (1988). Radiative transfer through arbitrary shaped optical media, Part 1 - A general method of solution. *J. Atmos. Sci.*, **45**, 1818–1835.

Ganapol, B.D., D.E. Kornreich, J.A. Dahl, D.W. Nigg, S.N. Jahshan, and C.A. Temple (1994). The searchlight problem for neutrons in a semi-infinite medium. *Nucl. Sci. Eng.*, **118**, 38–53.

Marshak, A., A. Davis, W.J. Wiscombe, and R.F. Cahalan (1995). Radiative smoothing in fractal clouds. *J. Geophys. Res.*, **100**, 26247–26261.

Kornreich, D.E. and B.D. Ganapol (1997). Numerical evaluation of the three-dimensional searchlight problem in a half-space. *Nucl. Sci. Eng.*, **127**, 317–337.

Davis, A., A. Marshak, R.F. Cahalan, and W.J. Wiscombe (1997). The Landsat scale-break in stratocumulus as a three-dimensional radiative transfer effect, Implications for cloud remote sensing. *J. Atmos. Sci.*, **54**, 241–260.

Davis, A.B., R.F. Cahalan, J.D. Spinhirne, M.J. McGill, and S.P. Love (1999). Off-beam lidar: An emerging technique in cloud remote sensing based on radiative Green-function theory in the diffusion domain. *Phys. Chem. Earth (B)*, **24**, 757–765.

Romanova, L.M. (2001). Narrow light beam propagation in a stratified cloud: Higher transverse moments. *Izv. Atmos. Oceanic Phys.*, **37**, 748–756.

Platnick, S. (2001). Approximations for horizontal photon transport in cloud remote sensing problems. *J. Quant. Spectrosc. Radiat. Transfer*, **68**, 75–99.

Davis, A.B. and A. Marshak (2001). Multiple scattering in clouds, Insights from three-dimensional diffusion/P_1 theory. *Nucl. Sci. Eng.*, **137**, 251–288.

Davis, A.B. and A. Marshak (2002). Space-time characteristics of light transmitted by dense clouds, A Green function analysis. *J. Atmos. Sci.*, **59**, 2713–2727.

Polonsky, I.N. and A.B. Davis (2003). Exponential tails in lidar returns from dense clouds: A theoretical proof and the dependence on physical parameters. *S.P.I.E. Proceedings*, **5059**, 15–20.

(4) *New transport kernels and RT equations:* Chapter ??? is devoted to "stochastic" RT, which usually means in binary Markovian binary media. It covers in detail mean-field theory for a special kind of random medium that has a vast literature in its own right in atmospheric optics, astrophysics and neutronics. Here we list some other kinds of mean-field investigations that produce new transport equations for multiple scattering, or new kernels for propagation between the scatterings.

Borovoi, A.G. (1984). Radiative transfer in inhomogeneous media. *Dok. Akad. Nauk SSSR*, **276**, 1374–1378. (English version in *Sov. Phys. Dokl.*, **29**(6).)

Stephens, G.L. (1988). Radiative transfer through arbitrarily shaped media, Part 2 - Group theory and closures. *J. Atmos. Sci.*, **45**, 1836–1848.

Davis, A. and A. Marshak (1997). Lévy kinetics in slab geometry: Scaling of transmission probability. In *Fractal Frontiers*, M.M. Novak and T.G. Dewey (Eds.), World Scientific, Singapore, pp. 63–72.

Evans, K.F. (1993). A general solution for stochastic radiative transfer. *Geophys. Res. Lett.*, **20**, 2075–2078.

Cairns, B., A.W. Lacis, and B.E. Carlson (2000). Absorption within inhomogeneous clouds and its parameterization in general circulation models. *J. Atmos. Sci.*, **57**, 700–714.

Kostinski, A.B. (2001). On the extinction of radiation by a homogeneous but spatially correlated random medium. *J. Opt. Soc. Am. A (18*, 1929–1933.

Shaw, R.A., A.B. Kostinski, and D.D. Lanterman (2002). Super-exponential extinction of radiation in a negatively-correlated random medium. *J. Quant. Spectrosc. Radiat. Transfer*, **75**, 13–20.

Knyazikhin, Y., A. Marshak, W.J. Wiscombe, J. Martonchik, and R.B. Myneni (2002). A missing solution to the transport equation and its effect on estimation of cloud absorptive properties. *J. Atmos. Sci.*, **59**, 3572–3585.

Davis, A.B. and A. Marshak (2004). Photon propagation in heterogeneous optical media with spatial correlations: Enhanced mean-free-paths and wider-than-exponential free-path distributions. *J. Quant. Spectrosc. Rad. Transf.*, **84**, 3–34.

(5) *New instrumental designs that exploit 3D RT:* Here we exclude high-resolution O_2 band/line spectroscopy because it has an entry of its own in the above item (2), and a whole chapter further on in this volume by Stephens, Heidinger, and Gabriel (Chap. ???). It is to be considered as a new and promising technique even though it has been under consideration and even testing for a long while. The references by von Savigny et al., Marshak et al. and Barker et al. use a simple zenith- or nadir-looking radiometer that records radiance time-series at one or more non-absorbed solar wavelengths as the clouds are advected above the ground station or scanned from an aircraft. Davis et al., Love et al. and Evans et al. use a pulsed laser as a source and examine the information about clouds contained in the "off-beam" (i.e., multiple-scattering) returns.

Savigny, C. von, O. Funk, U. Platt, and K. Pfeilsticker (1999). Radiative smoothing in zenith-scattered skylight transmitted through clouds to the ground. *Geophys. Res. Lett.*, **26**, 2949–2952.

Davis, A.B., R.F. Cahalan, J.D. Spinhirne, M.J. McGill, and S.P. Love (1999). Off-beam lidar). An emerging technique in cloud remote sensing based on radiative Green-function theory in the diffusion domain. *Phys. Chem. Earth (B)*, **24**, 757–765.

Marshak, A., Y. Knyazikhin, A.B. Davis, W.J. Wiscombe, and P. Pilewskie (2000). Cloud-vegetation interaction). Use of normalized difference cloud index for estimation of cloud optical thickness. *Geophys. Res. Lett.*, **27**, 1695–1698.

Love, S.P., A.B. Davis, C. Ho, and C.A. Rohde (2001). Remote sensing of cloud thickness and liquid water content with Wide-Angle Imaging Lidar (WAIL). *Atm. Res.*, **59–60**, 295–312.

Barker, H.W., A. Marshak, W. Szyrmer, A. Trishchenko J.-P. Blanchet, and Z. Li (2002). Inference of cloud optical depth from aircraft-based solar radiometric measurements. *J. Atmos. Sci.*, **59**, 2093–2111.

Evans, K.F., R.P. Lawson, P. Zmarzly, D.O'Connor, and W.J. Wiscombe (2003). In situ cloud sensing with multiple scattering lidar). Simulations and demonstration. *J. Atmos. and Oceanic Tech.*, **20**, 1505–1522.

(6) *Further considerations on surface reflectance properties and/or reciprocity:* A few recent studies worth consulting are listed below, to go beyond the references given in Sect. 3.10.3.

Loeb, N.G. and R. Davies (1996). Observational evidence of plane parallel model biases: Apparent dependence of cloud optical depth on solar zenith angle. *J. Geophys. Res.*, **101**, 1621–1634.

Di Girolamo, L. (1999). Reciprocity principle applicable to reflected radiance measurements and the searchlight problem. *Appl. Opt.*, **38**, 3196–3198.

Diner, D. J., G. P. Asner, R. Davies, Y. Knyazikhin, J.P. Muller, A. W. Nolin, B. Pinty, C. B. Schaaf, and J. Stroeve (1999). New directions in Earth observing: Scientific application of multi-angle remote sensing, *Bull. Amer. Meteor. Soc.*, **80**, 2209–2228.

Knyazikhin, Y. and A. Marshak (2000). Mathematical aspects of BRDF modeling: Adjoint problem and Green's function. *Remote Sens. Review, 18*, 263–280.

Martonchik, J.V., C.J. Bruegge, and A. Strahler (2000). A review of reflectance nomenclature used in remote sensing. *Remote Sensing Reviews*, **19**, 9–20.

Snyder, W.C. (2002). Definition and invariance properties of structured surface BRDF. *IEEE Trans. Geoscience Rem. Sensing*, **40**, 1032–1037.

(7) *More studies on cloud models with non-plane-parallel geometry:* In the introduction to main text, we covered the historical (pre-1980) period where horizontally finite (fundamentally non-plane-parallel) clouds where a popular topic, especially using the diffusion approximation. In the 1990s, the trend was to return to plane-parallel geometry for the outer geometry but the models were rife with internal 2D or 3D variability. We predict a renewed interest in horizontally finite clouds to cope with cumulus-type clouds. In Sect. 3.9.2, we discussed a recent application by one of the authors (Davis and Marshak, 2002) to remote-sensing that capitalized on a closed-form diffusion theoretical result for spherical clouds. Here are a few references from the 1980s where horizontally finite clouds are investigated in isolation or in (random or regular) arrays, always going beyond diffusion theory.

Welch, R. and W. Zdunkowski (1981). The radiative characteristics of noninteracting cumulus cloud fields, Part I - Parameterization for finite clouds. *Contrib. Atmos. Phys.*, **54**, 258–272.

Welch, R. and W. Zdunkowski (1981). The radiative characteristics of noninteracting cumulus cloud fields, Part II - Calculations for cloud fields. *Contrib. Atmos. Phys.*, **54**, 273–285.

Harshvardhan and J. Weinman (1982). Infrared radiative transfer through a regular array of cuboidal clouds. *J. Atmos. Sci.*, **39**, 431–439.
Harshvardhan and R. Thomas (1984). Solar reflection from interacting and shadowing cloud elements. *J. Geophys. Res.*, **89**, 7179–7185.
Welch, R.M. and B.A. Wielicki (1984). Stratocumulus cloud field reflected fluxes: The effect of cloud shape. *J. Atmos. Sci.*, **41**, 3085–3103
Preisendorfer, R.W. and G.L. Stephens (1984). Multimode radiative transfer in finite optical media, I: Fundamentals. *J. Atmos. Sci.*, **41**, 709–724.
Stephens, G.L. and R.W. Preisendorfer (1984). Multimode radiative transfer in finite optical media, II: Solutions. *J. Atmos. Sci.*, **41**, 725–735.
Joseph, J. and V. Kagan (1988). The reflection of solar radiation from bar cloud arrays. *J. Geophys. Res.*, **93**, 2405–2416.

(8) *Selected readings on the independent pixel/column approximation:* This is simple idea of applying 1D RT to the column under every (computational) grid-point or (satellite) pixel in the horizontal projection of a 3D cloud field. We see this as the "IPA" or "ICA," a prediction for the 2D horizontal field of reflected or transmitted fluxes or the heating rate at a given level. Some authors would consider the IPA/ICA to include the next step which consists in spatially or statistically averaging this predicted field. At any rate, the now popular IPA/ICA terminology was introduced during the 1990s to describe an already common practice. In a sense, this is the default approach to radiative budget estimation in climate models as well as in remote sensing operations when unresolved variability is ignored. If reasonable assumptions are made about the unresolved variability the averaging can, at least under some circumstances, predict the domain-average quite accurately. So the IPA/ICA has become a real workhorse in contemporary 3D RT. It was mentioned in the main text only in connection with two early publications of primarily historical interest: one that appeared in the Former Soviet Union (Mullamaa et al., 1972), and another in the West (Ronnholm et al., 1980), later and independently of course. In this volume alone, the IPA/ICA is used extensively in Chaps. ???, ??? and ??? either as a benchmark (from which to measure "true" 3D RT effects mediated by horizontal flux divergences and convergences) or as a framework (for producing domain-average properties by accounting for the variability but ignoring the horizontal fluxes). Below is a sampler of studies where the IPA/ICA is applied (some even before the abbreviations were adopted), assessed (by comparison with more accurate 3D RT methods), and improved upon (without sacrificing efficiency).

Applications of the IPA/ICA:

Stephens, G.L. (1985). Reply (to Harshvardan and Randall). *Mon. Wea. Rev.*, **113**, 1834–1835.
Stephens, G.L., P.M. Gabriel, and S.-C. Tsay (1991). Statistical radiative transport in one-dimensional media and its application to the terrestrial atmosphere. *Transp. Theory and Statis. Phys.*, **20**, 139–175.
Cahalan, R.F., W. Ridgway, W.J. Wiscombe, T.L. Bell, and J.B. Snider (1994). The albedo of fractal stratocumulus clouds. *J. Atmos. Sci.*, **51**, 2434–2455.

Barker, H.W. (1996). A parameterization for computing grid-averaged solar fluxes for inhomogeneous marine boundary layer clouds - Part 1, Methodology and homogeneous biases. *J. Atmos. Sci.*, **53**, 2289–2303.

Barker, H.W., B.A. Wielicki, and L. Parker (1996). A parameterization for computing grid-averaged solar fluxes for inhomogeneous marine boundary layer clouds - Part 2, Validation using satellite data. *J. Atmos. Sci.*, **53**, 2304–2316.

Oreopoulos, L. and H.W. Barker (1999). Accounting for subgrid-scale cloud variability in a multi-layer 1D solar radiative transfer algorithm. *Quart. J. Roy. Meteor. Soc.*, **125**, 301–330.

Deviations from the IPA/ICA:

Cahalan, R.F., W. Ridgway, W.J. Wiscombe, S. Gollmer, and Harshvardhan (1994). Independent pixel and Monte Carlo estimates of stratocumulus albedo. *J. Atmos. Sci.*, **51**, 3776–3790.

Marshak, A., A. Davis, W.J. Wiscombe, and G. Titov (1995). The verisimilitude of the independent pixel approximation used in cloud remote sensing. *Remote Sens. Environ.*, **52**, 72–78.

Marshak, A., A. Davis, W.J. Wiscombe, and R.F. Cahalan (1995). Radiative smoothing in fractal clouds. *J. Geophys. Res.*, **100**, 26247–26261.

Chambers, L., B. Wielicki, and K.F. Evans (1997). On the accuracy of the independent pixel approximation for satellite estimates of oceanic boundary layer cloud optical depth. *J. Geophys. Res.*, **102**, 1779–1794.

Davis, A., A. Marshak, R.F. Cahalan, and W.J. Wiscombe (1997). The Landsat scale-break in stratocumulus as a three-dimensional radiative transfer effect, Implications for cloud remote sensing. *J. Atmos. Sci.*, **54**, 241–260.

Titov, G.A. (1998). Radiative horizontal transport and absorption in stratocumulus clouds. *J. Atmos. Sci.*, **55**, 2549–2560.

Davis, A.B. and A. Marshak (2001). Multiple scattering in clouds, Insights from three-dimensional diffusion/P_1 theory. *Nucl. Sci. Eng.*, **137**, 251–288.

Savigny, C. von, A.B. Davis, O. Funk, and K. Pfeilsticker (2002). Time-series of zenith radiance and surface flux under cloudy skies: Radiative smoothing, optical thickness retrievals and large-scale stationarity, *Geophys. Res. Lett.*, **29**(17), 1825–1828, doi:10.1029/2001GL014153.

Corrections to the IPA/ICA:

Gabriel, P.M. and K.F. Evans (1996). Simple radiative-transfer methods for calculating domain-averaged solar fluxes in inhomogeneous clouds. *J. Atmos. Sci.*, **53**, 858–877.

Marshak, A., A. Davis, R.F. Cahalan, and W.J. Wiscombe (1998). Nonlocal independent pixel approximation: Direct and inverse problems. *IEEE Trans. Geosc. and Remote Sens.*, **36**, 192–205.

Faure, T., H. Isaka, and B. Guillemet (2001). Neural network analysis of the radiative interaction between neighboring pixels in inhomogeneous clouds. *J. Geophys. Res.*, **106**, 14465–14484.

Polonsky, I.N., M.A. Box, and A.B. Davis (2003). Radiative transfer through inhomogeneous turbid media: Implementation of the adjoint perturbation approach at the first-order. *J. Quant. Spectrosc. Radiat. Transfer*, **78**, 85–98.

Finally, we note that the "adjacency" effect covered under item (3) is a 3D RT process that nonlinearly mixes surface reflectances in satellite imagery. This radiometric mixing mediated by the ambient aerosol is what defeats the clear-sky equivalent of the IPA: satellite pixels can no longer be analyzed separately to infer surface properties. Because the aerosol atmosphere is optically thin, methods used in that context are interestingly different from those favored by the cloud radiation community.